NOTE TO USERS

158

uOttawa

L'Université canadienne
Canada's university

FACULTÉ DES ÉTUDES SUPÉRIEURES ET POSTOCTORALES

uOttawa

L'Université canadienne
Canada's university

FACULTY OF GRADUATE AND POSDOCTORAL STUDIES

Rachel M. McBride
AUTEUR DE LA THÈSE / AUTHOR OF THESIS

M.Sc. (Cellular and Molecular Medicine)
GRADE / DEGREE

Department of Cellular and Molecular Medicine
FACULTÉ, ÉCOLE, DÉPARTEMENT / FACULTY, SCHOOL, DEPARTMENT

The genetic mapping and characterization of the M196 craniofacial and fin mutation in zebrafish

TITRE DE LA THÈSE / TITLE OF THESIS

M-A. Akimenko
DIRECTEUR (DIRECTRICE) DE LA THÈSE / THESIS SUPERVISOR

CO-DIRECTEUR (CO-DIRECTRICE) DE LA THÈSE / THESIS CO-SUPERVISOR

EXAMINATEURS (EXAMINATRICES) DE LA THÈSE / THESIS EXAMINERS

C. Martin

D. Bulman

Gary W. Slater
LE DOYEN DE LA FACULTÉ DES ÉTUDES SUPÉRIEURES ET POSTDOCTORALES /
DEAN OF THE FACULTY OF GRADUATE AND POSTDOCORAL STUDIES

The genetic mapping and characterization of the *m196* craniofacial and fin mutation in zebrafish

Rachel M. McBride

This thesis is submitted as a partial fulfillment of the Master of Science program in Cellular and Molecular Medicine.

University of Ottawa
Department of Cellular and Molecular Medicine
Ottawa, Ontario, Canada

May, 2005

Your file Votre référence
ISBN: 0-494-11346-4
Our file Notre référence
ISBN: 0-494-11346-4

Abstract

The *m196* mutation, a result of an ENU mutagenesis screen in zebrafish, disrupts embryonic development resulting in a delay of proper gill arch cartilage differentiation and a disruption of median and pectoral fin fold development. Mutant phenotypes arise at 24 hours post fertilization (hpf) with the onset of fin fold development and lead to early mortality between 30 hpf and 2 weeks from unknown causes. *m196* delay and disruption of craniofacial chondrogenesis is possibly due to the initial displacement of the pharyngeal pouches and dismorphogenesis of the branchial arches. Cells expressing genetic markers of the fin fold and neural crest accumulate in a disorganized manner along the tail. Using meiotic mapping techniques, we have mapped the m196 mutation to a SSLP marker zCtg37A on LG17. We are analyzing candidate genes in search of the m196 mutation. These results will lead to the identification of a genetic factor essential for craniofacial and fin development in zebrafish.

Table of Contents:

List of Figures:

List of abbreviations

aa, amino acid

AER, apical ectodermal ridge

Asmt, acetylserotonin O-methyltransferase

bp, base pairs

BCIP, 5-bromo-4-chloro-3-indolyl phosphate

BSA, bovine serum albumin

cDNA, complementary deoxyribonucleic acid

cldn, claudin

cM, centiMorgan

CNS, central nervous system

col2a1, collagen 2a1

cR, centiRay

DAB, 3,3'-diaminobenzidine tetrahydrochloride

dd, dorsal diencephalon

dlx, distal-less

dpf, days post fertilization

dscr1l2, down syndrome candidate region gene 1-like 2

e2f2, e2f transcription factor 2

ECM, extracellular matrix

ENU, N-ethyl N-nitrosourea

EST, expressed sequence tag

EtOH, ethanol

fb, forebrain

fec, facial ectoderm

fgf, fibroblast growth factor

ga, gill arch

gdf7, growth/differentiation factor 7

grhl3, grainyhead-like 3

HCh1, Human chromosome 1

het, heterozygote

HK, Hong Kong

Hox, homeobox transcription factor

hpf, hours post fertilization

hy, hyoid

id3, inhibitor of differentiation/DNA binding 3

ISH, *in situ* hybridization

kb, kilobase pairs

LG17, linkage group 17

MCh4, Mouse chromosome 4

MeOH, methanol

mhb, midbrain-hindbrain boundary

mRNA, messenger ribonucleic acid

msx, muscle segment homeobox

NBT, nitroblue tetrazolium

NCC, neural crest cell

ng1, novel gene 1

˚C, degrees Celsius

os, optic stalk

ot, otic vesicle

PAC, P1-artificial chromosome

PBS, phosphate buffered saline

PBST, phosphate buffered saline and Tween-20

PCR, polymerase chain reaction

PFA, paraformaldehyde

RAPD, random amplified polymorphic DNA

recs, recombinants

RNA, ribonucleic acid

rps6ka1, ribosomal protein S6 kinase polypeptide 1

Shh, sonic hedgehog

SSLP, simple sequence length polymorphism

SSCP, single strand conformation polymorphism

tb, tail bud

TGF-ß, transforming growth factor ß

TL, Top Long-fin

Acknowledgements

First I would like to express much gratitude to my supervisor Dr. Marie-Andree Akimenko for the opportunity to tackle this project and invaluable guidance. I would also like to thank my advisory committee Drs. Marc Ekker, Margaret Sonnenfeld, and Dennis Bulman for their counsel and fresh, enthusiastic perspective. I would also like to thank the members of my examining committee Drs. Christofre Martin and again Dennis Bulman.

The mapping of this mutant would not have been accomplished with such speed and grace were it not for the four months I spent with our collaborators in the Knapik Lab in Munich, Germany (currently based at Vanderbilt University, Nashville, Tennessee). I would like to acknowledge Dr. Ela Knapik for her mentorship and honesty as well as Dr. Mercedes Montero for taking me under her wing. I would like to thank Dr. Sherri Sackdev and Mark Reims for beginning this project prior to my involvement and accomplishing the initial bulk segregant analysis in the summer of 2000. I wish to express many thanks to Drs. Michael Lang, Alejandro Barrallo-Gimeno, Georg Schmidt, and Jun Honda for their laughter and impressive work ethic.

As well many thanks go to the members of the Akimenko and Ekker laboratories and the Ottawa Health Research Institute (OHRI). Thanks to Danielle Guay and Lindsay Quayle for maintaining the zebrafish facilities, to Lucille Joly for the LN54 mapping results. I would also like to thank Drs. Fabien Avaron and Luc Poitras for their invaluable advice and unique martial arts demonstrations as well as Dr. Padhi Bhaja for his positive attitude. I would like to

acknowledge Daniel Kolcinski for continuing this project for his own graduate work- may the force be with you. As well many thanks go to my fellow graduate students Amanda Smith, Olga Jarinova, Purva Wagh, Jing Zhang, and Noel Ghanem for creating a pleasant work environment and assisting with practical jokes.

Finally I would like to thank my close family and friends without which none of this would have been possible. I am grateful to Christopher, Jill, Aaron, and Ashley for their understanding, inspiration, and active encouragement as well as Echo for her conditional loving purrs. I owe immense gratitude to my big little brother Iain for checking in every once in a while and to my wonderful parents Doreen and Dr. R. Garth McBride for their love and unconditional support.

I. Introduction

1. Zebrafish as a model organism

The teleost zebrafish (*Danio rerio*) has become an important model in the study of developmental biology and genetics. These resilient, freshwater fish originating from India along with *Caenorhabditis elegans* became more widely used in research in the 1970s. The small size of *D. rerio*, about 2-4 cm, allows a large number of fish to be housed in a relatively small area. After reaching sexual maturity at 3 months of age, zebrafish are able to lay up to a few hundred eggs per clutch. The resulting embryos grow rapidly; within 24 hours post fertilization (hpf) the basic body structure is established (Figure 1B), and within 3 days post fertilization (dpf) embryogenesis is complete (Figure 1C). Zebrafish embryos are also unique because they remain transparent up to 2 dpf. Therefore observation of early developmental processes and organ systems deep within the living embryo can be easily followed with the aid of a basic dissecting microscope (Figure 1). Additionally gene expression patterns can be observed directly within the whole mount embryos through *in situ* hybridization (ISH) using labeled antisense RNA probes (Nuesslein-Volhard and Dahm, 2002).

Furthermore, external development of zebrafish offspring allows embryos to be readily manipulated genetically or through cell transplantations. Transgenic strains of zebrafish can be created by microinjection of constructs into one- or two-cell fertilized eggs. Although a lack of homologous recombination means a knockout approach is currently unfeasible, microinjection of chemically-modified

antisense oligonucleotides, called morpholinos (Summerton, 1999), into one- or two-celled fertilized eggs can create genetic knockdown phenotypes up to 5 dpf (Nasevicius and Ekker, 2000). These short oligonucleotides are designed to bind to specific targets within the transcript and inhibit translation *in vivo*. The zebrafish model allows researchers to bridge the genetic gap between *Drosophila* and mammals and provides a model organism facilitating the use of genetic approaches along with embryological technique (Nuesslein-Volhard and Dahm, 2002).

Zebrafish genomics are greatly enhanced by the creation of genomic mapping panels as well as the current genome sequencing project undertaken by the Sanger Institute in Cambridge, United Kingdom. Meiotic (Knapik *et al.*, 1998) and radiation hybrid (Geisler *et al.*, 1999; Hukriede *et al.*, 2001; Hukriede *et al.*, 1999) maps allow for the placement of sequences on zebrafish chromosomes or linkage groups (LGs). As well sequencing of the zebrafish genome is on the verge of completion. Analysis of this sequence will lead to the discovery of many novel genes and genetic elements and will greatly assist the cloning of mutants such as *m196*.

Recently a number of genetic mutagenesis screens in zebrafish have been completed in order to analyze the function of developmentally significant genes (Driever *et al.*, 1996; Haffter *et al.*, 1996). In particular the *m196* mutant is of interest to the Akimenko lab because of the defects in fin development, as well as our collaborators in the Knapik lab currently based at Vanderbilt University in Nashville, Tennessee due to the craniofacial phenotype. The following overview

of specific developmental processes in zebrafish provides a background for understanding the *m196* phenotype and may offer some insights into the genetic and cellular pathways that may be affected in the *m196* mutation.

2. Brief overview of neural crest cells

The craniofacial and fin structures, affected in the *m196* mutants, are contributed to in part by cells of neural crest origin. Neural crest cells (NCCs) are induced in the region of the neural keel in zebrafish, or neural folds in other vertebrates, that meet to form the neural tube. These cells delaminate from the neural tube and migrate along distinct pathways, differentiating during their passage. They will eventually contribute significantly to cartilage and bone, neurons and glia, pigment cells, and connective tissues of the organism (Figure 2). Cranial NCCs are found to contribute significantly to the segmented branchial arches migrating in three streams: mandibular, hyoid, and vagal (Schilling and Kimmel, 1994). Neural crest cells from more rostral and mid-trunk regions have been shown in zebrafish to contribute to a number of different ganglia and glia, smooth muscle, and connective tissues in the heart and tail regions as well as fin mesenchyme (Vaglia and Hall, 1999). Recently they have also been found to populate the adrenomedullary and pronephric regions (Vaglia and Hall, 2000). Therefore, based on their anterior-posterior positioning along the body axis, NCCs populate distinct regions and tissues essential for zebrafish survival.

Figure 1: The early developing wild type *Danio rerio* embryo. (A) The mid-somitogenesis embryo at 14 hpf (10-somite stage), (B) 24 hpf, and (C) 6 dpf. Lateral view, anterior to the left.

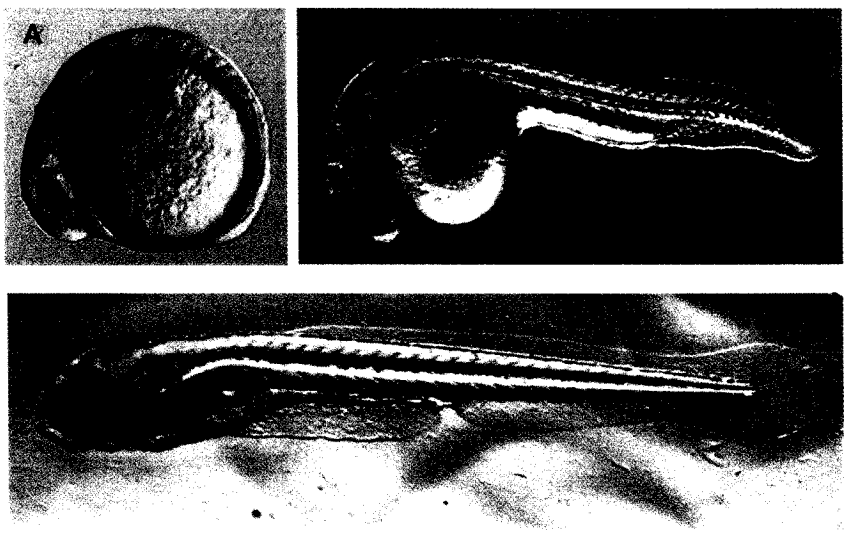
A

Figure 2: Neural crest cells populate distinct tissues along the anterior-posterior axis of the zebrafish embryo. The cartoon represents a dorsal view of the zebrafish embryo. Thin dotted lines divide the original regions of premigratory cranial, cardiac, and trunk neural crest. Shading marks a proposed transition region between cardiac and trunk crest populations thought to occur, possibly between somites 3 and 5 (s3 and s5). Solid black bars demonstrate tissues along the anterior posterior axis which are contributed to by cranial, cardiac, and/or trunk neural crest, but do not encompass the potential of neural crest populations to differentiate into tissues other than specified. fb, forebrain; mb, midbrain; r1-r7, rhombomeres 1-7; s1-6, somites 1-6 (Adapted from Vaglia and Hall, 1999).

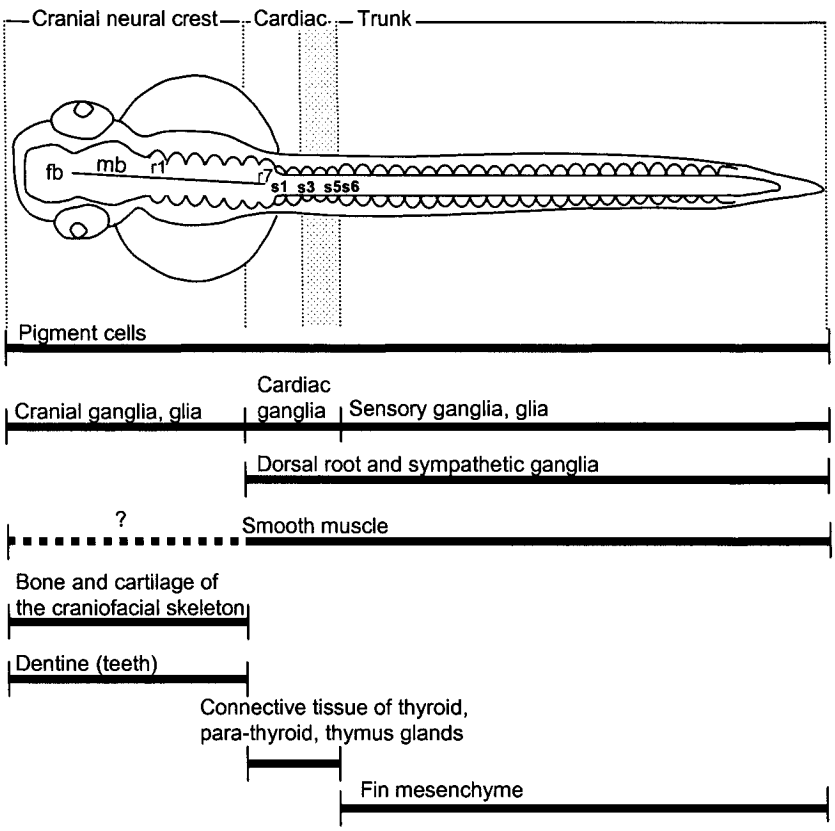
Cranial neural crest
Cardiac
Trunk
fb
mb
r1
r7
s1 s3 s5s6
Pigment cells
Cardiac
Cranial ganglia, glia
ganglia
Sensory ganglia, glia
Dorsal root and sympathetic ganglia
?
Smooth muscle
Bone and cartilage of
the craniofacial skeleton
Dentine (teeth)
Connective tissue of thyroid,
para-thyroid, thymus glands
Fin mesenchyme

3. Posterior zebrafish development

3.1 Tail bud elongation

Tail extension and differentiation in zebrafish involves coordinated genetic and morphological factors during development. Differential cell movement and proliferation rates in the posterior body provide insight into how the tail bud extends from the body core. As the tail region develops beyond the yolk around 17-18 hpf, there appears to be a strong posterior movement of dorsomedial cells found in the anterior trunk which acts as the driving force during tail elongation. Cell proliferation is greater in this more anterior-medial area than at the posterior tip where cells actually move more laterally and/or anteriorly (Kanki and Ho, 1997). Ventral cells of the tail bud display significantly less caudal movement than dorsally located cells. The active migration and proliferation of the dorsal tissues and inactivity of the ventral cells possibly contributes to the initial ventral curve to the tail during the first 30 hours of zebrafish development (Figure 1B). Together this suggests that elongation of the tail is a mechanism of the rostral trunk rather than an extension of the posterior tail tip (Kanki and Ho, 1997).

The posterior-most region of the elongating tail bud in vertebrates is not necessarily a homogenous blastema, but rather contains distinct regions specified to defined cell fates that play a role in proper tail elongation and differentiation (Nakao and Ishizawa, 1984; Smithberg, 1954; Tucker and Slack, 1995). One such region implicated in mediating elongation of the tail bud is the developing notochord. Differentiation of axial cells into large, cuboidal notochord

cells may be part of the tail extension mechanism (Kanki and Ho, 1997). This is supported by the zebrafish *no tail* mutation in which the notochord fails to form and the tail is severely reduced (Halpern *et al.*, 1993). However in the zebrafish *floating head* mutation, although embryos form no notochord, tail development is primarily wild type at 24 hpf (Talbot *et al.*, 1995). Conversely embryos with inhibited *Wnt8* expression develop an intact notochord but completely lack an extended tail (Agathon *et al.*, 2003). Therefore, although the notochord may play some role, it is unlikely elongation of the tail is solely mediated by notochord differentiation.

In fact, a ventral tail organizer has been characterized in zebrafish, able to form secondary tails when grafted ectopically (Agathon *et al.*, 2003). A dorsal organizer in zebrafish has been previously established (Shih and Fraser, 1996) analogous to the organizer activity of the dorsal blastopore lip in amphibians which is able to induce a secondary embryonic axis when grafted ectopically (Spemann and Mangold, 1924). Similarly, grafting regions of the dorsal margin of zebrafish mid-gastrula embryos (approximately 8 hpf) into the animal pole of host sphere stage embryos (approximately 4-4.5 hpf) result in ectopic axial structures such as notochord and floor plate (Agathon *et al.*, 2003) In contrast, similar grafts of regions derived from the ventral margin will establish an ectopic secondary tail including non-axial tail tissues derived from mesoderm and ectoderm (i.e. caudal and ventral fins, somites, neural tube and blood cells) (Agathon *et al.*, 2003). This organizer activity is mediated by overlapping bmp, wnt, and nodal signaling in this ventral margin. Downregulation of the Bone

Morphogenic Protein (bmp) signaling pathway creates embryos with axial, but not non-axial, structures of the tail (Schmid *et al.*, 2000). Inactivation of the wnt8 signaling pathway results in comparable phenotypes (Lekven *et al.*, 2001). Similarly, a decrease in both maternal and zygotic nodal signals prevents axis and tail formation (Thisse *et al.*, 2000). Misexpression of all three signals in the embryonic animal pole can recapitulate the induction of a secondary tail axis and recruit animal pole tissues to form differentiated ectodermal and mesodermal structures (Agathon *et al.*, 2003). Thus the tail formation in zebrafish is mediated by Bmp, Wnt8 and Nodal signaling from the ventral organizer of the embryo. A similar bmp-regulated tail bud initiator is also found in *Xenopus*, giving evolutionary significance to this developmental feature (Beck *et al.*, 2001).

3.2 Median fin development

Late in tail bud elongation, the zebrafish fin development begins to occur. This involves the formation of the paired and unpaired fins (Figure 3). Paired fins include the pectoral and pelvic fins, homologous to tetrapod fore- and hindlimbs respectively. Unpaired fins include the dorsal, caudal, and anal fins which are represented by the median fin fold during embryonic development.

3.2.1 Development of the larval and adult fins

Median fin fold development begins around 22 hpf, prior to pectoral limb bud extension, as a rapidly elongating dorsal-ventral outgrowth around the posterior end of the embryonic tail bud (Kimmel *et al.*, 1995). The fin fold is characterized by a thin keel of distally elevated epidermal cells supported by a more proximal

core of mesenchyme and extracellular matrix (ECM) that separates the epidermal layers laterally along the body wall (Dane and Tucker, 1985). In *Xenopus* this thick ECM, consisting of collagen, fibronectin, tenascin and glycosaminoglycans, mediates trunk neural crest and mesenchyme migration into the fin fold (Collazo *et al.*, 1993; Epperlein *et al.*, 1988). Similar matrix components are found in zebrafish along trunk neural crest pathways (Vaglia and Hall, 2000). Further fin outgrowth develops along with the onset of dermal skeleton (actinotrichia, lepidotrichia, and dermal bones) and endoskeleton (paired fin radials and caudal fin hypural complexes) within later weeks of zebrafish development.

3.2.2 The initial fin skeleton

The endoskeleton of the unpaired fins adjoins the free fin with the axial skeleton of the fish. Beginning shortly after epithelial extension, small structural fibrils called actinotrichia are deposited synchronously along with both pectoral and median fin fold extension (Figure 3B,D,F). These fibers are deposited in a distal to proximal manner in both the pectoral and median fin folds early in epidermal extension. Although their origin and composition have been debated for decades, it is now understood that these non-mineralized elements contain a non-collagenous, glycosylated protein rich in tyrosine and cysteine called elastoidin (Bouvet, 1974; Geraudie, 1977; van Eeden *et al.*, 1996). Using the fibrils as a substrate, mesenchymal and neural crest cells migrate between these arrays into the fin fold in a contact guidance-mediated manner (Thorogood and Wood, 1987; Wood and Thorogood, 1984) and provide the skeletogenic cells

necessary for further chondro- and osteogenesis in the fins (Smith *et al.*, 1994). During the first four weeks of development the zebrafish median fin fold is replaced by three adult fins: the unpaired anal (ventral), dorsal and caudal fins. Subsequently cartilaginous endoskeletal radial and hypural bones start to form within the fins, followed by the bony fin rays, or lepidotrichia.

3.2.3 Neural crest contribution

Early experiments have shown the importance of neural crest cells for the induction and development of the median fin fold. By vital cell dye (DiI) labeling of the dorsal neural keel of zebrafish, caudal trunk NCCs from this region were found to migrate into the forming dorsal, ventral and caudal fins along the actinotrichial arrays (Smith *et al.*, 1994). As mentioned above, actinotrichia may actually act to provide contact-guidance cues to mesenchymal cells as they move distally into the developing fin (Wood and Thorogood, 1984; Wood and Thorogood, 1987). Smith and colleagues (Smith *et al.*, 1994) also found that labeled NCCs migrate to positions that correlate with later lepidotrichial elements of the dermal skeleton. Therefore these results suggest that the NCCs within the median fin fold may have significant skeletogenic potential.

Furthermore NCCs play an essential role in early fin fold induction. Extirpation of the trunk neural folds in axolotls and lamprey results in the loss of fin development in the corresponding regions (DuShane, 1935; Newth, 1956). Grafting experiments by Twitty and Bodenstein (1941) demonstrate that the underlying tail mesenchyme, containing neural crest, is able to determine anterior-posterior polarity of the overlying fin fold ectoderm in frogs. Dorsal

epidermis also appears to be induced most likely by the dorsal neural keel to form the fin fold (Twitty and Bodenstein, 1941). These experiments also found that this inductive signal lies in a developmental window, before neural crest migrate distally but after closure of the neural keel. When transplanted elsewhere, neural crest-induced dorsal ectoderm is able to recruit underlying mesenchyme to form an ectopic fin (Bodenstein, 1952). Hence early NCCs initiate powerful axis-specific inductive signals within the epidermis necessary for fin fold formation.

3.2.4 Differential development of the dorsal and ventral caudal fins

A recent study in *Xenopus* has noted the differential development of the dorsal versus the ventral fins (Tucker and Slack, 2004). This is further exemplified in a number of zebrafish mutants. Dorsalizing mutations such as *tolloid/minifin* and *lost-a-fin* show a loss of ventral tail fin (Bauer *et al.*, 2001; Connors *et al.*, 1999), whereas ventralizing mutations such as *mercedes* and *dino* result in an enlarged or duplicated ventral fin phenotype (van Eeden *et al.*, 1996). In amphibians, trunk crest cells migrate by means of two pathways into the ventral fins: the tail tip and enteric pathways (Collazo *et al.*, 1993). The former dorsal migration route is initiated prior to the enteric route and follows in a medial line along the dorsal fin around the posterior tail tip, providing cells to the more posterior ventral tissues, as well as dorsal fin and pigment stripe. The enteric pathway involves direct migration ventrally within the space between the neural tube/notochord and the somites towards the proctodeum (Collazo *et al.*, 1993). These two novel pathways are unlike those of amniotes which follow a more intrasomitic route.

Tucker and Slack (2004) however show that development of the ventral fin is not as dependent on a neural crest contribution as the dorsal fin fold. Instead they propose the presence of a mesodermal ventral fin inducer, lying just under the blastopore lip, active in the mid to later stages of embryonic neurulation. Interestingly, as mentioned above, this same area is noted in zebrafish and *Xenopus* as a tail organizer (Agathon *et al.*, 2003; Beck *et al.*, 2001). Thus the ventral inducer initiates and physically contributes to the formation of the ventral fin fold in the same way that the dorsal neural crest induces and populates the dorsal fin fold.

4. Pectoral fin development

The formation of the paired appendages is highly conserved among vertebrates. In zebrafish the paired fins are embodied in the pectoral and pelvic fins similar to the fore- and hindlimbs limbs in tetrapods respectively. Limb/fin development is first initiated by the specification of a limb field defined as an area along the embryonic body capable of forming a limb. This is followed by the establishment of limb/fin bud anteroposterior, proximodistal, and dorsoventral axes. Basic limb morphology is then completed by the formation of the distal-most structures such as the fin fold in zebrafish and digits in tetrapods. This fin to limb transition represents a major step from the aquatic to terrestrial lifestyle in vertebrate evolution.

First limb field specification results from coordinated *Hox* gene expression that provides positional identity cues along the anterior-posterior axis. For example, in fishes, amphibians, birds and mammals, forelimb development

appears to take place at the anterior-most border of the *Hoxc6* expression domain (Gilbert, 2000). *Hoxc8* and *Hoxb5* are also expressed in the lateral plate mesoderm of the prospective forelimb/pectoral fin and loss of one of these factors affects the position of limb components, suggesting that these specific combinations of *hox* gene expression are necessary for limb positional information (Nelson *et al.*, 1996; Rancourt *et al.*, 1995). The T-box family of transcription factors, including the T (brachyury) locus, and Wnt signaling pathway also play an important role in defining the anterior versus posterior fin bud. While *Tbx4* and *Wnt8c* are expressed in the hindlimb/pelvic fin, *Tbx5* and *Wnt2b* are expressed in the forelimb/pectoral fin in tetrapods and zebrafish (Gibson-Brown *et al.*, 1996; Kawakami *et al.*, 2001; Ng *et al.*, 2002). Together these signaling pairs specify chick, mouse, and zebrafish limb identity (Ng *et al.*, 2002; Rodrıguez-Esteban *et al.*, 1999; Takeuchi *et al.*, 1999) and act to initiate downstream signaling, such as Fgf10, necessary for limb/fin bud outgrowth (Kawakami *et al.*, 2001; Ng *et al.*, 2002).

Following identification of a limb field, mesenchyme from the lateral plate mesoderm (skeletal precursors) and somites (muscle precursors) accumulate under the epidermal tissue creating a circular bulge known as the limb bud (Gilbert, 2000). In tetrapods extensive proliferation of these mesenchymal tissues forms the bulk of the resulting appendage. However in the teleost fin, bud growth is arrested early on and the distal epidermis extends out from the bud as the fin fold.

Axis specification in the developing limb is in many ways conserved between mouse, chick, and zebrafish. Limb development is mediated by the establishment of the main signaling centers involved in limb outgrowth and differentiation, namely the apical ectodermal ridge (AER) and the mesodermal zone of polarizing activity (ZPA; Figure 3A). A coordinated Fgf-signaling loop within the mesoderm signals to the overlying ectoderm to express *Fgf8* and establishes the AER which defines the anterior-posterior limb axis (Capdevila and Belmonte, 2001). The maintenance of the AER in chick and mouse is essential for the distal outgrowth of the limb (Saunders, 1948; Todt and Fallon, 1984). Although the presence of an AER in zebrafish pectoral fin development is still controversial, the distal apical epidermis of the zebrafish pectoral fin appear to be morphologically as well as genetically homologous to the AER of the tetrapod limb during early fin development. Loss of signals from the apical ectoderm results in a lack of fin bud outgrowth (Neumann *et al.*, 1999; van Eeden *et al.*, 1996) similar to results in tetrapods mentioned above. Also supporting the presence of AER activity in zebrafish are two recently cloned *buttonhead* (*btd*)-like zinc (Zn) finger transcription factors, *sp8* and *sp9* (Kawakami *et al.*, 2004). Activity of these genes is necessary for maintaining the apical epidermis and *fgf8* expression in mouse, chick, and zebrafish limbs (Bell *et al.*, 2003; Kawakami *et al.*, 2004). Both *sp8* and *sp9* act downstream of *fgf10* and, in the case of *sp8*, is mediated by Wnt/ß-catenin signaling (Kawakami *et al.*, 2004) which play a major roles in limb development. In fact conserved *sp8* sequences are found in beetle (Beerman *et al.*, 2004), and murine Sp8 is able to functionally replace mBtd in

Drosophila (Treichel *et al.*, 2003). Therefore the genetic mechanisms in establishing the limb AER and fin distal epidermis are highly conserved in limb formation, even in aspects of invertebrate development.

Signals from the overlying ectoderm then induce the ZPA within the posterior mesoderm (Figure 3A). This area in the posterior limb bud is characterized by a marked expression of *sonic hedgehog* (*shh*) which defines the anterior-posterior axis of the limb/fin (Riddle *et al.*, 1993). Combinatorial expression of *fgf8* from the AER and *hox* genes, such as *hoxb-8* in mouse (Charite *et al.*, 1994), help to define this *shh* expression domain. Retinoic acid signaling is also critical for limb bud initiation and ZPA induction in the chick (Stratford *et al.*, 1996) in an anterior-posterior gradient (Bryant and Gardiner, 1992). In zebrafish, not only does *shh* expression in the pectoral fin buds mirror that found in tetrapods (Akimenko and Ekker, 1995a; Krauss *et al.*, 1993), but this expression appears to be controlled by conserved mechanisms. Duplication of *shh* expression in the pectoral fin bud by general administration of retinoic acid (Akimenko and Ekker, 1995a) echoes previous results in chick which also form an anterior node of Shh signaling and develop a mirrored duplicate set of digits (Riddle *et al.*, 1993). Thus the ZPA, defining the anterior-posterior axis, is conserved within zebrafish and tetrapods.

Teleost fin bud growth is arrested much earlier than in tetrapods as the epidermal fin fold begins to extend and the first endoskeletal elements appear (Dane and Tucker, 1985; Sordino *et al.*, 1995). In tetrapods, sustained mesodermal proliferation is mediated by continued signaling from the AER and is

followed by the formation of the digit-forming autopod of the distal limb not present in teleosts. Therefore, folding of the epidermal tissues to form the fin fold in zebrafish may disrupt these proliferative signals from the apical ectoderm and arrest further bud growth (Sordino *et al.*, 1995). The evolutionary transition from fin fold to digits is represented in part by an alteration in *Hox* gene expression. The *hoxd* expression patterns provide a good example of this shift. In teleost fins *hoxd11,-12* and *-13* are expressed in a distal to proximal manner within tip of the fin bud. Tetrapods retain this expression pattern in their developing limb buds as well; however a second pattern of *Hoxd* expression is later shifted to the posterior edge of the limb and a new domain of *Hoxd13, -12,* and *-11* appears in the distal region of the bud which delineates the digit-forming autopod (Coates, 1995; Sordino *et al.*, 1995). Therefore shifts in gene expression domains and tissue movements help to explain the divergence of later paired fin/limb development between fish and tetrapods.

Two weeks after fertilization the second phase of pectoral fin development occurs involving the subsequent formation of skeletal elements. The endoskeletal disc, which has condensed within in the bud mesenchyme by approximately 2 dpf, subdivides into the proximal endoskeletal components (Grandel and Schulte-Merker, 1998), homologous to the more proximal bones in tetrapod limbs (Wagner and Chui, 2001). Bony fin ray endoskeletal elements form within the fin fold region (Grandel and Schulte-Merker, 1998) similar to more caudal fin development described above.

Figure 3: Pectoral fin bud growth involves coordinated induction signals from the distal epidermis and ZPA in the posterior mesenchyme and consequent epithelial outgrowth including early formation of structural actinotrichia. (A, C, E) Dorsal view of the developing fin. Distal to the right. Green arrows represent signals from the overlying distal epidermis (de). Red represents signaling from the zone of polarizing activity (ZPA). B, D, F pertains to median as well as pectoral fin fold extension and represents cross-sections at mid-fin (Adapted from Bouvet, 1974; Dane and Tucker, 1985). Distal to the top. a, actinotrichia; ff, fin fold; m, mesenchyme; e, epidermis; pe, peridermis.

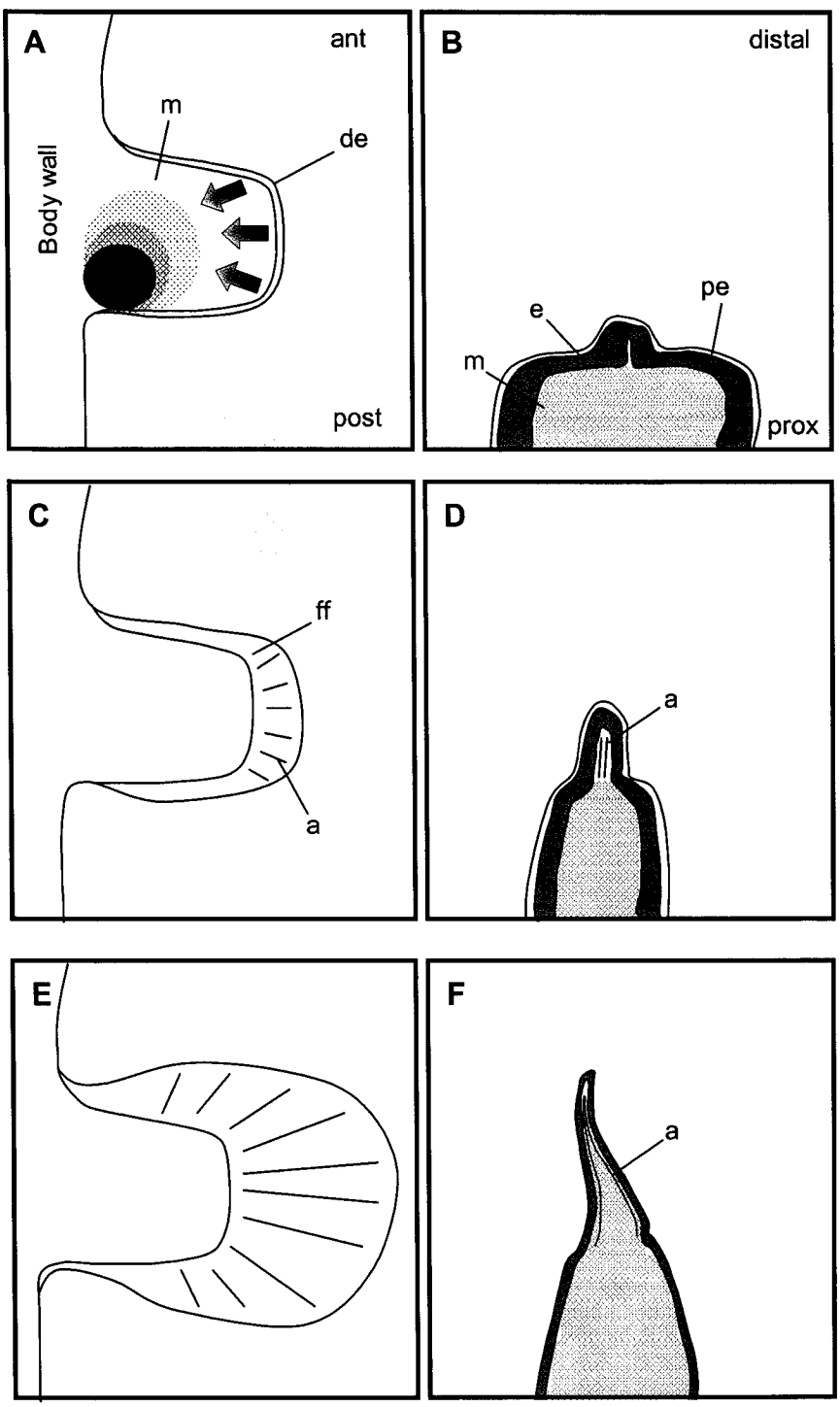
A
ant
m
de
Body wall
post
B
distal
pe
e
m
prox
C
ff
a
D
a
E
F
a

5. Craniofacial development

5.1 Branchial arch morphogenesis and differentiation

The formation of the zebrafish cranium involves coordinated morphogenesis and differentiation of the anterior-most ectoderm, mesoderm, endoderm, and neural crest cells into seven branchial arches: the first mandibular arch, the second hyoid arch, and the five gill arches. Between 15-19 hpf in zebrafish, cells begin to migrate laterally from the embryonic midline forming transverse rows, 4-5 cells thick in the mandibular and hyoid arches and 2 cells thick in the more caudal arches (Schilling and Kimmel, 1994). Cranial NCCs, which provide the structural connective tissues and skeletal components (Smith and Hall, 1990), migrate into the branchial arches from the developing neural ectoderm. Mesodermal contributions form the future musculature and endothelia of the arch arteries (LeDouarin *et al.*, 1994; Noden, 1988; Trainor *et al.*, 1994). The primordial arches are covered by ectodermal epidermis and arch-associated sensory ganglia (Couly and LeDouarin, 1990). Two transverse rows of endodermal cells, the pharyngeal pouches, separate each arch (Schilling and Kimmel, 1994), and form the epithelial lining of the pharynx as well as the endocrine glands of the pharyngeal region (thyroid, parathyroid, and thymus) (Cordier and Haumont, 1980; Warga and Stainier, 2002). At 60 hpf this endodermal core will open to form a small mouth opening located between the eyes just dorsal to the developing mandibular and hyoid arches (Kimmel *et al.*, 1995).

Patterning of the branchial arches in zebrafish has been shown in some cases to be specified early in development before paraxial mesoderm and cranial neural crest have begun to migrate laterally from the centre axis of the embryos (Schilling and Kimmel, 1994). Lineage tracing and fate mapping results from the Kimmel lab have shown that many premigratory mesodermal and NCCs will give rise to single cell types and that cell lineages are restricted to specific cranial segments along the anterior-posterior axis. For example, cells located just caudal to the eye will populate the mandibular arch, whereas cells located more posteriorly, between the otic vesicle and the anterior boundary of the forming somites, will contribute to the gill arches. Medial-lateral axis location also predicts the type of derivative the cranial neural crest will form. Lateral cells are more likely to form neurons, whereas more medial cells will contribute almost exclusively to cartilage and connective tissues (Schilling and Kimmel, 1994). Therefore, cranial neural crest tissues are defined early in development along the anterior-posterior and medial-lateral axes and play a major role in arch patterning.

5.2 Craniofacial cartilage development

Whereas dorsal cartilages are proposed to form from paraxial mesoderm (Kimmel *et al.*, 1998), as mentioned above cranial neural crest cells migrate into the seven segmented arches. Figure 4 illustrates the larval cranial cartilages formed from these tissues. The first mandibular arch will form the jaw, namely the Meckel's and palatoquadrate cartilages. The basihyal and hyosymplectic jaw support structures are formed from the second branchial arch, and arches 3-7

form the five gill arches consisting of the basibranchial, hypobranchial, and ceratobranchial cartilages. Cartilage development involves several key phases including morphogenesis of the segmented arches, differentiation of the cartilage precursors, and growth of the resulting cartilage. Early in pharyngeal development at approximately 36-48 hpf, craniofacial endoskeletal formation begins with the condensation of ectomesenchyme. Condensation is initiated by increased mitotic activity and/or aggregation of cells and is necessary for proper cartilage differentiation (Hall and Miyake, 1992). The cartilaginous elements then grow along with larval maturation. Early cartilage growth between 2.5 and 4 dpf in zebrafish primarily involves an increase in cell size rather than cell number. Later cartilage growth relies more on cell proliferation than hypertrophy (Kimmel *et al.*, 1998). By adulthood some cranial elements will further develop into bone while others retain their cartilaginous state.

Figure 4: Cranial cartilages of the wild type zebrafish larva at 7 dpf. Cartoons in A', B' and C' illustrate cartilaginous elements from the lateral (A), ventral (B), and dorsal (C) views of the larval head stained with alcian blue which outlines individual chondrocytes. (A, A') Lateral view of dorsal and ventral cartilages. Anterior to the left, dorsal to the top. (B, B') Ventral view of the cranium focused on the cartilages derived from the branchial arches. Anterior to the top. (B') Cartilages diagrammed are colour coded based on arch derivative: branchial arch 1 (ba1, light/dark blue), ba2 (orange), ba3 (green), ba4 (pink), ba5 (brown), ba6 (purple), ba7 (yellow). (C, C') Dorsal cartilages dissected from the ventral cartilages and overlying tissues for better visualization. Dorsal view, anterior to the top. bb, basibranchial; cb, ceratobranchial; ch, ceratohyal; ep, ethmoid plate; hb, hypobranchial; hs, hyosymplectic; m, Meckel's; not, notochord; ot, otic capsule; pq, palatoquadrate; pc, parachordal; tr, trabeculae cranii.

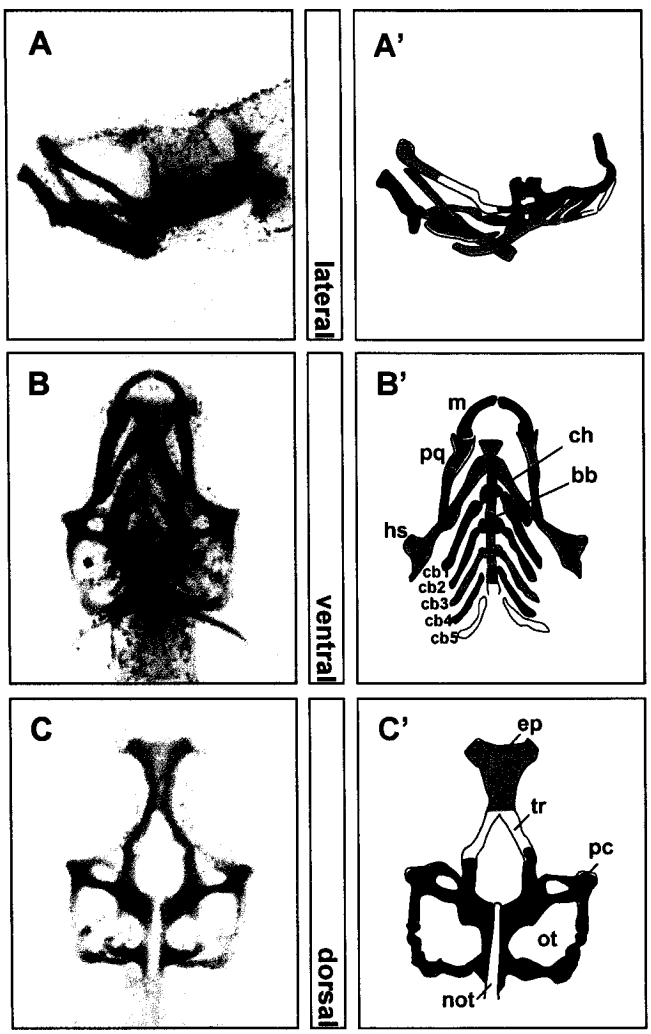
A
lateral
A'
B
ventral
B'
m
ch
pq
bb
hs
cb1
cb2
cb3
cb4
cb5
C
dorsal
C'
ep
tr
pc
ot
not

5.2.1 Genetic factors involved in chondrogenesis

Differentiation of precursor cells to chondrocytes involves a number of similar genetic factors among craniates. Bone Morphogenic Proteins (BMP) are part of the TGF-ß superfamily and have been shown to play a role in supporting the transition of mesenchymal cells into chondrocytes both *in vitro* in mouse (Shukunami *et al.*, 1998) and *in vivo* in chick (Macias *et al.*, 1997). In fact, the absence of BMP signaling by exposure to a BMP antagonist Noggin hinders cartilage formation in mice. As well cranial development is hyperplastic in *Noggin*-deficient mice in which BMP signaling is uninhibited (Brunet *et al.*, 1998). In mouse cell lines, BMP proteins have been shown to work alone or in combination with other molecules such as additional BMPs or Hedgehog during chondrogenesis (Nakamura *et al.*, 1997). Differential BMP receptor expression may also play a key role in cartilage differentiation. BMP type I receptor A possibly regulates apoptosis in precartilaginous cells and receptor B marks prehypertrophic chondrocytes. Therefore chondrogenesis is not only affected by secreted BMP signaling molecules but also in part by a fluctuation in spatial and temporal distribution of BMP receptors (Zou *et al.*, 1997).

Collagen type IIA (col2a1 in zebrafish) is a cartilage matrix protein that surrounds chondrocytes as they differentiate. A potential upstream regulator of Col2a1 is intranuclear protein Sox9, which has been found in mouse to bind and activate chondrocyte-specific enhancer elements in collagens and other cartilage-related genes (Lefebvre *et al.*, 1997). Campomelic dysplasia (CD) is a human syndrome resulting from a dominant lethal mutation in *SOX9* (Mansour *et*

al., 1995). Symptoms, which include a substantial disruption of cartilage development throughout the skeleton including numerous craniofacial defects, suggest SOX9 is necessary for cartilage differentiation (Foster, Dominguez-Steglich *et al.* 1994). In zebrafish, two *sox9* genes, *sox9a* and *sox9b*, were cloned by Chiang *et al.* (2001). The complementary expression patterns of these two tetrapod *SOX9* orthologs corresponds to that of *col2a1* in cartilage-forming arches (Chiang *et al.*, 2001). Therefore the expression pattern suggests that the role of *sox9a/sox9b* and *col2a1* is conserved in teleost craniofacial development and cartilage specification.

Wnt signaling has also been shown to interact with Sox9 in cartilage differentiation. N-Cadherin and ß-Catenin assembly of cadherin-catenin-actin adhesion complexes facilitate cell-cell interactions during chondrogenic condensations (Delise and Tuan, 2002). Overexpression of *Sox9* creates a phenotype reminiscent of loss-of-function mutations of ß-catenin in mice. Conversely downregulation of *Sox9* expression results in a phenotype similar to the constitutive activation of *ß-catenin* (Akiyama *et al.*, 2004). Both cases show a disruption of cartilage formation, suggesting that these two molecules functionally interact during chondrocyte differentiation. Therefore chondrogenesis appears to involve complex signaling pathways conserved among most vertebrates.

5.2.2 Cranial chondrogenesis and endoderm requirement

As previously mentioned, branchial arch development involves the formation of endodermal pouches that separate each arch. There is substantial evidence pointing to the important role of pharyngeal endoderm in cranial segmentation

and chondrogenesis. Pouches begin as epithelial outpocketings from the more axially located endodermal pharynx and foregut. Pouches move distally through the surrounding mesenchyme to contact the ectoderm. Cell migration appears to be the primary mechanism that drives the endoderm into the pouch shape. Lateral cytoplasmic movements within the cell suggest that environmental chemotactic or substrate cues guide this migration process (Crump *et al.*, 2004a). In chick, proper pouch morphogenesis along the proximodistal axis is directed in part by supra-cellular actin cables. N-cadherin adherens junctions join these actin fibers along the apical plasma membrane of the pharyngeal endodermal cells (Quinlan *et al.*, 2004). In fact proper pouch structure has recently been shown to be an essential factor for pharyngeal cartilage patterning in zebrafish. Alterations in pouch size and shape give rise to misshapen cranial cartilages (Crump *et al.*, 2004a). Therefore the proper functioning of the cell cytoskeleton and migration of the pouches is important for the formation of other cranial structures associated with meso- and ectodermal derivatives.

Disruption of genetic factors within the endoderm associated with cell migration and tissue integrity lead to a loss of pouch formation. Integrins are heterodimeric receptor proteins which bind fibronectin and laminin in the extracellular matrix and have important functions in tissue integrity, differentiation, migration and survival (Bokel and Brown, 2002). Zebrafish expressing integrinα5 mutated in an important ligand binding site show variable disruption in endodermal pouch formation, as well as dismorphogenesis of associated craniofacial cartilages, muscle, and nerve (Crump *et al.*, 2004b).

Therefore cell migration, cell adhesion and tissue integrity maintenance factors are all important for proper pouch formation and play a significant role in craniofacial development.

Moreover, proper segmentation of the pharyngeal region requires endodermal pouch formation. The endoderm appears to contribute signals which are necessary for patterning and survival of the neural-crest derived cartilage (Piotrowski *et al.*, 2003; Piotrowski and Nuesslein-Volhard, 2000). Recently David *et al* (2002) found fgf3 to be a major signaling molecule from the pharyngeal pouches essential for posterior branchial arch development in zebrafish. General inhibition of FGF signaling with a FGF antagonist results in the complete ablation of branchial cartilage, a phenotype reminiscent of endoderm-deficient mutants such as *Bonnie and clyde* (*bon*) and *Casanova* (*cas*) (David *et al.*, 2002). *Fgf8*$^{-}$*;fgf3*-morpholino injected zebrafish embryos do not form pharyngeal pouches. The disruption in neural crest cells in these *fgf*-deficient embryos is probably due in part to a loss of Fgf8 or Fgf3 survival factors from the absent pouches (Crump *et al.*, 2004a). Even in the presence of pouch epithelium, knockdown of endodermal *fgf3* expression results in a complete loss of the more posterior arches, though introduction of fgf3 in endoderm-deficient mutants is unable to rescue gill arch formation (David *et al.*, 2002). Therefore although fgf3 is a necessary endodermal signaling molecule, other factors must be required from the pouch epithelium for proper cartilage development.

There is substantial evidence revealing that close contact with endoderm is a prerequisite for cranial neural crest chondrogenesis to occur in chick (Bee

and Thorogood, 1980; Smith and Thorogood, 1983), frog (Seufert and Hall, 1990), axolotl (Gravenson and Armstrong, 1987), and more recently zebrafish (Crump *et al.*, 2004a; David *et al.*, 2002). Pharyngeal endoderm, but not more posterior gut-forming endoderm, is able to induce chondrogenesis in axolotl cranial neural crest (Gravenson and Armstrong, 1987), including more anterior amphibian neural crest which do not normally contribute to cranial cartilage (Seufert and Hall, 1990). Direct contact of neural crest cells to the epithelium or epithelial matrix is necessary for chondrogenesis to occur in zebrafish, suggesting that this process is not mediated by diffusible factors (Smith and Thorogood, 1983). A conserved requirement for the presence of endoderm is therefore crucial for proper chondrogenesis.

6. Large scale mutagenesis screens in zebrafish

Gene function is characteristically determined by analyzing the loss-of-function phenotype, structural and biochemical properties of protein structure, and the temporal and spatial expression patterns of gene products throughout the organism. Creation of loss-of-function mutations through genetic mutagenesis screening allows for the selection of a relatively small number of genes with unique or at least partially redundant activities. Large scale mutagenesis screens in the past have been key in elucidating pattern-forming pathways by identifying groups of genes sharing similar phenotypic traits in numerous developmental models including *C. elegans* (Hirsh and Vanderslice, 1976) and *Drosophila* (Nuesslein-Volhard and Wieschaus, 1980). This has proven to be more difficult in vertebrates because of long generation times and high cost of

maintaining and breeding large numbers of organisms such as mouse and chicken.

Recently two major chemical mutagenesis screens have been performed in zebrafish (Driever *et al.*, 1996; Haffter *et al.*, 1996). As described above, zebrafish as a model organism is ideal for large scale screening based on the ability to process a very high number of transparent embryos for phenotypic traits under a simple dissecting microscope. The creation of these loss-of-function recessive mutant strains has enabled researchers the potential to characterize thousands of genes essential for vertebrate embryo and larval development. These zebrafish mutant screens were performed using the chemical mutagen N-ethyl N-nitrosourea (ENU). ENU induces point mutations randomly within the genome (Russell *et al.*, 1979; Singer and Grunberger, 1983). Generation of ENU-induced mutations within the male zebrafish germ line is highly efficient, ranging from one induced mutant allele per 300 to 2000 mutagenized genomes (Driever *et al.*, 1996). Males incubated in ENU are crossed to wild type females of the same inbred genetic background (AB in this case) and the resulting F_1 progeny raised to adulthood (Figure 5). Males from this F_1 family theoretically heterozygote for a mutation are again crossed to a wild type AB female. The resulting F_2 generation contains ½ wild type fish and ½ fish heterozygous for the ENU-induced mutation. Crossing two fish heterozygous for the same induced mutation will result in ¼ of the F_3 progeny as mutant based on simple Mendelian genetics (Driever *et al.*, 1996; Haffter *et al.*, 1996). Mutants of the Driever study (1996) such as *m196* were classified based on four different phenotypes: (1)

widespread non-specific degeneration assumed to be associated with genes essential for general cell survival, (2) developmental delay including a syndrome of affected tissues such as brain, eye, branchial arches, pectoral fins, and internal organs, (3) degeneration of the central nervous system (CNS), and (4) developmental defects arising in specific regions, tissues, or organs. The concurrent zebrafish mutagenesis screens published in 1996 isolated over 3500 mutant strains (Driever *et al.*, 1996; Haffter *et al.*, 1996).

These large scale mutagenesis screens, however, have a few disadvantages and limitations. First, genes expressed maternally or zygotically would be difficult to isolate. Maternal-effect genes are only recoverable if fourth generation progeny are screened. Therefore mutations in maternally-derived genes only expressed within early development would not be isolated. Embryos expressing dominant lethal maternal-effect mutations would die within the F_2 progeny. The strains bearing these mutations would be impossible to establish. Heterozygotes of dominant lethal zygotic-effect mutations, expressed in the F_1 generation, would be eliminated since F_2 progeny would not survive. Hence many genes of maternal or zygotic contribution are not addressed in this screen. Secondly, because of the redundancy of many large families of genes, mutations in individual genes might have only a slight or complete lack of phenotype. The subtleties of such genes could only be elucidated through double or triple mutants. Additionally, statistical analysis of the allele distribution reveals that only a portion of mutable genes in the zebrafish genome able to create a visible phenotype have been affected in this screen (Driever *et al.*, 1996). Therefore

this screen failed to produce a set of mutations saturating the genome. However this means that certain areas were therefore mutated more frequently than others and further supports the notion of hotspots in the genome more susceptible to mutation (Driever *et al.*, 1996). Despite such limitations to the screen, the insights into developmental pathways, once these mutations are characterized and mapped within the zebrafish genome, will be significant.

Since 1996 technologies involved in large scale mutagenesis screens have evolved dramatically. Although techniques are improving to identify ENU-induced mutations (Rawls *et al.*, 2003), identification of chemically mutated genes is still slow and laborious and also uses primarily the candidate gene approach biased to known genes and pathways. New mechanisms for the creation of such mutagenesis screens allow for an enhanced look at genetic activity within zebrafish development. Among the most compelling technologies is insertional mutagenesis. A number of different methods for mutagenic insertions are currently being investigated. Transposon systems, similar to the *Drosophila* P element, have been identified and designed in zebrafish such as the *Sleeping beauty* cassette (Ivics *et al.*, 1997) and the *Tol2* element found in the medaka fish *Oryzias latipes* (Kawakami *et al.*, 2000), although their efficiency as a large scale screening system is still being refined. Of significant success has been the insertional mutagenesis system involving the infection of zebrafish embryos with a pseudotyped retrovirus (Gaiano *et al.*, 1996). These retroviruses insert their genome randomly creating a clean and stable mutagenic lesion within a host chromosome. As well, such insertions knockdown/knockout gene

expression rather than possibly create hypo- or neomorphs as in chemical mutagenesis. Identification of genes affected in these mutant lines is as simple as sequencing from this conveniently inserted molecular tag. Recently a large-scale mutagenesis screen has been reported using this technique (Amsterdam *et al.*, 1999). Although the frequency of mutations is only approximately one-ninth that of ENU-induced chemical mutations (Amsterdam *et al.*, 1999), the ease of identifying the mutagenized genetic element far outweighs this constraint. Hence these new technologies such as insertional mutagenesis overcome many of the limitations set by chemical mutagenesis screens and are providing a different approach to the identification of new genes, genetic elements and developmental pathways.

Figure 5: Schematic outline of the creation of the mutant (*m196*)/AB strain by ENU mutagenesis. Initial ENU-treated parent (P) males are bred to wild type females. F1 males heterozygous for one mutant genome are outcrossed to sibling females. F2 adult progeny are screened for heterozygotes by random in-crosses, one quarter of which will result in the pairing of two heterozygotes. 25% of the resultant progeny will be phenotypically mutant. M, mutant; WT, wild type; het, heterozygote (Adapted from Haffter *et al.*, 1996).

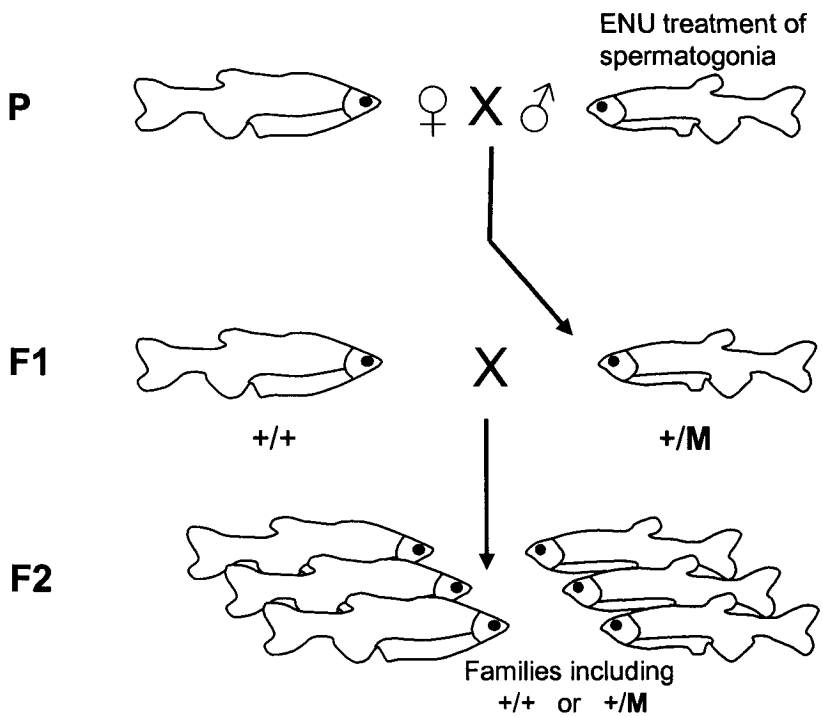
ENU treatment of
spermatogonia
P
♀ X ♂
F1
X
+/+
+/M
F2
Families including
+/+ or +/M
F3
Random crosses:
+/+ X +/+
+/+ X +/M
+/M X +/+
+/M X +/M
100% WT
50% WT
50% het
50% WT
50% het
25% WT
50% het
25% Mutant

6.1 Zebrafish as a model for human disease

These and other mutant analyses in zebrafish have shown this teleost fish to be a powerful tool in studying human disease. A number of genes responsible for these mutations have already been identified and have also been associated with related human disease (Davidson *et al.*, 1999; Zon, 1999), such as the isolation of several blood-related mutations. The erythroid synthase δ-aminolevulinate synthase, or ALAS-2, gene mutation of the *sauternes* (*sau*) strain is reminiscent of the ALAS-2 mutation in humans causing sideroblastic anemia (Brownlie *et al.*, 1998). The *yquem* (*yqe*) mutant encodes uroporphyrinogen decarboxylase (UROD), which is found to be deficient in patients with porphyria (Wang *et al.*, 1998) and *dracula* mutant has established a zebrafish disease model for erythropoietic protoporphyria (Childs *et al.*, 2000). Diseases such as these involving single tissues, i.e. blood cells, are therefore recapitulated in these zebrafish mutants.

Most notably the well-conserved role of TBX5 has been shown in the significant similarity in phenotype of the zebrafish *heartstrings* (*hst*) mutation and Holt-Oram syndrome in humans. Both display reduced upper limbs/pectoral fins and cardiac defects, characterized in zebrafish by slight brachycardia and a later absence of heart looping. The restriction of defects to the limb/fin and heart in both human and zebrafish demonstrates the remarkable retention of deficiency syndromes associated with a loss of TBX5 activity (Garrity *et al.*, 2002). Additionally, expression of the *van gogh* (*vgo*) mutant alleles, encoding truncated tbx1 proteins, strikingly resembles that of the human DiGeorge deletion

syndrome (DGS) which affects neural crest-derived craniofacial development (Piotrowski *et al.*, 2003). Piotrowski and colleagues (2003) established regulatory interactions between *vgo/tbx1*, *edn1*, and *hand2* that are implicated in pharyngeal arch development as well as in DGS. Therefore, the *hst* and *vgo* mutants play a major role in understanding the genetics of more complicated human disease and recognize the significance of evolutionarily conserved genetic interactions.

7. Mapping technique

These induced mutations within the zebrafish genome are isolated in part by meiotic and radiation hybrid mapping techniques, positional cloning, and candidate gene searches. In the past decade an integrated physical and genetic map of the zebrafish genome has been consistently updated. Mapping of this genome involves a number of different high-resolution panels, including meiotic and radiation hybrid maps. Postlethwait and colleagues (1994) constructed the first zebrafish genetic linkage map based on random amplified polymorphic DNAs (RAPDs). Soon after, a linkage map anchored with simple-sequence length polymorphisms (SSLPs) was developed by Knapik *et al* (1998). SSLP genetic markers utilize di-, tri- and tetra-nucleotide repeats that are found to be polymorphic between certain inbred zebrafish wild type strains, for example between the AB and HK (Hong Kong) or TL (Top Long-fin) commonly used zebrafish strains. Meiotic distance of an induced mutation from a closely-associated marker is calculated using the number of recombination events of the marker for every meiotic event (Figure 6). The SSLP-anchored genetic map is

capable of providing a maximum resolution of 0.1 centiMorgans (cM) (Knapik *et al.*, 1998). The zebrafish genome is made up of 25 pairs of chromosomes, or linkage groups, spanning a genetic length of 2635 cM and a physical size of 1.7 x 10^9 base pairs (bp) (Postlethwait *et al.*, 1994). With 1 cM equaling approximately 625 kilobase pairs (kb), a physical resolution of 62.5 kb is possible. Therefore simple rates of genomic recombination can be used to map mutant alleles to a very high resolution.

Another panel used to map genes is the radiation hybrid (RH) panel. RH mapping is a somatic cell genetic technique first initiated to create an integrative map of human and mouse chromosomes (Cox *et al.*, 1990). These maps use statistical analysis to determine distances between DNA markers and their order on chromosomes based on x-ray breakage. In zebrafish the LN54 (Hukriede *et al.*, 2001; Hukriede *et al.*, 1999) and T51 (Geisler *et al.*, 1999) RH panels are used to map genes, cDNAs and ESTs within the genome. Radiation hybrid maps are measured in centiRays (cR). In the T51 panel one cR is equivalent to 61 kb, therefore a maximum resolution of 350 kb is obtainable (Geisler *et al.*, 1999), whereas mapping resolution for the LN54 panel is 500 kb, with one cR equivalent to 118 kb (Hukriede *et al.*, 1999). Although it is of lower resolution than meiotic mapping, RH panels are able to determine the general chromosomal location of an allele of interest.

Positional cloning can be used to create a contig of large overlapping genomic fragments spanning the region of interest. Large insert libraries, using PACs (P1-based artificial chromosomes) and BACs (bacterial artificial

chromosomes), hold up to 100 and 82 kb inserts of genomic DNA per clone respectively (Amemiya *et al.*, 1996; Amemiya *et al.*, 1999a). A chromosomal walk is initiated by isolating clones containing a close marker. Rescreening libraries with sequences derived from the initial clone ends will locate overlapping PAC or BAC clones. This makes positional cloning of these mutations possible by screening with close markers and other sequence tags.

Currently, the Sanger Institute is well on its way to completing the sequence. Numerous premature sequence assemblies have been published online and are annotated with relevant predicted gene information. By placing relevant SSLP and RAPD markers within the sequence, the genomic sequence can be used to locate potential candidate genes affected by the mutation. Candidates are then mapped to the mutation using single strand polymorphism (SSCP) analysis (see Methods and Materials) and sequenced to search for mutant-specific base pair changes. Unfortunately, because the current genome sequence configurations are still somewhat error-prone and newly updated releases rather unpredictable, relying on the genomic sequence in its current state is often more of a hindrance than a help. Despite these current limitations, the completed genome sequence will be an invaluable tool for candidate identification.

Figure 6: Schematic outline of the mapping technique of bulk segregant analysis. Adult fish heterozygous for the mutation (in the AB background) and the TL polymorphic wild type strain are bred to create phenotypically wild type and mutant diploid embryos. Genomic DNA is then isolated from individual embryos. PCR amplification of SSLP or RAPD marker "A", which is closely linked to the mutant allele will amplify the 200 bp TL allele in homozygous wild type embryos and the 300 bp AB (m196) allele in homozygous mutant embryos. Phenotypically wild type but genotypically heterozygous embryos will amplify both the AB and TL allele.

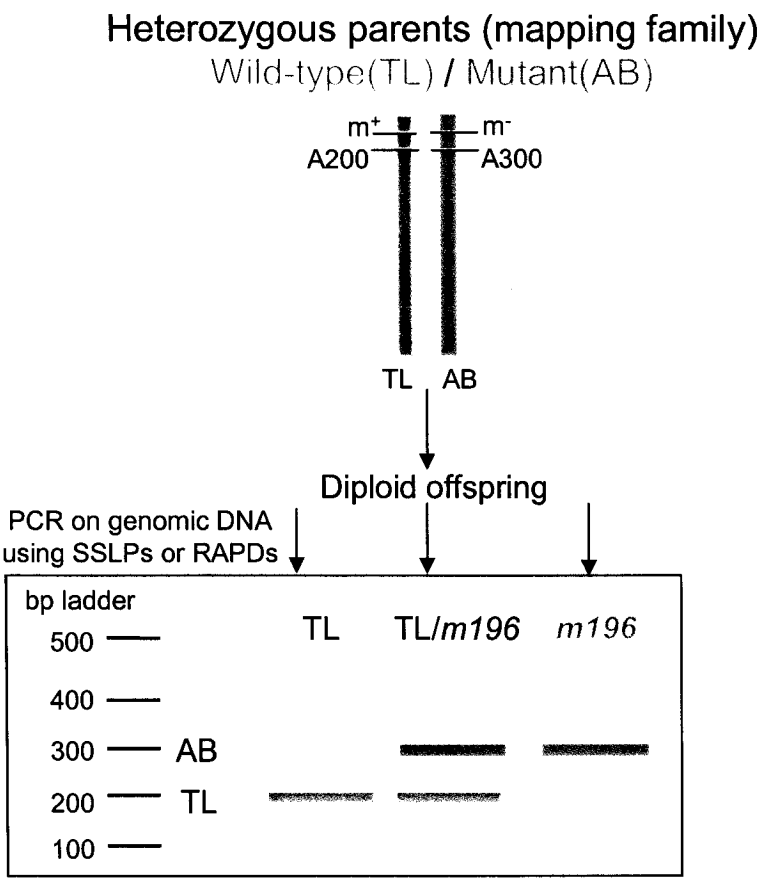
Heterozygous parents (mapping family)
Wild-type(TL) / Mutant(AB)
m+
m-
A200
A300
TL
AB
Diploid offspring
PCR on genomic DNA
using SSLPs or RAPDs
bp ladder
500
400
300
200
100
AB
TL
TL
TL/m196
m196

8. The *m196* mutant

The Akimenko lab is primarily interested in studying fin development and regeneration in the zebrafish. The *m196* mutation, a result of the large ENU-mutagenesis screen from Driever *et al.* (1996), is characterized by a disruption in median and pectoral fin fold development as well as a loss of craniofacial structures. The characterization and cloning of this mutation is a collaborative effort with the Knapik lab whose research focuses mainly on zebrafish craniofacial development. The *m196* mutant phenotype is first visible by dissecting microscope in embryos 24 hpf (Figure 7) as a shortened tail and disruption of median fin fold extension. As the median fin fold begins to extend in wild type embryos, the *m196* mutants display a significant although variable defect in fin fold extension (Figure 7,8). A disruption in pectoral fin bud outgrowth and fin fold extension is also observed and most easily detected at 2-3 dpf (Figure 9). By 6 dpf the median fin fold has begun to regenerate though no mutant larvae ever regains a completely wild type structure. A pigment phenotype is also observed in most mutants as an accumulation of black melanocytes around the tip of the tail (Figure 8, 10, 11). Some of these pigment cells are also found ectopically within the posterior-most fin fold. At 48 hpf the beginnings of the facial phenotype can be seen, characterized by the ventral flattening of the head along the large yolk. As the head begins to straighten out and lift from the yolk, a distinct cavitation is observed in ventral underside of the head and more ventral structures in the head (Figure 12) appear to be absent when compared with wild type. The *m196* mutants die between 30 hpf and

approximately 2 weeks post fertilization from unknown causes. The nature of this fin and craniofacial phenotype may therefore indicate a defect in neural crest cell formation, differentiation, migration, and/or neural crest interaction with other cells.

9. Objectives

Therefore the aim of this project is to identify a genetic factor essential for fin and craniofacial development through analysis of the *m196* mutant zebrafish strain. The objectives of this study in order to achieve this goal were as follows:

1. The phenotypic characterization of the *m196* mutation involving the development of the pectoral fins, median fins, and cranium.

2. The mapping of the *m196* mutation to a specific chromosomal location.

3. An effort to identify and clone candidate genes or genetic elements affected by the *m196* mutation.

Figure 7: The early *m196* mutant phenotype at 24 hpf. *m196* embryos (B, C) compared with wild type (A) at 24 hpf. Note the partial growth of the ventral fin fold in some mutants (asterisk).

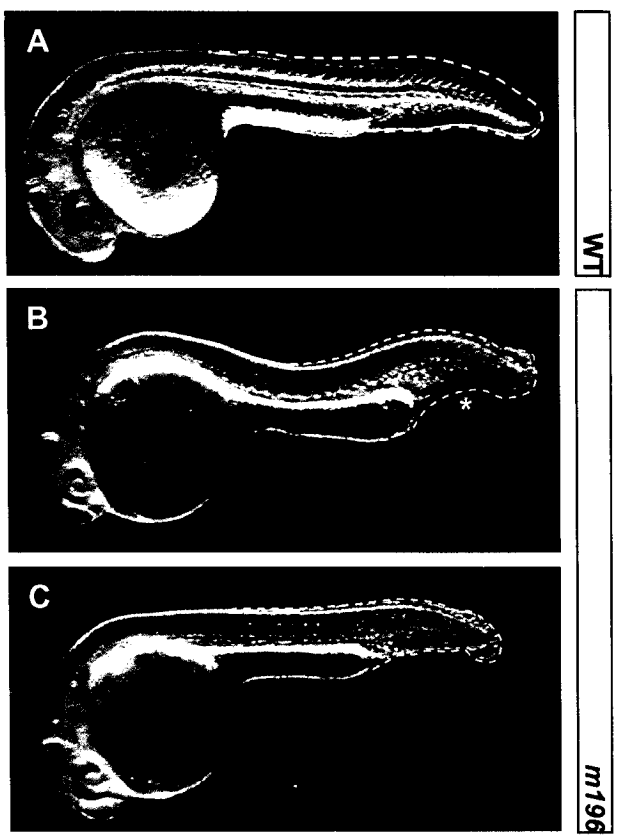
A
B
C
*
WT
m196

Figure 8: The *m196* mutant phenotype at 3 dpf. Wild type (A) and 3 individual *m196* mutant (B-D) embryos at 3 dpf. Lateral view, anterior left. White dotted line in A marks the limit of the wild type median fin fold. A portion of the ventral fin fold is present at this stage in some mutants (asterisk). Arrowhead marks edema in the pericardial region found in some mutants.

A
B
C
D
*
WT
m196

Figure 9: The *m196* mutant phenotype at 6 dpf in the pectoral fin. Pectoral fin development in the 6 dpf mutants (C-F) compared with wild type (A-B). (A, C, E) ventral view, anterior to the left. (B, D, E) Dorsal side of the pectoral fin from each respective larva, distal to the top.

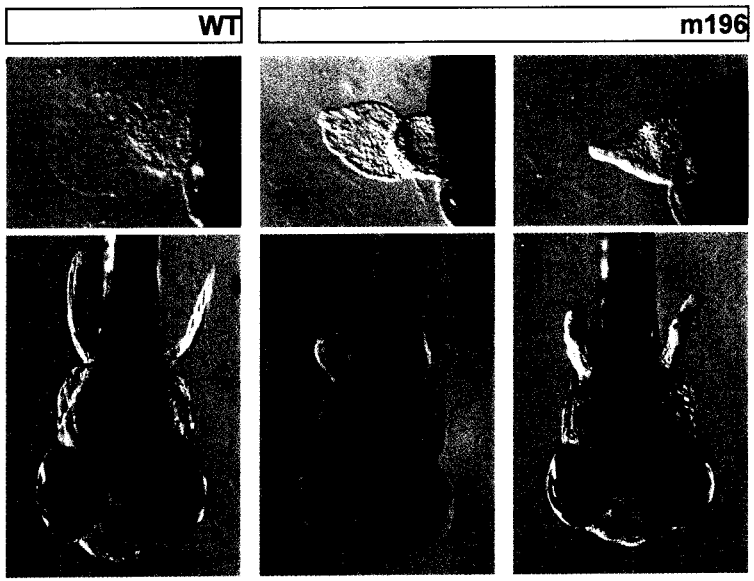
WT
m196

Figure 10: The *m196* mutant phenotype in the 6 dpf larva. *m196* mutants (B-E) compared to a wild type larva (A) at 6 dpf. Lateral view, anterior to the left. Some larvae have continued edema in the pericardial region at this stage (arrowhead). Asterisk marks ventral fin folds that partially develop.

WT
m196
C
D
E

Figure 11: The median fin fold in *m196* larvae surviving to 12 dpf. Lateral view of the posterior body of wild type (A) and *m196* mutant (B-E) larvae at 12 dpf. Arrowhead marks the ventral fin fold. The wild type pigment-free region in the ventral tail is completely absent in most mutants at this stage (asterisk).

A
B
C
D
E
WT
m196

Figure 12: The *m196* mutant displays a cavitation in the ventral cranium resulting in two lateral protrusions from the jaw. Wild type (A) and mutant (B-C) larvae at 6 dpf. Dorsal to the top. Black arrowhead indicates ventral cavitation. Note the mouth is not open in mutants as it is in wild type larvae at this stage (white dotted line).

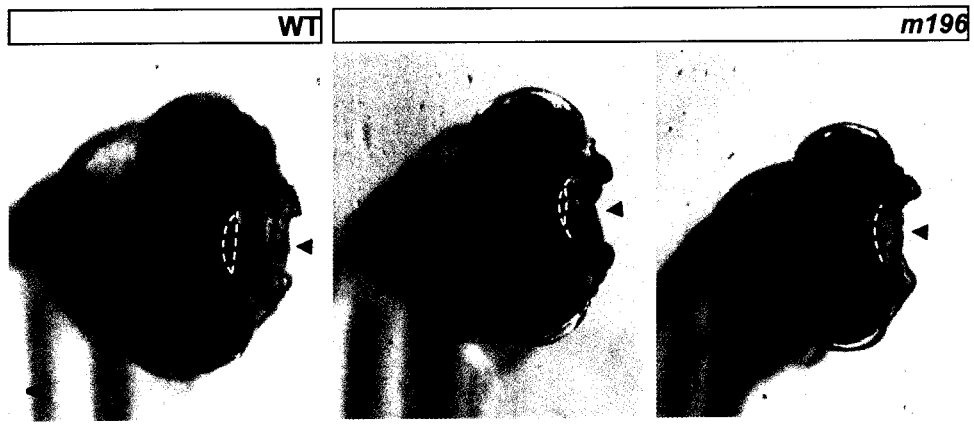
WT
m196

II. Materials and Methods

1. Fish maintenance and breeding

Fish were raised and kept under standard laboratory conditions at 28.5°C (Westerfield, 1995). In order to obtain embryos, one male and one female fish was placed in a breeding tank (Aquatic Habitats) over night. Breeding tanks consist of two stacked plastic containers where the base of the top container includes holes large enough to allow fertilized eggs to fall in the space between. Eggs were collected shortly after spawning the next morning induced by the onset of the photoperiod. Embryos were staged, anaesthetized in tricaine (Westerfield, 1995), and fixed in 4% paraformaldehyde (PFA) in phosphate-buffered saline (PBS; 137 mM NaCl, 2.7 mM KCl, 10 mM Na_2HPO_4, 2 mM KH_2PO_4) at specific hours or days after fertilization (hpf or dpf) as described by Kimmel *et al.* (1995). In order to better visualize internal structures, whole mount in situ hybridization experiments embryos were incubated with 200 mM 1-phenyl-2-thiourea (PTU, Sigma) to inhibit the formation of pigment. The *m196* mutant strain is derived from the N-ethyl-N-nitrosourea (ENU) mutagenesis screen performed by Driever *et al.* (1996). The *m196* allele was maintained in an AB wild type strain background for phenotype analysis and crossed to Hong Kong (HK) or Top-Long fin (TL) background (Johnson and Zon, 1999) for genetic mapping experiments (Knapik *et al.*, 1998).

2. *In vitro* transcription of RNA probes

Whole mount in situ hybridization (WISH) was carried out using digoxigenin-labeled antisense riboprobes synthesized *in vitro* from a linearized plasmid DNA template. The probe-synthesizing transcription reaction, containing 1 μg linearized DNA, 2 μl NTP labeling mix (10mM ATP, 10mM CTP, 10mM GTP, 6.5mM UTP, 3.5mM DIG-11-UTP (Roche), 10X transcription buffer, 20 Units RNase Inhibitor (Promega), 20 Units RNA polymerase (T7, T3, SP6; Roche), was incubated at 37°C for 2 hours. The synthesized probe was then precipitated with lithium chloride (500mM) and 100% ethanol and pelletted for 30 minutes at 4°C in a microcentrifuge (Baxter). After washing the pellet with 70% ethanol and respinning for 5-10 minutes, the probe was dried and resuspended in DEPC-treated water for a final concentration of approximately 100ng/ml.

The following probes were used: *crestin* (Rubenstein *et al.*, 2000), *dlx2* (Akimenko *et al.*, 1994), *sox9b* (Chiang *et al.*, 2001), *foxD3* (Odenthal and Nuesslein-Volhard, 1998), *fgf8* (Fuerthauer *et al.*, 1997), *msxC* (Akimenko *et al.*, 1995b), *col2a1* (Yan *et al.*, 1995), *2-H06* (Padhi *et al.*, 2004). For more details on probes, see Appendix 1.

3. Whole mount *in situ* hybridization

Embryos were fixed overnight in PFA at 4°C, then washed in PBS/0.1% Tween-20 (PBT), dehydrated stepwise into methanol and stored at -20°C. After rehydration embryos older than 10 hpf were digested with proteinase K (10 μg/ml), refixed in 4% PFA, washed with PBT, incubated at 70°C for greater than

1 hour in hybridization mix (65% formamide, 5x SSC (0.75 M NaCl, 75 mM sodium acetate) , 50 μg/ml heparin, 20 μg/ml yeast tRNA (Sigma), 0.1% Tween-20, 9.2 mM citric acid pH 6), and hybridized overnight with 500ng RNA probe. Embryos were transferred into 0.05x SSC at 70°C by graded washes with hybridization mix and then into PBT by graded washes with SSC at room temperature. Samples were blocked 1 hour with PBT/2% calf serum/2 mg/ml bovine serum albumin (BSA) and incubated over night at 4°C in preadsorbed anti-digoxigenin FAB fragment antibody (1:2000 dilution, Roche). After extensive washes at room temperature in PBT, embryos were rinsed 3 times 15 minutes in NTMT staining buffer (100 mM Tris-HCl pH 9.5, 50 mM MgCl2, 100 mM NaCl, 0.1% Tween-20). The alkaline phosphatase staining reaction was revealed using NTMT staining buffer containing 225 μg/ml Nitro Blue Tetrazolium (NBT, Sigma) and 175 μg/ml 5-bromo-4-chloro-3-indolyl phosphate (BCIP, Sigma). Embryos were refixed in 4% PFA and stored in 80% glycerol/20% PBT or 4% PFA at 4°C.

4. Whole mount immunohistochemistry

Whole mount immunostaining experiments were carried out as per Nuesslein-Volhard and Dahm (2002). Fixed and dehydrated embryos were rehydrated into PBT with graded MeOH:PBS dilutions. Embryos were then blocked 1 hour at room temperature in blocking solution (10% goat serum, 40 mg/ml BSA in PBT). Embryos were incubated over night at 4°C in a 1:500 dilution of the primary antibody zn-5 (Eugene, Oregon) in blocking solution. The next day, specimens were washed four times 30 minutes in blocking solution and incubated overnight

at 4°C in 1 μg/ml biotinylated anti-mouse IgG secondary antibody (Vector Laboratories). Then, after four 30 minute washes in blocking solution, the avidin/biotinylated horseradish peroxidase (AB) complex substrate (from ABC Vecta Stain kit, Vector Laboratories) was added to embryos and incubated 45 minutes at room temperature. Embryos were subsequently washed again in blocking solution and finally PBT. Bound antibody was visualized using 1 mg/ml 3,3'-diaminobenzidine (DAB) in PBT plus 2μl 0.3% H_2O_2 for approximately 15-30 minutes. After rinsing in PBT, embryos were stored in 4% PFA or 80% glycerol/20%PBS.

5. Whole mount cartilage staining

Alcian blue, a tetracationic dye, reacts strongly with glycosaminoglycans and acidic glycoproteins found in cartilage ECM (Junquiera *et al.*, 1998). For the Alcian Blue staining, embryos of 3-7 dpf were fixed overnight in 4% PFA at 4°C and washed in PBS. Embryos were bleached in 10% H_2O_2 supplemented with 0.1M KOH for 1 hour. Embryos were then stained in 0.1% alcian blue diluted in 70% acidic ethanol (70% ethanol, 5% concentrated HCl) and destained for at least 5 hours in acidic ethanol. After dehydration into ethanol, embryos were stored in 80% glycerol/20%PBS.

6. Whole mount acridine orange cell death assay

Apoptosis in *m196* mutants was assessed by staining live embryos with the vital dye Acridine Orange. This dye is able to permeate acid lysosomal vesicles and become fluorescent. After growing to the desired time point, live embryos were

incubated for 15-20 minutes in a 5 μg/ml solution of Acridine Orange (Sigma) diluted in system water from a 300x filtered stock solution. Embryos were then washed three or more times in system water and observed under a fluorescent dissecting microscope (Leica).

7. Cryostat sectioning

Embryos previously stained with alcian blue and stored in 80% glycerol in PBS were incubated in a series of 5 minute washes of glycerol/PBS dilutions (75% glycerol:25% PBS, 50% glycerol:50% PBS, 25% glycerol:75% PBS) and finally two 5 minute washes in 100% PBT. Embryos were embedded in a liquefied 5% sucrose/1.5% agarose solution containing PBS. The solidified block with the enclosed embryo was cut to size with a scalpel and placed in a 30% sucrose PBS solution overnight at 4°C. Blocks were to be sectioned were mounted on a cryostat chuck, covered in cryomatrix (VWR) and frozen in 2-methyl butane (-80°C) for sectioning on a cryostat (2800 Frigocut, Leica). 12 µm sections were collected on glass slides, dried overnight at 42°C, and mounted using Aquatex (EM Science).

8. Genetic mapping

8.1 Bulk segregant analysis and fine mapping

m196 was mapped in a F_2 intercross using bulk segregant analysis (Michelmore *et al.*, 1991).The F_1 generation was obtained by crossing *m196* heterozygous fish in an AB background and wild type TL fish. Using sibling single pair crosses we

identified mutation-carrying F_2 heterozygotes. F_2 embryos were scored at 30-48 hpf for the *m196* mutation. In order to isolate genomic DNA, the F_2 *m196* embryos were then frozen in 20 µl fish system water and boiled for 10 minutes with 50 µl lysis buffer (10 mM Tris pH 8.0, 50 mM KCl, 0.3% Tween-20) and chilled on ice. 5 µl of 10 mg/ml proteinase K was added and samples incubated overnight at 55°C. After boiling for 10 minutes, DNA from a single embryo was diluted up to 200 µl with 0.1x TE (1mM Tris pH 8.0, 0.1 mM EDTA). Two pools of 10 *m196* and 10 wild type sibling embryos were created and screened with polymorphic SSLP markers evenly spaced throughout the zebrafish genome (approximately every 20 centiMorgans (Knapik *et al.*, 1998)). PCR products were resolved by electrophoresis on 2-3% agarose gels. When a linked marker was found, individual embryos were tested with polymorphic markers within the linkage group in order to establish a critical interval.

Higher resolution was needed to detect small size differences between the TL and AB polymorphic fragments from flanking marker z30467. We used 5-10 µCi of [α-^{32}P]-dATP (Amersham) in a radiolabeling PCR analysis for this marker and resolved the products on an 8% denaturing polyacrylamide gel for 1.5-2 hours at 4000 Volts/200milliAmps on a vertical gel electrophoresis system (Interscience Biotechnologies, Inc.). Gels were then transferred to Whatman paper, dried on a heated vacuum manifold (Savant), and exposed on a storage phosphor screen (Molecular Dynamics). Screens were scanned on a Typhoon 8600 Variable Mode Imager.

8.2 Single strand conformation polymorphism analysis

In order to map candidate genes, we use SSCP (single strand conformation polymorphism) analysis (Foernzler *et al.*, 1998). This involves the PCR amplification of regions within the 5' and 3' untranslated region (UTR) of candidate genes that contain single base pair polymorphisms between the AB and TL background mapping strains. Amplified fragments are then denatured and allowed to reanneal as single stranded DNA. These DNA fragments, run on a non-denaturing polyacrylamide gel, separate within the gel matrix based on secondary structure. SSCP analysis of various candidate genes was performed by amplifying a 250-300 bp region of the candidate 5' or 3' untranslated regions (UTR) by PCR including 5-10 μCi of [α-^{32}P]-dATP (Amersham). Denatured, radiolabeled-PCR products were resolved in 8% polyacrylamide non-denaturing gels electrophoresed at 400 Volts/15 milliAmps for 20-24 hours on a vertical gel electrophoresis system (Interscience Biotechnologies, Inc.). Gels were then dried and exposed as described above.

8.3 Positional cloning

8.3.1 Random priming probe synthesis

A zebrafish P1 artificial chromosome (PAC) library (Amemiya and Zon, 1999b) obtained from RZPD was screened using random primed probes for flanking markers and candidate genes. Probes were synthesized by adding pdn6 hexanucleotide (Amersham) to 50-100 ng of gel-purified PCR fragment and boiling the mixture for 3 minutes to denture. After cooling on ice, a synthesis

reaction was prepared by adding 10X React 2 buffer (Roche), 10X dNTP mix (Invitrogen), 50 µCi [α-^{32}P]-dATP (Amersham), and large fragment DNA polymerase (Roche) to the template. The reaction was then incubated for 1 hour at 37°C and purified in a spin column using G-25 Sephadex for 2 minutes at 1400 RPM after mixing with 100 µl Dextran blue.

8.3.2 Screening of PAC genomic clone library

PAC genomic library filters were prehybridized for at least 30 minutes at 65°C in Church Medium (7% Sodium Lauryl Sulphate (SDS), 0.5 M Sodium Phosphate pH 7.2, 1 mM EDTA, 100 µg/ml sheared and boiled salmon sperm DNA). Filters were then hybridized over night at 65°C with the random priming probe in Church Medium. The next day, filters were then rinsed once in fresh Church Medium for 30 minutes at 65°C and washed twice in a stringent wash (40 mM Sodium Phosphate pH 7.2, 0.1% SDS). Library filters were exposed and scanned on a storage phosphor screen and scanned as described above. Resulting positive PAC clones were used to initiate a chromosomal walk. PAC ends were sequenced and subsequently synthesized as probes for rescreening the library.

9. cDNA cloning

9.1 mRNA isolation

Whole RNA was extracted from 24 or 36 hpf embryos. Approximately 50 embryos were dechorionated and fixed in 1 ml Trizol overnight. Samples were homogenized with an insulin syringe and centrifuged at 12,000 x g for 10 minutes

at 4°C. The supernatant was chloroform extracted and precipitated with isopropanol. The dried pellet was resuspended in DEPC-treated deionized water.

Messenger RNA (mRNA) was isolated by adding 2 volumes of dilution buffer (Promega) to the whole RNA solution and 1 µl oligo (dT)n (Promega). The mixture was incubated for 5 minutes at 70°C and left to cool to room temperature for 30 minutes. The cooled RNA solution was incubated for 5 minutes in a 200 µl magnetic bead solution (Promega) washed with 0.5X SSC. A magnetic stand was used to capture and wash beads three times with 200 µl 0.5X SSC. mRNA was eluted with 300 µl DEPC-treated deionized water and precipitated with 3M sodium acetate and isopropanol. The dried whole mRNA pellet was used for further first strand 3' RACE (rapid amplification of cDNA ends) synthesis.

9.2 TA-cloning and sequencing

First strand 3' RACE synthesis from mRNA was carried out by adding 4 µl water and 1 µl of 10 µM 3'CDS primer (5'-AAGCAGTGGTATCAACGCAGAGTAC (T)30 VN-3', where V is any base but T) to the whole mRNA pellet mentioned above. This was then incubated for 2 minutes at 70°C and 2 minutes on ice. Next the reverse transcription reaction was initiated by adding 2 µl 5X reverse transcription buffer (Gibco), 1 µl 20 mM DTT, 1 µl 10 mM dNTP mix (Invitrogen), 1 µl RNase inhibitor (Promega), and 1 µl Reverse Transcriptase (RNA-dependent DNA polymerase, Gibco). The reaction was incubated at 42°C for 1.5

hours. 250 µl TE was then added to the reaction which was subsequently incubated for 7 minutes at 72°C and stored at -20 °C. Amplification of cDNAs was accomplished through PCR on these first strand preps. The reaction mix included 10-100 ng template, 5 µl 10X PCR buffer (100 mM Tris-HCl ph 8.3, 500 mM KCl, 15 mM $MgCl_2$), 6.5 µl 2mM dNTP mix (Invitrogen), and 1 µl *Taq* DNA polymerase. Reactions were carried out on a PTC-225 Peltier Thermal Cycler (MJ Research) for 30 cycles with the following cycling parameters: denaturing at 96°C for 30 seconds, primer annealing at 50-65°C for 30 seconds, elongation at 72°C for 1 minute per kb of desired product size. RT-PCR products were immediately ligated into the pDrive TA-cloning vector (Qiagen kit). Resulting clones were screened for inserts of the correct size by restriction digest with *EcoR*1 (Fermentas). Clean plasmid preparations of positive clones were obtained using a Promega Wizard plus SV mini prep kit. Clones were then sent for sequencing at the Ottawa Health Research Institute Sequencing Service on an Applied Biosystems 3730 DNA analyzer. Sequence analysis and multi-transcript alignments were done through SeqWeb (http://www.uottawa.bioinformatics.org). Motif prediction for phf17 was accomplished through Eukaryotic Linear Motif (ELM) resource (http://elm.eu.org). For all identification numbers as well as mapping and cloning primer sequences see Appendix 2.

III. Results

1. Phenotypic characterization

1.1 Initial m196 phenotype

The *m196* fin and craniofacial mutant is a result of the above mentioned ENU mutagenesis screen performed by Driever and colleagues (1996). Embryos homozygous for the *m196* allele show a phenotype recognizable by dissecting microscope beginning at approximately 24 hpf. This is characterized at this stage by a general absence or reduction in median fin fold extension along the dorsal and ventral midline of the posterior embryo (Figure 7). At this stage the craniofacial region in mutants is indistinguishable from wild type. A significant number of *m196* mutants have edema in the pericardial region to varying extents beginning around 24 hpf. Extreme edema in some mutants is often associated with slight tachycardia and low blood cell counts or, rarely, a complete loss of blood cells (data not shown). However a majority of these embryos regain normal cardiac behavior by 3-6 dpf, and this edema is not associated with an earlier mortality.

At 2 dpf the disruption in the cranial region of *m196* embryos is first observable. There is a more ventral curvature of the head which is flattened along the underlying yolk. Also at this stage when the pectoral fin fold begins to extend in wild type embryos, fin fold extension is often reduced in mutants. The median fin fold also continues to be diminished or absent. Melanocyte pigmentation in the posterior part of the embryo is readily observed at this time.

In wild type embryos these cells form a tidy medial line around the tip of the chordal neural hinge. In *m196* mutants these black pigment cells accumulate in the far caudal region of the tail in a disorganized manner.

At 6 dpf mutants display a distinct cavitation in the ventral jaw region, resulting in two points jutting from the very anterior underside of the head (Figure 12). The median fin fold has also begun to partially develop in a number of mutants. A slight extension of caudal epithelium can be observed in most mutant embryos (Figure 10). Melanocytes which migrate medially along the dorsal and ventral sides of the embryo continue to gather around the end of the tail tip, a number of which are ectopically located in the posterior-most fin fold that has formed. These pigment cells are normally absent in a small region on the ventral side of the tail. A significant number of *m196* embryos consistently show a loss of this pigment-free zone as melanocytes migrate into this area (Figure 13). Additionally the ventral fin fold, which initially fails to develop, is rescued to varying extent in a significant number of mutants.

Around 8-12 dpf the ventral region of the head continues to display a distinct cavitation. The amount of median fin fold extension ranges in older mutants and is also reflective of the extent of pectoral fin fold disruption (Figure 13). A small subset of mutants show a complete lack of ventral fin folds although most regain a partial growth or are only slightly wavy in shape (Figure 11). Interestingly, although the extent of the pectoral fin fold defects appears to correlate with that of the median fin fold, this does not seem to be the case for the ventral versus median fin fold defects. As well actinotrichia which are

important for initial fin fold stability are present in all mutants with significant epithelial extension at this stage (Figure 14). These actinotrichia however do not extend straight out from the larval body as in wild type but appear to be curved caudally along the dorsal and ventral midline. Additionally in some larvae at 8 and 12 dpf, the ends of some actinotrichia have no surrounding epithelial cells and can be seen extending beyond the distal-most fin fold (Figure 13, 14). Nevertheless *m196* mutants are unable to develop to adulthood, dying between 36 hpf and 2 weeks post fertilization from unknown causes.

Figure 13: Variable defects correlate between the pectoral and median fin folds of the same *m196* larva. The posterior tail tip (A, D, G, J, M) and associated pectoral fin pairs (B, C, E, F, H, I, K, L, N, O) of wild type (A-C) and 4 *m196* mutant (D-O) larvae at 8 dpf. Dotted line in C outlines the margin of the fin bud. Asterisks delineate ventral region usually free of pigment in wild type larvae. Arrowheads show actinotrichia in mutant pectoral and median fins which lack surrounding epithelial cells in the distal-most regions. Arrow marks an example of an ectopic pigment cell in the median fin fold.

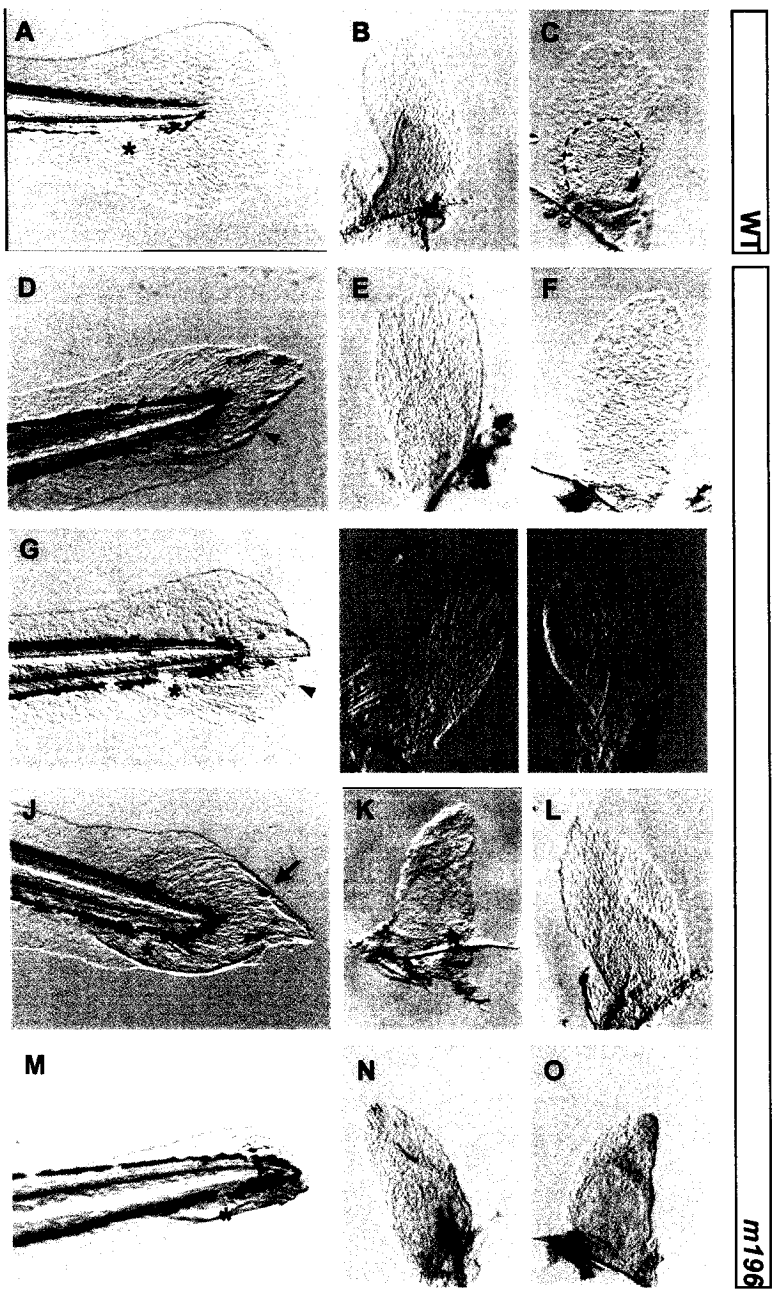
A
B
C
D
E
F
G
J
K
L
M
N
O
WT
m196

Figure 14: Actinotrichia in the posterior tail tip are present but bent caudally in the *m196* mutants. Posterior tail region of 7 different live *m196* mutants (B-F) compared to wild type (A) at 8 dpf. Black lines trace actinotrichia observed within the fin fold. Anterior to the left, dorsal to the top. Asterisk marks the region of the ventral tail free from melanocytes in wild type larvae.

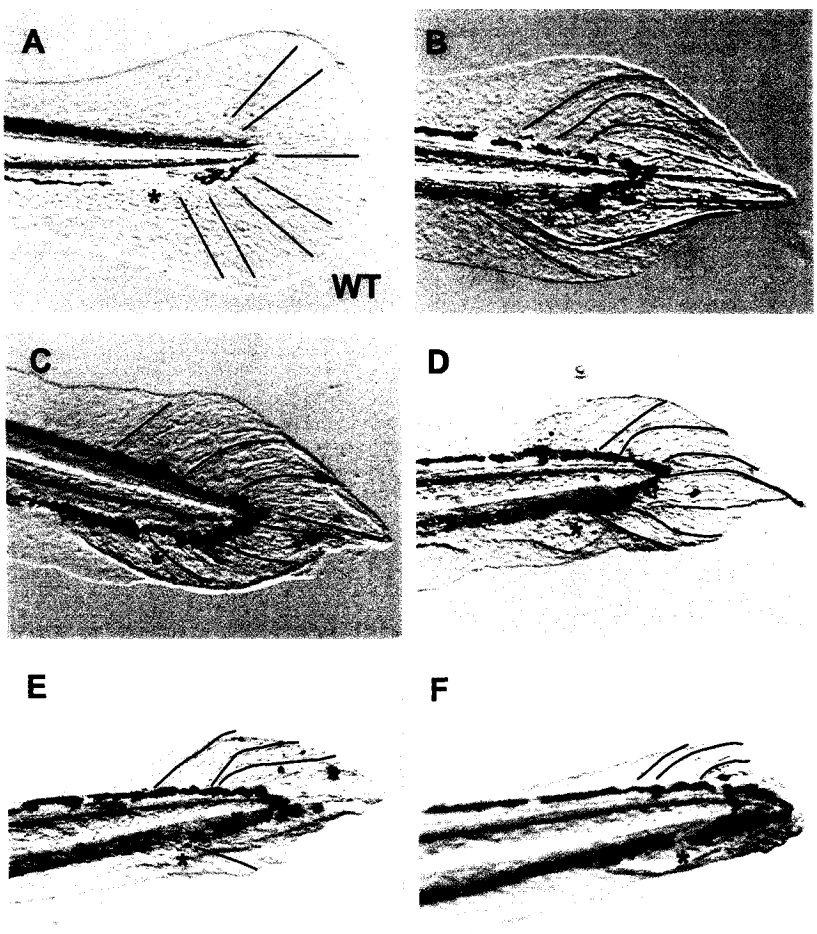
A
WT
B
C
D
E
F

1.2 Basic morphology of the craniofacial cartilage precursors

Observation of the cranial regions of *m196* mutant embryos under dissecting microscope reveals an obvious developmental alteration in the ventral head, particularly in larvae 3 dpf and later when the head is curved slightly more ventral toward the yolk than in wild type. In order to determine whether this is a result of a defect in the head skeleton, we assessed the formation of cranial cartilages using alcian blue which binds to glycoproteins within the matrix surrounding differentiated chondrocytes. Dorsal cartilages, which will eventually form the ethmoid plate, trabeculae cranii, anterior basicranial commissure, parachordal, and auditory capsule, show a normal morphology and alcian blue staining beginning at 3 dpf through 12 dpf (data not shown). Therefore initial chondrogenesis in the dorsal cartilages not associated with the segmented branchial arches is unaffected.

However, more ventral cartilage, which develop from the 7 branchial arches (see Introduction), appear to be disrupted in a number of ways. As mentioned above, a cavitation in the underside of the larval head is seen most distinctly at approximately 6 dpf. Observing alcian blue staining of larval heads at 3 through 12 days reveals a displacement of the hyoid and gill arches dorsally within the head closer to the dorsal cartilages above (Figure 15). The characteristic lateral points seen on the underside of the *m196* larval head appears to be the result of a sharp angle created by the Meckel's and palatoquadrate cartilages of the mandibular arch. The 1st arch Meckel's cartilage

is distinctly angled towards the anterior dorsal cartilage, and the remaining branchial arches are displaced dorsally within the larval head in *m196* mutants which exposes the sharp angle of the anterior mandibular structures.

1.3 Cartilage differentiation in the gill arches

Along with the general displacement of these ventral branchial arch cartilages, a variable disruption in alcian blue staining of cartilage matrix in these structures is seen between 3 and 12 dpf. Generally the cranial region remains significantly smaller in mutants compared with wild type from 3-12 dpf. *m196* mutants display an initial delay in cartilage differentiation in the 5 posterior gill arches. Although the general morphology of the precartilage condensations is visible, the alcian blue does not appear to stain these structures at 3 dpf in *m196* mutants (Figure 16). Later at 6 dpf alcian blue is able to stain these gill arches suggesting that differentiation has occurred properly although delayed. These cartilages in *m196* mutants appear consistently more crowded along the anterior-posterior axis within the cranium than their wild type counterparts (Figure 16). Analysis at 12 dpf, alcian blue staining in the gill arch cartilage in most mutants is normal though still crowded. However, a subset of mutants display a lack of alcian staining in specific gill arches, most often arches 3 and 4 (Figure 17). Thus after an initial delay in chondrogenesis, most *m196* mutant larvae retain normal alcian staining within the cartilages, although some gill arches remain undifferentiated.

This early delay in differentiation may be caused by a disruption in the chondrogenesis pathway. In order to determine whether upstream components of this pathway were properly initiated in the *m196* cartilages, we looked at

expression of *collagen2a1* (*col2a1*) associated with cartilage differentiation by *in situ* hybridization (ISH) analysis. As mentioned above *col2a1* is expressed in precartilage condensations and differentiating cartilage within the zebrafish cranium and is a necessary component of the cartilage differentiation pathway (Lefebvre *et al.*, 1997; Yan *et al.*, 1995). At 2 and 3 dpf larval ISH analysis reveals *col2a1* to be expressed in regions of all dorsal and ventral cartilage structures in *m196* mutants (Figure 18) suggesting that this step in the chondrogenesis pathway is properly initiated. Interestingly, distinct morphological differences are observed in *m196* mutants at this stage based on the *col2a1* staining (Figure 18). *Col2a1* expression shows that the angle of the gill arches in *m196* mutants is again located more dorsally within the cranium. Therefore although these expression results provide little insight into the delay in chondrogenesis, the displaced nature of the branchial arch precartilage condensations mirrors previous alcian blue results documenting hyoid and gill arch cartilage located in a similar position.

Figure 15: The gill arch and hyoid cartilages are displaced and early gill arch chondrogenesis is delayed in the *m196* mutant. Alcian blue staining of the cartilage matrix in wild type (A, B) and *m196* (C, D) larvae at 3 dpf. (A, C) Lateral view, anterior to the left. (B, D) ventral view, anterior to the top. Eyes are removed for better visualization of the staining. D, dorsal cartilage; ga, gill arches; hy, hyoid; m, mandible.

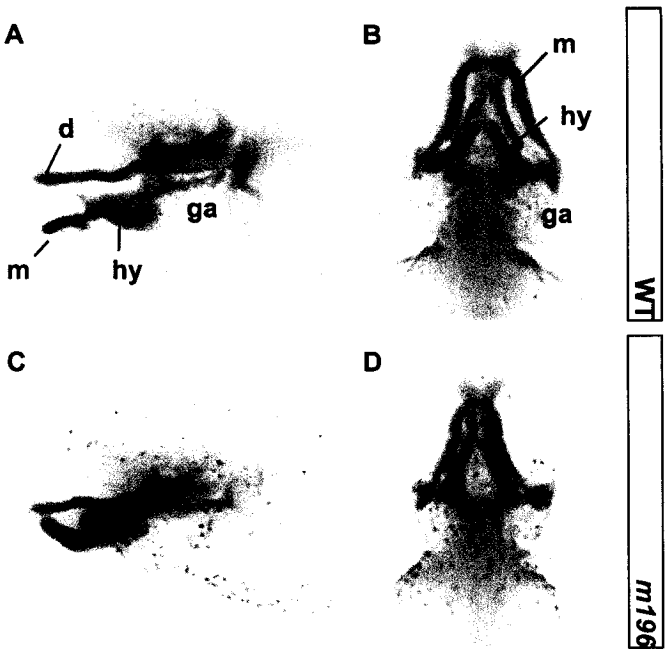
A
d
ga
m
hy
B
m
hy
ga
WT
C
D
m1196

Figure 16: Later branchial arches differentiate into cartilage in *m196* mutants. Alcian blue staining of the cartilage matrix in wild type (A, B) and *m196* (C, D) larvae at 6 dpf. (A, C) Lateral view, anterior to the left. (B, D) Ventral view, anterior to the top. Eyes are removed for better visualization of the staining.

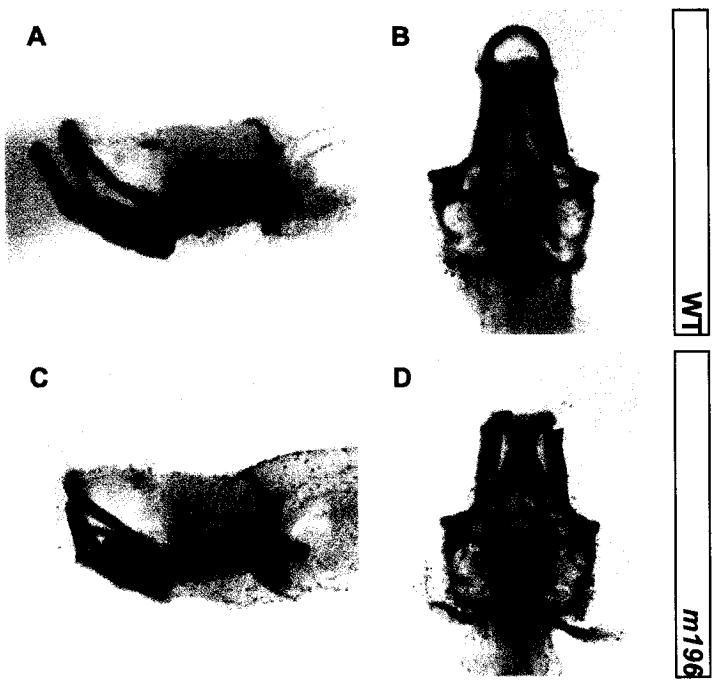
A
B
C
D
WT
m196

Figure 17: Some gill arches show a lack of chondrogenesis in a number of *m196* mutants at 12 dpf. Alcian blue staining of the cartilage matrix in wild type (A, B) and *m196* (C-F) larvae at 12 dpf. (C, D) Asterisks represent gill arches 3 and 4 that have not stained with alcian blue. (E, F) Most m196 embryos retain normal chondrogenesis in the gill arches. (A, C, E) Lateral view, anterior to the left. (B, D, F) Ventral view, anterior to the top. Eyes are removed for better visualization of the staining.

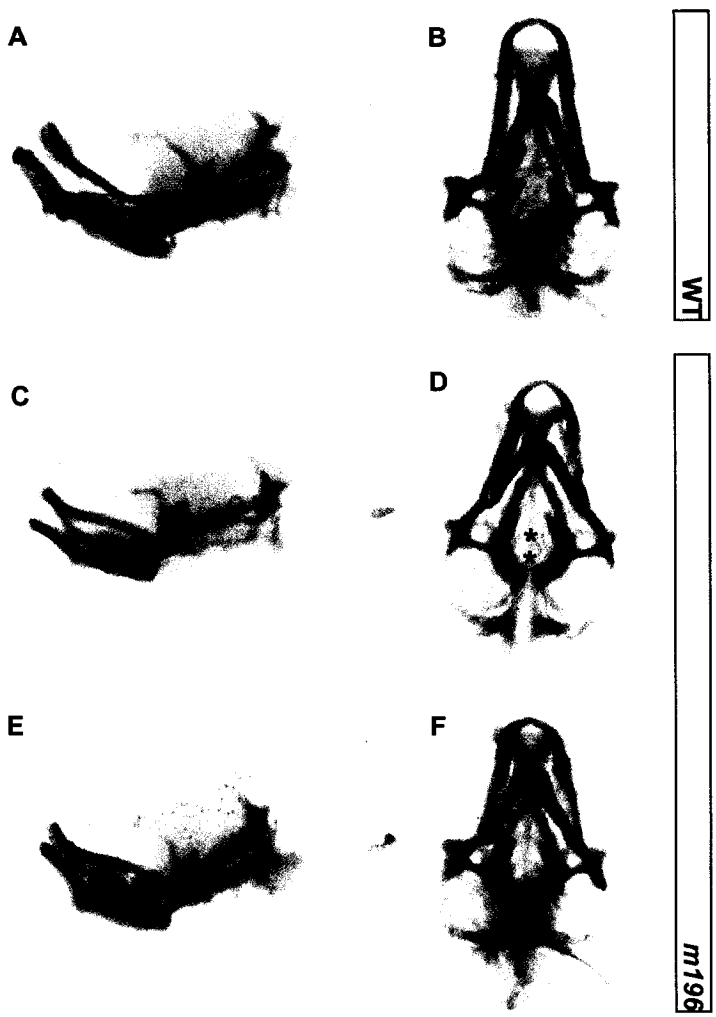
A
B
C
D
E
F
WT
m196

Figure 18: Precartilage condensations of gill arches in 3 dpf *m196* embryos are displaced dorsally in the larval cranium. *In situ* hybridization with a digoxygenin-labeled antisense RNA probe for *col2a1* on wild type (A, A') and *m196* (B, B') embryos at 3 dpf. Eyes were removed for better visualization of staining in A and B. A' and B' show the staining outline of the otic vesicle/dorsal cartilage and line of gill arches to illustrate the change in angle. Lateral view, anterior to the left. d, dorsal cartilage; ga, gill arches; ot, otic vesicle.

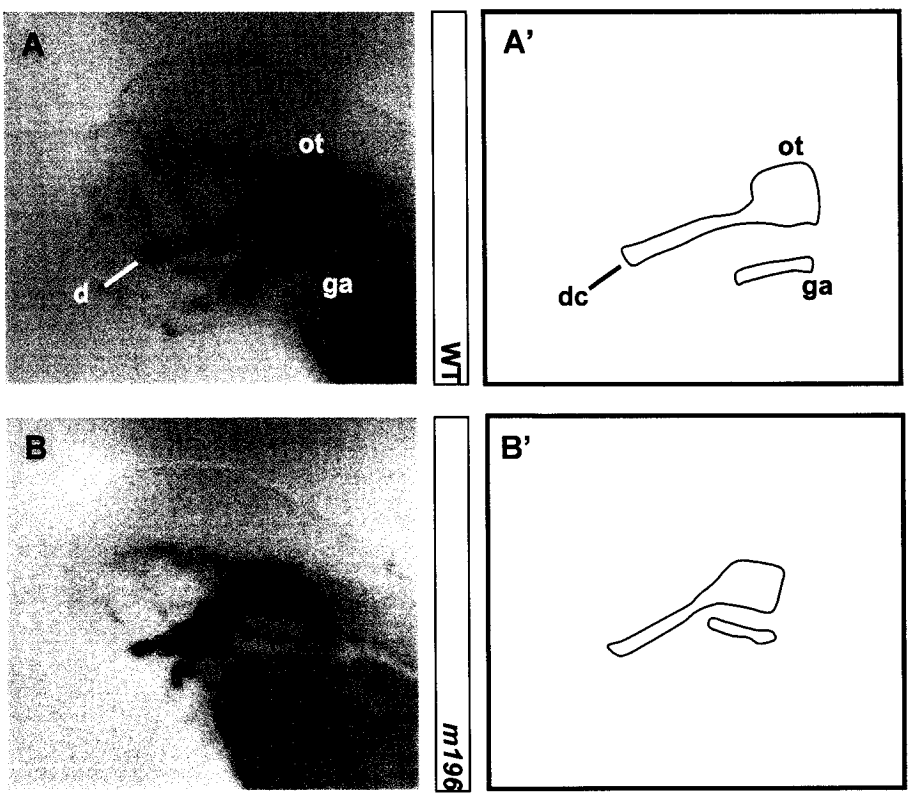
A
ot
d
ga
WT
A'
ot
dc
ga
B
m196
B'

1.4 Primary specification and induction of neural crest cells

Neural crest cells are induced within the neural keel during vertebrate development and migrate throughout the embryo into structures such as the cranial cartilage and median fin in zebrafish. In fact neural crest cells have been found to be necessary for proper cranial cartilage morphology (see Introduction). In order to establish the early induction of these neuroectodermal cells, we analyzed the expression of early neural crest markers *sox9b* and *foxD3* by ISH analysis. *FoxD3*, also known as *fkd6*, encodes a member of the fork head-domain transcription factors identified in *Drosophila*, zebrafish, mouse, and *Xenopus* (Odenthal and Nuesslein-Volhard, 1998). Although its role in zebrafish development is still rather elusive, it is strongly expressed in the premigratory neural crest cells beginning at 90% epiboly (9 hpf) as two anterior longitudinal stripes. Expression extends posteriorly during later stages of development, found as well in the tail bud mesoderm, and is downregulated as neural crest cells begin to migrate from the neural keel (Odenthal and Nuesslein-Volhard, 1998). *Sox9b* is also expressed at these stages in bilateral stripes of early neural crest cells similar to *foxD3* (Chiang *et al.*, 2001). Embryos obtained by in-crossing fish heterozygous for the *m196* mutation show no differences in both *foxD3* (Figure 19) and *sox9b* (Figure 20) expression within the neural keel at 10 and 12 hpf (bud and 6-somite stages, respectively). This suggests that premigratory neural crest cell induction is not affected in the *m196* mutant.

Figure 19: Early specification of the premigratory neural crest cells is unaffected in *m196* mutants: *foxD3*. *In situ* hybridization with a digoxygenin-labeled antisense RNA probe for *foxD3* on embryos derived from a cross of fish heterozygote for the *m196* mutation at 10 hpf (A) and 12 hpf (B). Arrows mark expression in the neural keel. Dorsal view, anterior to the top. tb, tail bud.

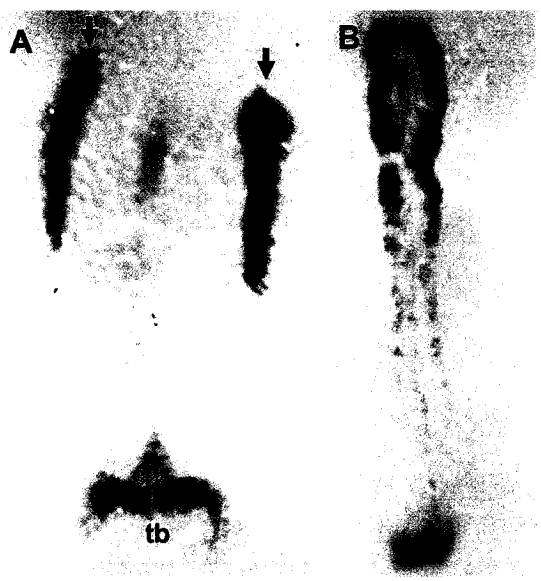
A
B
tb

Figure 20: Early specification of the premigratory neural crest cells is unaffected in *m196* mutants: *sox9b*. *In situ* hybridization with a digoxygenin-labeled antisense RNA probe for *sox9b* on embryos derived from a cross of fish heterozygote for the *m196* mutation at 10 hpf (A) and 12 hpf (B). Dorsal view, anterior to the top. Arrows mark expression in the neural keel.

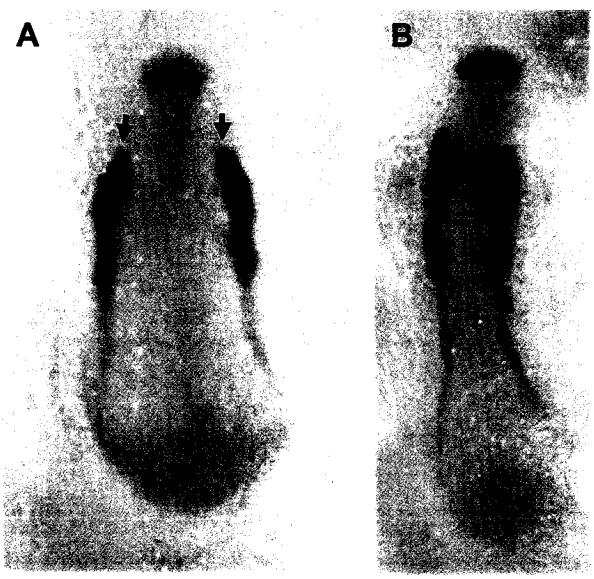
A
B

1.5 Formation of the branchial arches

Following induction, crest cells delaminate and travel along specified pathways. Pan-neural crest marker *crestin* is also expressed in the premigratory neural crest cells as well as later migratory and differentiating crest cells (Luo *et al.*, 2001). At 19 hpf migrating NCCs in the cranium form 3 main streams: the mandibular, hyoid and vagal pathways. The first two streams begin anterior to the otic vesicle and will populate the first two branchial arches, differentiating into the mandibular and hyoid cartilages as well as the associated connective tissues. The vagal pathway begins just posterior of the otic vesicle and will populate the five gill arches. No significant alteration in neural crest streams is seen in the vagal pathway of 19 hpf embryos derived from crosses of *m196* heterozygote pairs (data not shown). Fluctuation in staining of the first two mandibular and hyoid pathways within progeny from a heterozygote cross show no mutant-specific differences when compared with progeny derived from homozygous wild type crosses (data not shown). Later at 24 hpf no significant alteration in NCC number can be seen in *m196* mutant embryos when compared with wild type (data not shown). Therefore patterns of *crestin* expression suggest that initial neural crest migration is unaffected in *m196* mutants.

As NCCs travel into the branchial arches, these structures begin expressing members of the *distal-less* (*dlx*) family of transcription factors. Induction and maintenance of *dlx* expression is facilitated by surrounding pharyngeal structures. Therefore we used ISH analysis of *dlx* expression as an indication of proper arch structure including neural crest cell contribution.

Specifically, *dlx2* is found as early as 20 hpf in the branchial arches. At 20-30 hpf *dlx2* expressing cells are present in all arches of *m196* (Figure 21, 22). Although wild type expression is seen in arches 1 and 2, more diffuse expression is found in arches 3 and 4, particularly at 24 hpf (Figure 21). This pattern of expression is reminiscent of *dlx2* patterns seen at 20 hpf when transcripts are found in NCCs migrating into the arches. This suggests that migration of cells into the arches is delayed in *m196* mutants at 24hpf. At 24 and 30 hpf *dlx2*-expressing arches 3 and 4 are located distinctly further from the midline in *m196* mutants compared to wild type (Figure 22). Additionally these posterior arches in 20hpf mutants appear more oblong or teardrop-shaped. This branchial arch morphology is reiterated by similar expression of *dlx3* in the arches at 30 hpf (data not shown) Therefore shape and placement of *dlx* expression domains in the branchial arches of *m196* mutants suggest an initial delay in migration and later alteration in morphology within the early branchial arches.

Figure 21: Expression of *dlx2* shows a delay in early branchial arch morphogenesis and disorganization of epithelial tissues in *m196* embryos. *In situ* hybridization with a digoxygenin-labeled antisense RNA probe for *dlx2* on wild type (A, B) and *m196* (C, D) embryos at 24 hpf. A and C show the dorsal view at the level of the branchial arches. Anterior to the top. B and D show the lateral view of the embryonic tail bud. Anterior to the left.

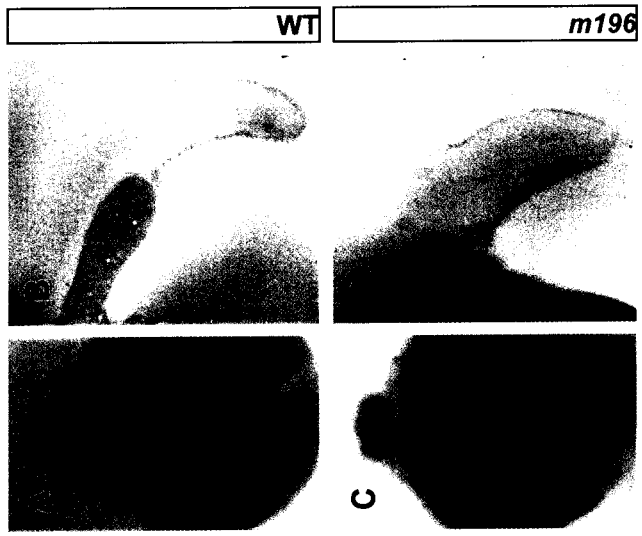
WT
m196
C

Figure 22: Branchial arches 3 and 4 are more oblong in shape and displaced laterally in *m196* embryos at 30 hpf. *In situ* hybridization with a digoxygenin-labeled antisense RNA probe for *dlx2* on wild type (A, B) and *m196* (C, D) embryos at 30 hpf. Dorsal view, anterior to the top. fb, forebrain; 1-4, branchial arches 1-4.

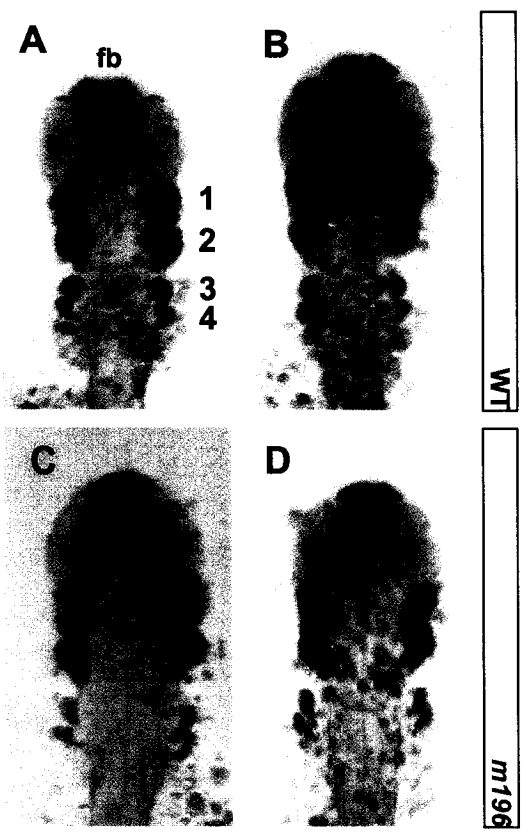
A
fb
1
2
3
4
B
WT
C
D
m196

1.6 Cranial endoderm development

There is substantial evidence pointing to the significant role of endoderm in cartilage differentiation as mentioned in the Introduction. In order to determine if pharyngeal pouch development was affected in these mutants, we used the anti-zn-5 zebrafish antibody, which recognizes dm-grasp, a member of the L2 family of cell surface molecules (Kanki *et al.*, 1994), to detect the pharyngeal pouches during gill arch formation and subsequent chondrogenesis (Schilling *et al.*, 1999). As early as 24 hpf, pouches 1 and 2 which divide the mandibular, hyoid and first gill arches (branchial arches 1-3) are visualized by anti-zn-5. In *m196* mutants, pouch formation appears to be initiated further out from the midline along the yolk surface compared to wild type (Figure 23) similar to the phenotype found in the location and shape of the branchial arches at this time (Figure 21). Later at 36 hpf the development of the endodermal pouches in this ectopic position is even more prominent in mutants (Figure 24). Twelve hours later at 2 dpf however, as precartilage condensations are forming in the branchial region, the anti-zn-5-labeled pharyngeal pouches are located in a more wild type mediolateral position ventrally in the head closer to the midline (Figure 25). Still the crowded nature of the arches is maintained in the pouches, similar to the mutant phenotype seen in the alcian blue-stained gill arch cartilages. Therefore, although the pharyngeal pouches appear to be ultimately located in the ventral cranium separating the forming cartilages, the initial displacement of the developing anterior endoderm may play a role in the later chondrogenesis disruption in *m196* mutants.

In addition to the alteration in pouch positioning it is possible that other endodermal structures within the cranium may be affected. In order to determine if the more centralized endodermally-derived structures, such as the mouth, pharynx, and foregut, were involved in the *m196* phenotype, we sectioned the cranial region of alcian blue stained larvae at 3.5 and 6 dpf. Alcian Blue not only stains cartilage matrix but also mucin secreted by mucosal cells within some gut epithelia (Jones and Reid, 1973). At 3.5 dpf the mouth and pharyngeal region of wild type larvae has formed a lumen. However, *m196* mutants have a completely unopened mouth (Figure 26A'-B'). At the level of the pharynx just posterior to the eye, the alcian-stained mucosal cells are found surrounding the open tract in wild type. Although a double layer of these epithelial tissues is present in mutants, no open lumen forms along the length of the pharynx (Figure 26C'-D'). Also found at this level is the opercular cavity and gill arch endoderm that form open pouches within the pharyngeal region. This space is not found within cross-sections of mutant pharyngeal regions. This collapse of the endodermal tube appears to be limited to the anterior mouth and pharynx. At the level of the esophagus, the gut tube has formed an open lumen with properly folded mucin-stained epithelium (Figure 26E'). This phenotype is reiterated at 6 dpf in the mouth and pharynx (Figure 27). However at this stage, the opercular cavity and pharyngeal pouches have formed an open space as in wild type. Therefore the failure of these epithelia to form an open anterior endodermal tube appears to be the major craniofacial phenotype in the *m196* mutant and may be involved in the ectopic mediolateral positioning of the pouches.

Figure 23: The initial development of the pharyngeal pouches dividing branchial arches 1-3 begins further from the midline in *m196* mutants. Immunostaining of whole mount wild type (A,B) and *m196* (C-F) embryos at 24 hpf with zn-5 antibody. (A,C,E) Dorsal view, anterior to the top. Arrows denote the distance from the edge of the neural tube to the proximal tip of the pouches. (B,D,F) Lateral view, anterior to the left. Arrowheads mark the anterior limit of the two early pouches. Dorsal view, anterior to the top.

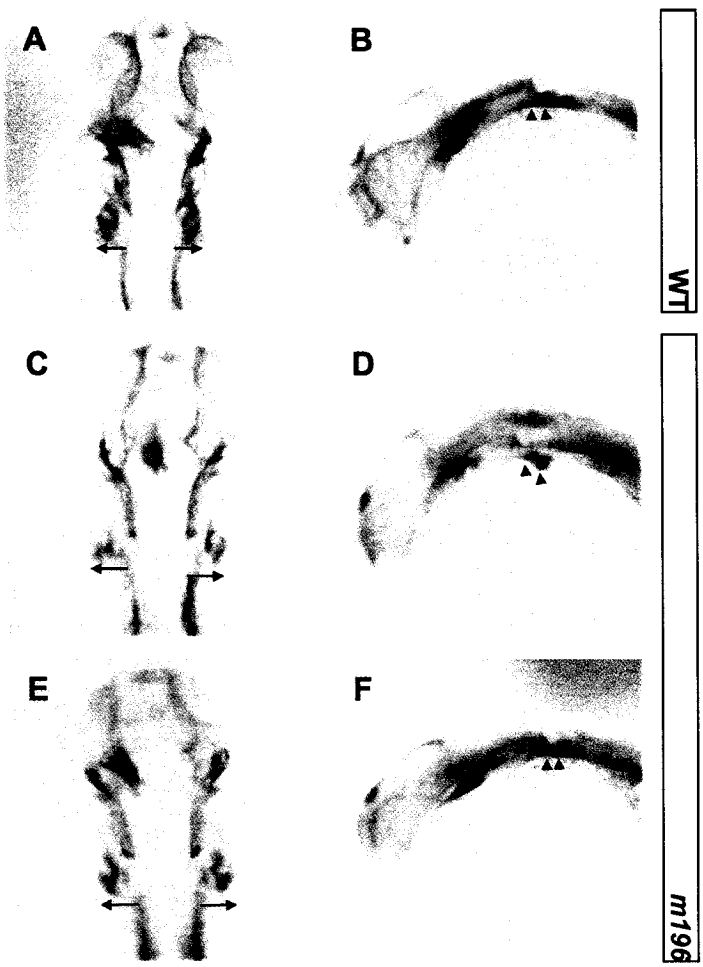
A
B
C
D
E
F
WT
m196

Figure 24: The pharyngeal pouches continue to develop further from the midline in *m196* mutants. Immunostaining of 36hpf wild type (A,B) and *m196* mutant (C-F) embryos with zn-5 antibody. (A,C,E) Dorsal view, anterior to the top. Arrows denote the distance between the limit of the left neural tube to the proximal posterior-most pouch. M, mandibular arch; H, hyoid arch; g1-4, gill arches 1-4. (B,D,F) Lateral view, anterior to the left. Arrowheads mark the anterior limit of each pouch.

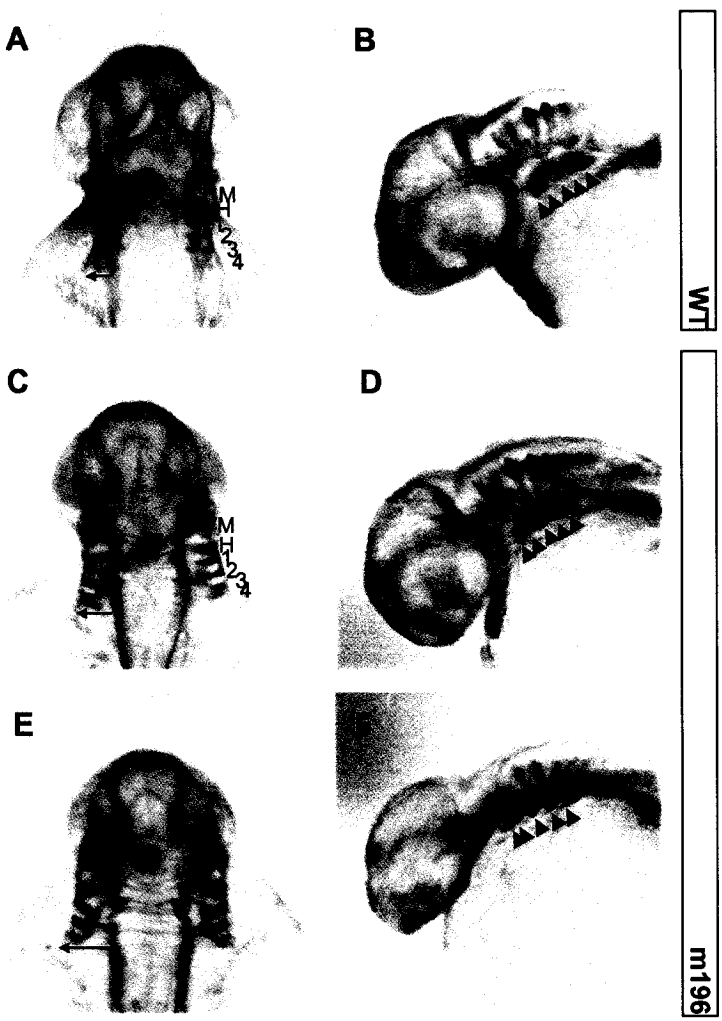
A
B
C
D
E
M
H
1
2
3
4
WT
m196

Figure 25: At the time of early chondrogenesis, pharyngeal pouches are crowded together but in a more wild type location closer to the midline in *m196* mutants. Immunostaining of 48hpf wild type (A) and *m196* mutant (B, C) embryos with zn-5 antibody. Arrowheads identify the anterior limit of the pharyngeal pouches. Lateral view, anterior to the left. M, mandibular arch; H, hyoid arch; g1-4, gill arches 1-4.

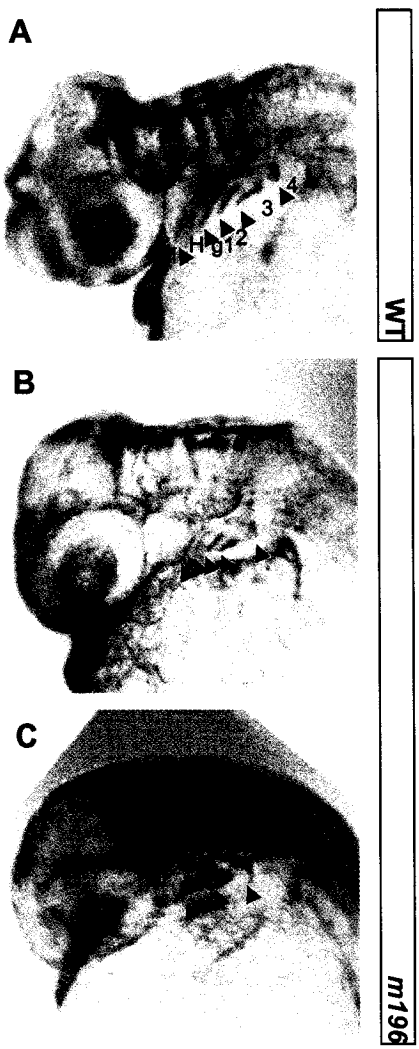
A
Hyl
2
3
4
WT
B
C
m196

Figure 26: The mouth and pharynx are unopened in *m196* mutants at 3.5 dpf. Cross-sections of 3.5 dpf wild type (A-E) and *m196* mutant (A'-E'). (F) Lateral view of a wild type Alcian Blue stained larva. Black lines indicate the level along the anterior/posterior axis represented by each section. bb, basibranchial; cb, ceratobranchial; ch, ceratohyal; ep, ethmoid plate; m, Meckel's; nc, notochord; pq, palatoquadrate; pc, parachordal; oper, opercular cavity; ot, otic vesicle; tr, trabeculae cranii.

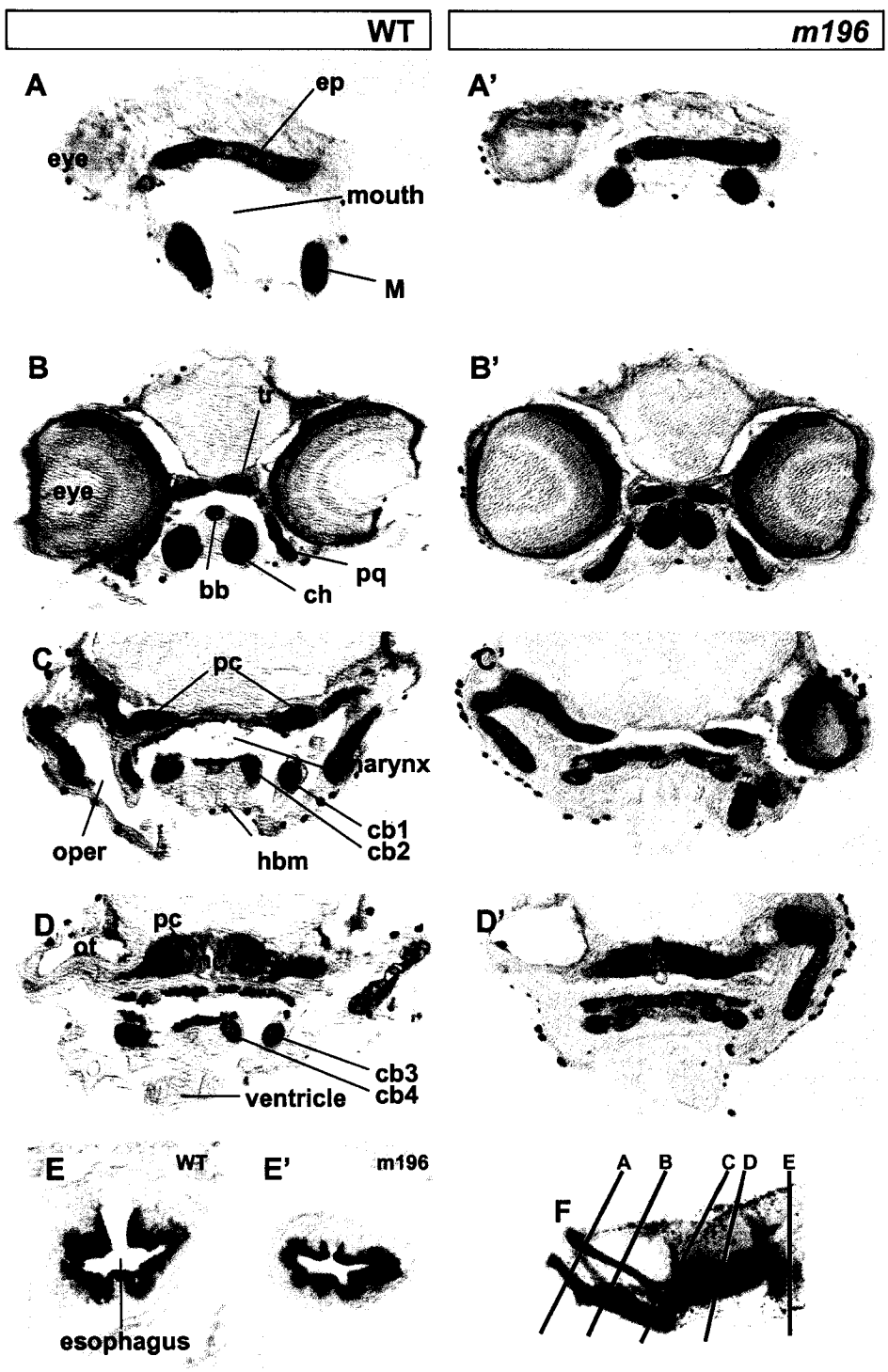
WT
m196
A
ep
eye
mouth
M
A'
B
tr
eye
bb
ch
pq
B'
C
pc
larynx
cb1
cb2
oper
hbm
C'
D
pc
ot
cb3
cb4
ventricle
D'
E
WT
esophagus
E'
m196
A
B
C
D
E
F

Figure 27: The mouth and pharynx are unopened in *m196* mutants at 6 dpf. Cross-sections of 6 dpf wild type (A,B) and *m196* mutant (A',B'). (C) Lateral view of a wild type Alcian Blue stained larva. Black lines indicate the level along the anterior/posterior axis represented by each section. bb, basibranchial; cb, ceratobranchial; ch, ceratohyal; hs, hyosymplectic; nc, notochord; oper, opercular cavity; ot, otic vesicle; pq, palatoquadrate; pc, parachordal; tr, trabeculae cranii.

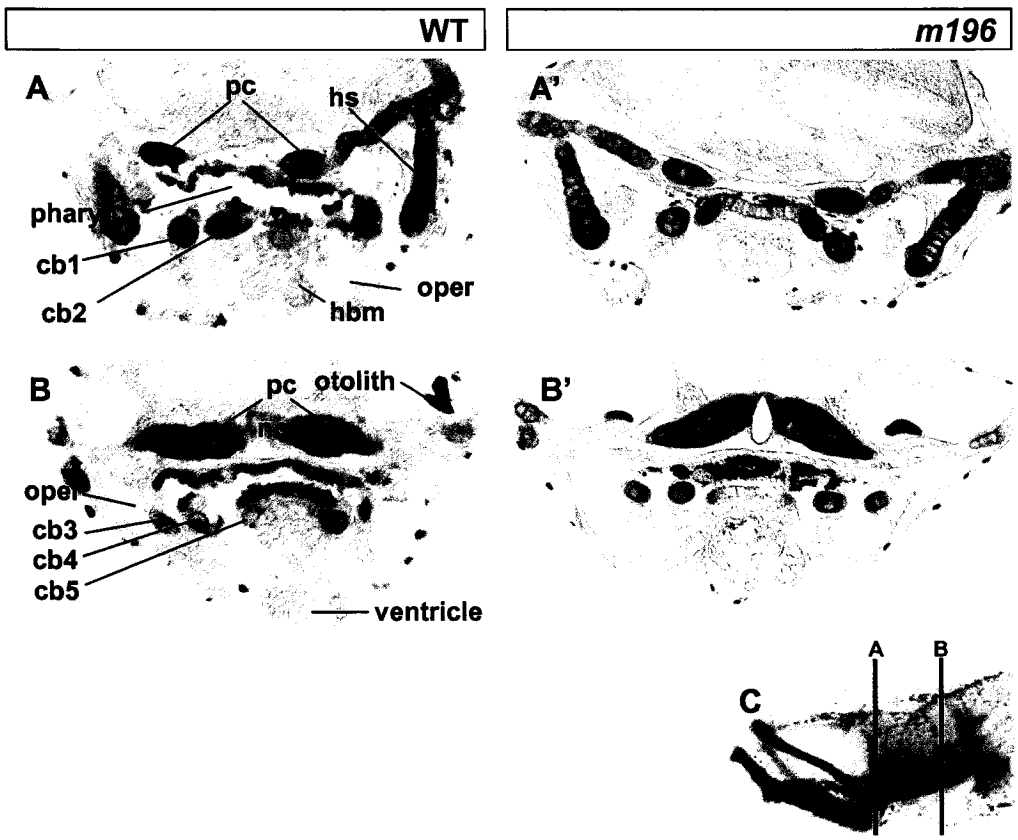
WT
m196
A
pc
hs
phar
cb1
cb2
hbm
oper
A'
B
pc
otolith
oper
cb3
cb4
cb5
ventricle
B'
C
A
B

1.7 Median fin development

The most consistent defect in the *m196* mutants is a disruption of the median fin fold. In order to determine if specific tissues of the median fin are properly specified in *m196* mutants a number of molecular markers were used. In wild type embryos *fgf8* is normally expressed around 24-28 hpf in the cranial region, such as the dorsal diencephalon, facial ectoderm, hyoid, and midbrain-hindbrain boundary (MHB), as well as the posterior embryo in the anterior boundary of the somites in the tail and the tail bud mesenchyme (Fuerthauer *et al.*, 1997). Although anterior expression of *fgf8* is unaffected in *m196* mutants (Figure 28), *in situ* hybridization analysis reveals a distinct upregulation of *fgf8* mRNA expression in the tail somites and mesenchyme at 28 hpf (Figure 29). In fact, overexpression of *fgf8* in zebrafish embryos has previously been found to cause similar posterior phenotypes to that of *m196*. In zebrafish recessive *aussicht* mutants overexpressing *fgf8* show a dorsoventrally widened tail bud (Heisenberg *et al.*, 1999). When injected with *in vitro*-synthesized *fgf8* RNA, the overexpression phenotype is manifested in the most weakly affected embryos at 36 hpf as a shortening of tail length and loss of ventral caudal fin fold (Fuerthauer *et al.*, 1997), a phenotype also found in *m196* mutants (Figure 7,8,10,11). Therefore the upregulation of *fgf8* and morphological characteristics seen in the developing tail bud of *m196* mutants coincides with that of other *fgf8*-overexpressing mutants and morphants.

Figure 28: Anterior expression of *fgf8* is unaffected in *m196* embryos. *In situ* hybridization with a digoxygenin-labeled antisense RNA probe for *fgf8* on wild type (A, B) and *m196* (C, D) embryos at 24 hpf. (A, C) Lateral view, anterior to the left. (B, D) Dorsal view, anterior to the bottom. dd, dorsal diencephalon; fec, facial ectoderm; mhb, midbrain-hindbrain boundary; os, optic stalk.

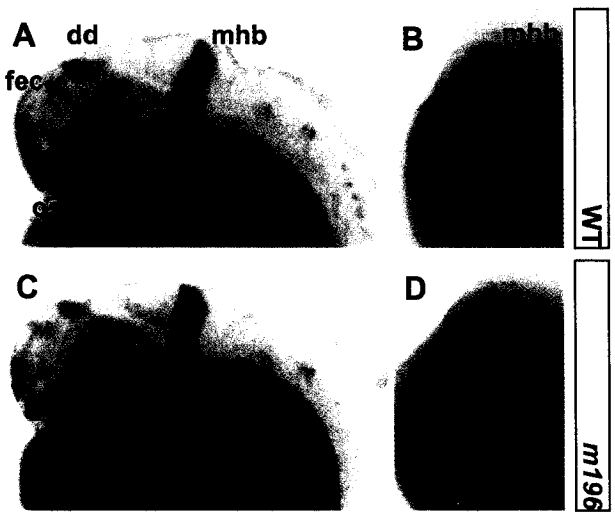
A
dd
mhb
fec
B
WT
C
D
m199

Figure 29: *Fgf8* is overexpressed in the tail bud of 28 hpf *m196* embryos. *In situ* hybridization with a digoxygenin-labeled antisense RNA probe for *fgf8* on wild type (A) and *m196* (B-D) embryos at 28 hpf. Lateral view, anterior left. Expression in the fin mesenchyme (fm), somites (s), tail bud (tb).

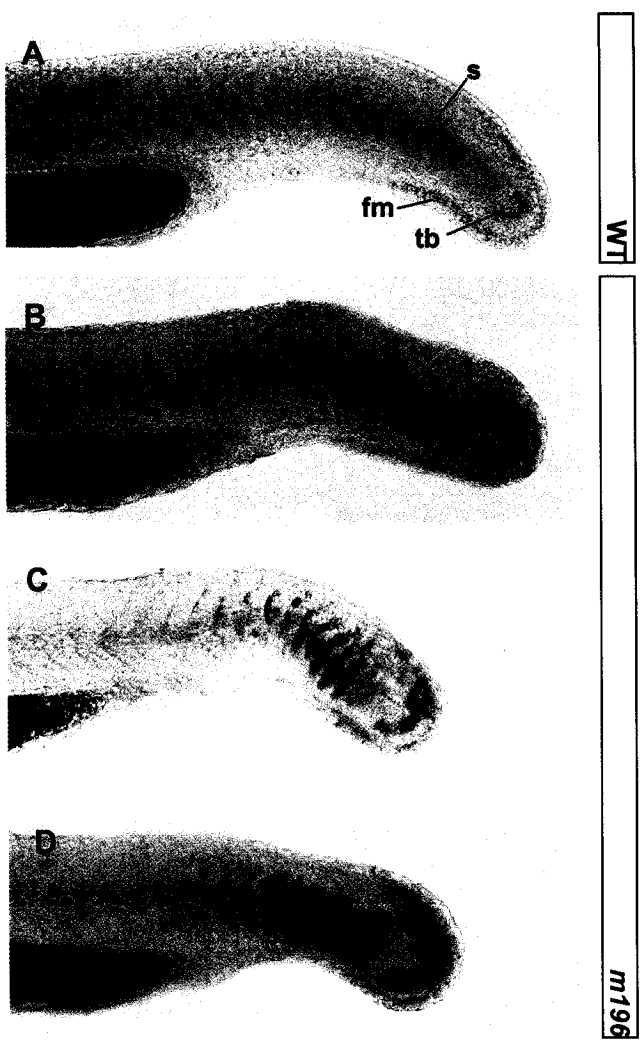
A
s
fm
tb
B
C
D
WT
m196

MsxC, a member of the *muscle segment homeobox* (*msx*) family of genes, is also expressed in the median fin region during development (Ekker *et al.*, 1997). Along the posterior dorsal and ventral midline of the zebrafish embryo, cells just distal to the tail mesenchyme express *msxC* during median fin fold outgrowth (Akimenko *et al.*, 1995b; Ekker *et al.*, 1997). We looked at *msxC* expression in order to determine if this subset of fin fold tissues is present in the *m196* mutant. In mutant embryos at 30 hpf *msxC*-expressing cells are in fact found along the dorsoventral midline of the posterior embryo. These cells however are arranged in a disordered manner unlike the straight line of expression seen in wild type embryos of the same stage (Figure 30). In some mutant embryos transcript-containing cells are found ectopically along the lateral sides of the end of the tail. As well the region of expression in cells surrounding the urogenital opening just posterior to the yolk end is also enlarged. Therefore median fin tissues expressing *msxC* are not limited to a midline stripe as in wild type but rather are unstructured around the posterior tail region.

Though the developmental significance of *dlx* signaling in the median fin fold is unknown, transcripts of a number of *dlx* genes are found within fin epithelial tissues throughout zebrafish development (Akimenko *et al.*, 1994; Ellies *et al.*, 1997). We looked specifically at expression levels of *dlx2* using ISH. *Dlx2* expression begins around 20 hpf just prior to fin fold extension and remains until approximately 30 hpf. In the *m196* mutant, *dlx2* expression is present in the fin epithelium at 20 hpf just prior to fin fold extension (Figure 31) as well as at 24 hpf just after the onset of extension (Figure 21). However transcript-containing, fin

epithelial cells are not found in a smooth, organized line along the midline of the tail such as in wild type. Instead these cells are disorganized and create a blotchy expression pattern in the mutant tail bud. Additionally at 20 hpf expression appears normal in the ventral fin although an accumulation of *dlx2*-expressing cells can be seen in the ventral tail a few hours later at 24 hpf. Therefore *dlx2* expression in the *m196* mutant tail epithelium is disorganized in the dorsal region but variably maintained ventrally just prior to and immediately after the onset of wild type fin fold extension.

Recently our lab cloned a novel fin fold-specific gene *2-H06* (Padhi *et al.*, 2004). *2-H06* is expressed exclusively within fin fold tissues beginning at 20 hpf just prior to median fin fold extension and continuing through larval development. We used *2-H06* in order to further confirm the presence of fin fold epithelial tissues in *m196* mutants. Although *m196* embryos at the same stage have little to no extended fin fold, *2-H06*-expressing cells are still present surrounding the tip of the embryonic tail (Figure 32). This expression shows a highly disorganized bunching of epithelial cells at the posterior end of the mutant embryos. These results support preceding observations of other fin fold marker expression within the tail between 20-30 hpf in suggesting that, even though the median fin epithelium is initially unable to extend from the embryonic body into a fin fold, genetic specification of these tissues is still occurring.

Furthermore in order to observe neural crest migration within the posterior embryo, we looked at the presence of *crestin*-positive cells at the time when fin fold extension would normally be in progress. Neural crest cells in the region of

the tail migrate posteriorly along the midline and around the tail tip in wild type embryos. At 36 hpf as these cell movements are occurring, there is an accumulation of *crestin*-containing cells along the dorsal tip of the tail (Figure 33). Ventrally located neural crest cells appear to be unaffected. Thus these results, along with the presence of ectopic neural crest-derived pigment cells in the posterior fin fold later in development (Figure 13-14), suggest a disruption of dorsal neural crest migration in the developing *m196* mutant tail.

Figure 30: Fin mesenchyme expressing *msxC* in the tail bud is disorganized in *m196* embryos at 30 hpf. *In situ* hybridization with a digoxygenin-labeled antisense RNA probe for *msxC* on wild type (A) and *m196* (B-C) embryos at 30 hpf. Arrowhead marks expression in the urogenital vent which marks the posterior boundary of the yolk. Lateral view, anterior left.

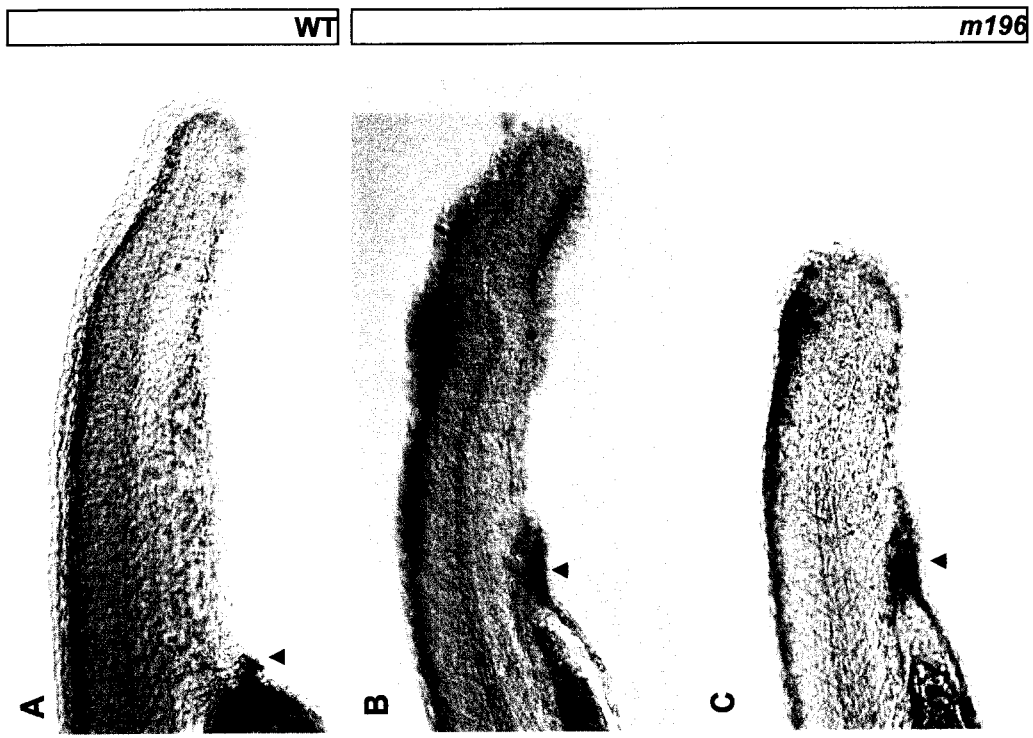
WT
m196
A
B
C

Figure 31: Expression of *dlx2* present but disorganized in the early epithelial tissue of *m196* mutants. Wild type (A) and *m196* mutant (B) embryos at 20 hpf. Arrowhead marks the dorsal region of the tail where expression appears rough.

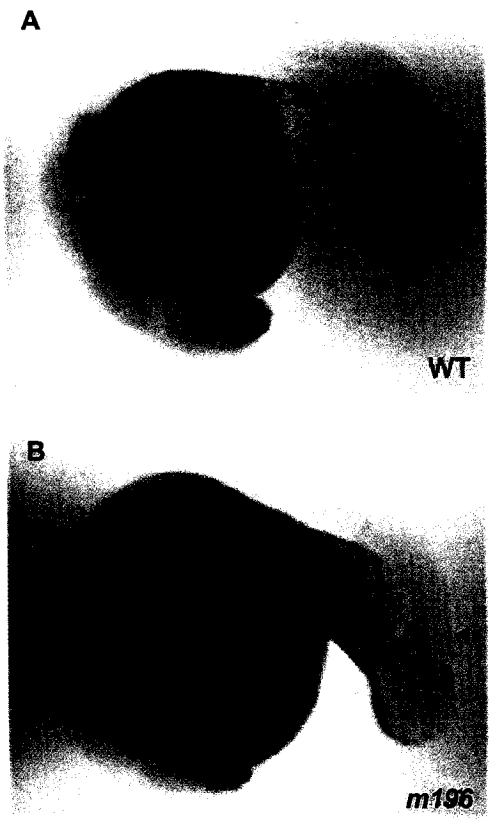
A
WT
B
m196

Figure 32: Epithelial tissues that normally comprise the fin fold remain disorganized and fail to extend in *m196* mutants during early median fin development. *In situ* hybridization with a digoxygenin-labeled antisense RNA probe for *2-H06* on wild type (A) and *m196* (B-D) embryos at 36 hpf. Lateral view, anterior left.

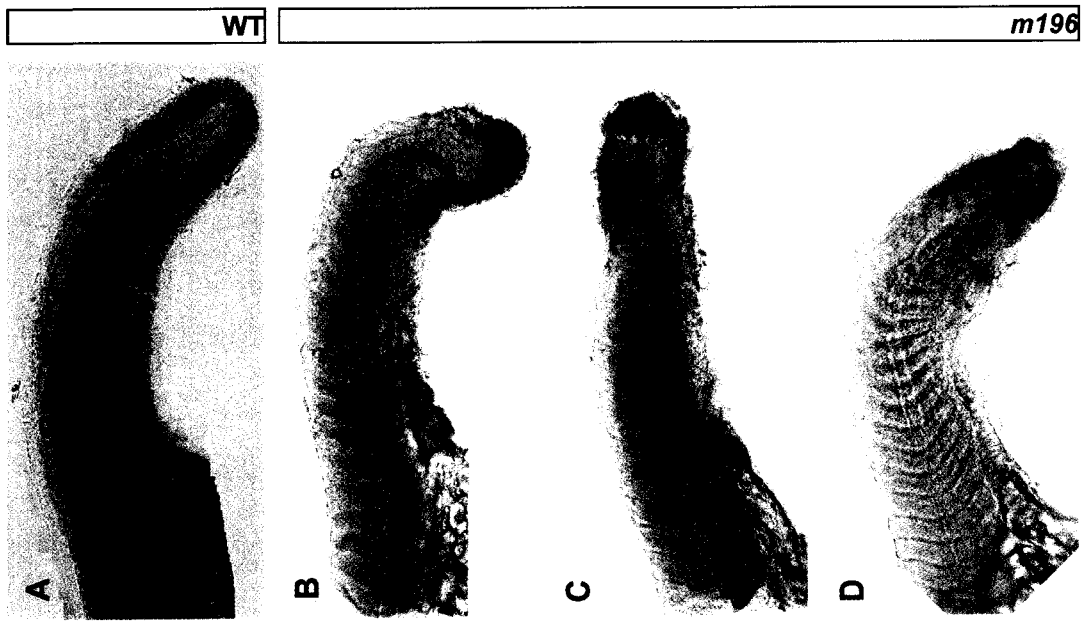
WT
m196
A
B
C
D

Figure 33: Migrating neural crest cells accumulate in the dorsal region of the posterior tail in *m196* mutants. *In situ* hybridization with a digoxygenin-labeled antisense RNA probe for *crestin* on wild type (A) and *m196* (B) embryos at 36 hpf. Lateral view, anterior to the left, dorsal to the top.

A
B
WT
m199

1.8 Pectoral fin development

Based on the observation that most mutants form an initial fin bud, we can assume that primary limb field specification proceeds normally in these mutants. Defects first appear to arise as a variable disruption of the pectoral fin fold extension. Pectoral fin folds of *m196* mutants are often smaller in size and are more narrow and triangular in shape when compared with wild type larvae (Figure 9, 13). Fin bud mesenchymal and epithelial markers were used to determine if early genetic signaling was initiated in the more distal regions of the fin buds of *m196* mutants. *MsxC* is expressed early in the embryonic limb bud mesenchyme prior to limb bud outgrowth at 24 hpf in wild type embryos. Later at 30 hpf *msxC* becomes restricted to the distal fin bud mesenchyme with an increased expression in the anterior region (Akimenko *et al.*, 1995b; Ekker *et al.*, 1997). At 24 hpf *m196* mutants with little or no fin bud outgrowth show either absent or severely reduced expression of *msxC* (Figure 34). At 30 hpf m*sxC* expression is present in the fin buds of all *m196* mutants suggesting an initial delay in expression (Figure 35). However the expression domain of *msxC* is more diffuse within the mesenchyme, extending beyond just the distal regions. The inability to maintain localized expression of this mesenchymal marker in the pectoral fin bud is comparable to the disrupted *msxC* expression in the median fin fold, suggesting that the defects in pectoral and median fin development are occurring in a similar manner.

Figure 34: Expression of *msxC* in the fin bud mesenchyme is decreased or absent in the pectoral fins of 24 hpf *m196* embryos. *In situ* hybridization with a digoxygenin-labeled antisense RNA probe for *msxC* on wild type (A) and *m196* (B, C) embryos at 24 hpf hpf. Arrowheads mark the regions of the pectoral fins. Dorsal view, anterior to the top.

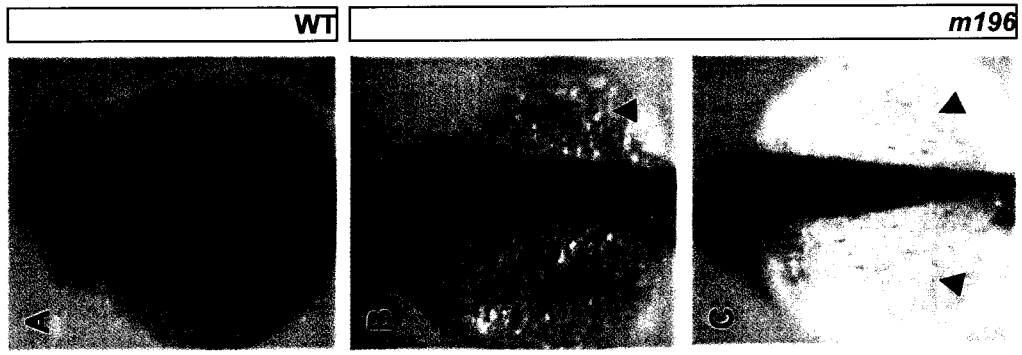
WT
m196
A
B
C

Figure 35: Later expression of *msxC* in the pectoral fins continues to be variably diffuse and/or decreased in *m196* embryos. *In situ* hybridization with a digoxygenin-labeled antisense RNA probe for *msxC* on wild type (A) and *m196* (B, C) embryos at 30 hpf. Arrowheads indicate pectoral fins. Dorsal view, anterior to the top.

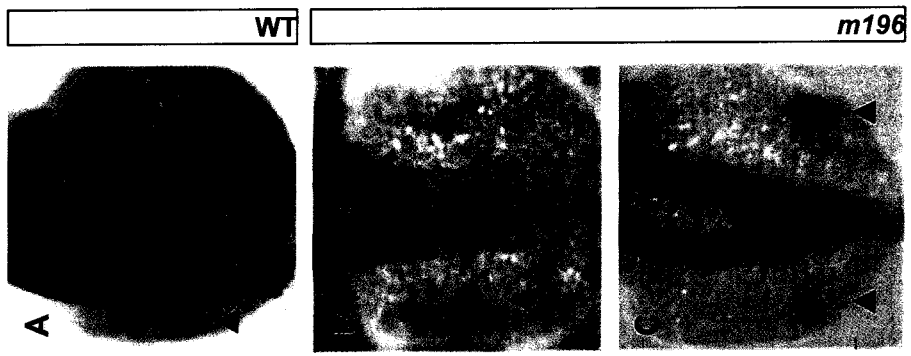
WT
m196
A

1.9 Cell cycle control

Mutants are significantly smaller in size than wild type embryos. Coupled with a loss of fin fold tissues, it is possible that a disruption in cell cycle control is occurring. This could manifest itself as either an increase in programmed cell death or decrease in proliferation. We used Acridine Orange to detect apoptotic cells in living embryos at stages during development as the affected structures are forming. Embryos stained at 20 hpf had no mutant specific alteration in apoptosis (data not shown). At 24 and 36 hpf acridine orange staining is found dramatically increased in mutants in the caudal-most region of the tail, specifically in the dorsal epithelium when compared with wild type embryos of the same stage (Figure 36). In some *m196* mutants Acridine stained cells are also found within the mesenchymal cells of the tail (Figure 36C). Cranial regions of 24 and 36 hpf *m196* mutants from the anterior-most region to the post-otic area show no significant apoptosis (Figure 37) other than that normally found in wild type embryos at this stage (Cole and Ross, 2001). Thus although apoptosis does not appear to be a major influence on the defects within the branchial region at these stages, cell death is highly increased in the tail tissues involved in the median fin fold structure at the time of extension.

Figure 36: Apoptosis is increased in the tails of live *m196* embryos at 36 hpf. Acridine orange staining of wild type (A) and *m196* (B-D) embryos at 36 hpf. Lateral view, anterior left. White dotted line in A represents the outer boundary of the wild type median fin fold.

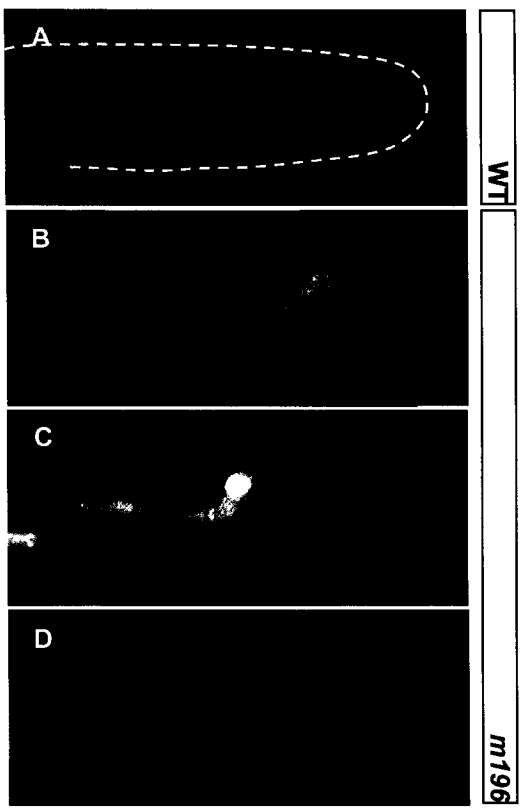
A
B
C
D
WT
m196

Figure 37: Apoptosis is unaffected in the cranial region of live *m196* embryos at 36 hpf. Acridine orange staining of wild type (A,B) and *m196* (C,D) embryos at 36 hpf. Lateral view, anterior to the top.

A
B
C
D
WT
m196

2. Mapping of the *m196* mutation

2.1 SSLP panel meiotic mapping

In order to map the *m196* mutation we used the simple sequence length polymorphism (SSLP) map created by Ela Knapik and colleagues (1998). Mapping began in the lab of Ela Knapik in Munich, Germany in July 2000 by Sherri Sachdev. Mapping family stocks of zebrafish were initially crossed into the Hong Kong background (HK) and subsequently screened for *m196*/AB/HK heterozygotes. Bulk segregant analysis revealed *m196* linkage to SSLP marker z9831 on linkage group (LG) 17 (Figure 38; Sachdev, S., unpublished). All initial *m196* embryos screened amplified the 175 bp AB allele. The z9831 marker amplified from wild type homozygous embryos is approximately 200 bp corresponding to the HK strain. In embryos heterozygous for both the HK and AB alleles, both the 200 and 175 bp fragments were amplified. New mapping families were also created in the TL (Top-Long fin) background which was found to contain a higher frequency of markers on LG17 polymorphic to the AB background and thus better for mapping experiments. The TL allele for z9831 marker when amplified from genomic DNA is approximately the same size as the previous HK allele. Therefore the z9831 marker is polymorphic within our mapping strains and is linked to the *m196* mutation.

Fine mapping was then used to create a critical interval spanning the mutation. We continued the fine mapping by screening individual mutant F_2 embryos from these same *m196*/AB/HK stocks as well as new *m196*/AB/TL fish

stocks. From the MGH meiotic mapping panel we found the z26685 marker to be polymorphic within our mapping families. The mutant (AB) z26685 allele is 150 bp and the HK and TL wild type alleles approximately 125 bp (Figure 38). z26685 was found to be the closest polymorphic flanking marker on the other side of the *m196* mutation with 9 recombinants out of 2148 meioses (2 meiotic events per embryo) or a meiotic distance of 0.42 cM (Figure 39). One centiMorgan is theoretically equivalent to approximately 600 kb (Knapik *et al.*, 1998), therefore 0.42 cM would equal 252 kb. Later within the mapping process, another polymorphic marker z30467 was found on the MGH mapping panel. This marker retains 3 recombination events of z9831 out of 2114 meioses or a meiotic distance of 0.14 cM (approximately 84 kb, Figure 39). Therefore the new critical interval for the *m196* mutation, flanked by markers z30467 and z26685 on LG17, is 0.56 cM or approximately 336 kb.

Finally in order to narrow down the critical interval a third important polymorphic marker zCtg37A was created through a new Simple Sequence Repeat search and primer design bioinformatics resource (http://danio.mgh.harvard.edu/markers/ssr.html) provided by Zebrafish Information Network (ZFIN) (Sprague *et al.*, 2001) which identifies new potentially polymorphic SSLP markers and associated primer pairs from specific sequence assemblies release by the Sanger zebrafish genome sequencing project. When amplified in the mutant embryos recombinant for flanking markers z30467 and z26685, this marker amplifies only the approximately 173 bp *m196*

(AB) allele. Therefore this new SSLP marker is linked to the *m196* mutation with 0 recombination events in 2148 meioses (Figure 39).

2.2 LN54 radiation hybrid mapping

The LN54 radiation hybrid panel created by Hukreide *et al.* (1999) was used to map candidates and markers to LG17. Fine mapping is not necessarily possible with the LN54 panel with a resolution of only approximately 400 kb or 3.38 cR (Hukriede *et al.*, 2001), but this can at least give a good indication of chromosomal placement of previously unmapped markers and genes of interest. Flanking marker z26685 maps to the 249.01 cR position on LG17 (Figure 40). The opposing flanking marker z30467 mapped 5.32 cR from the previously-mapped z9831 marker at the 241.09 cR position on LG17. According to these results, z30467 and z26685 create an interval of 7.92 cR or 935 kb. A number of other ESTs and genes of interest map within this region as well. Therefore although this is much greater than the 336 kb interval determined by meiotic mapping, radiation hybrid mapping further confirms the general location of the critical markers and genes of interest on LG17.

Figure 38: The *m196* mutation is flanked by the polymorphic SSLP markers z9831 and z26685. Separation of PCR-amplified alleles of z9831 (Lanes 1-4) and z26685 (Lanes 5-8) in wild type TL (1, 5), heterozygote *m196*/TL (2, 6), homozygous *m196* (3, 7) and recombinant *m196*/TL (4, 8) by agarose gel electrophoresis. The wild type allele is approximately 200 bp for z9831 and 125 bp for z26685. The *m196* mutant allele is approximately 175 bp for z9831 and 150 bp for z26685. M, 100 bp DNA ladder.

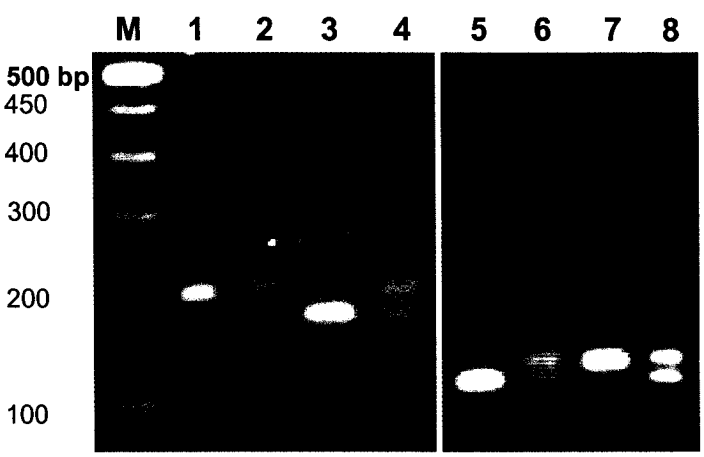
M
1
2
3
4
5
6
7
8
500 bp
450
400
300
200
100

Figure 39: *m196* is linked to zCtg37A and limited to a 0.235 cM critical interval. Meiotic map of the region of LG17 surrounding the *m196* mutation. Numbers to the right of each SSLP marker or gene represent the number of recombinants (recs) per number meioses. Recombinants of n*g1*, z30467 and PAC23SP6 are out of 2114 meioses. Recombinants of *id3* and *e2f2* are out of 2148 meioses. Numbers to the left give the meiotic distance (in centiMorgans, cM) of each marker or gene from the m196 mutation.

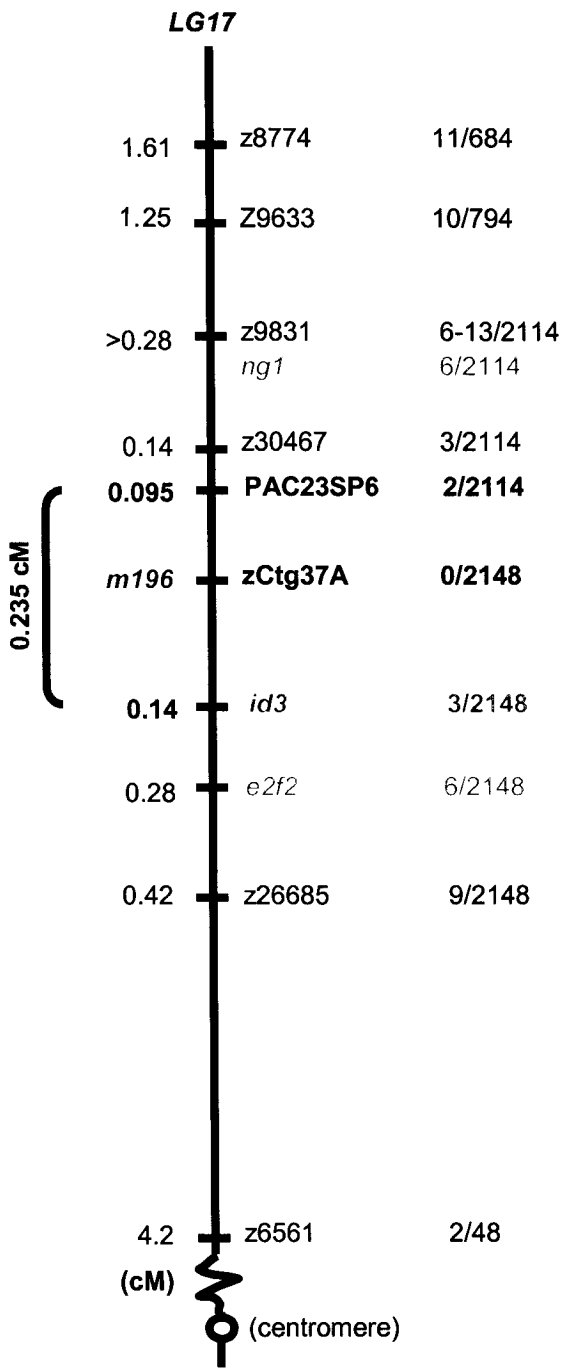
LG17
1.61
z8774
11/684
1.25
Z9633
10/794
>0.28
z9831
6-13/2114
ng1
6/2114
0.14
z30467
3/2114
0.095
PAC23SP6
2/2114
0.235 cM
m196
zCtg37A
0/2148
0.14
id3
3/2148
0.28
e2f2
6/2148
0.42
z26685
9/2148
4.2
z6561
2/48
(cM)
(centromere)

Figure 40: Flanking SSLP markers z30467 and z26685 as well as many candidates map to a similar region on LG17 by LN54 radiation hybrid mapping. LN54 map of the region on LG17 including ESTs and genes already mapped within the panel. Numbers on the right denote the map position of each element listed to the left in centiRays (cR). Mapped elements indicate results obtained during the current study (green) and those previously found within the panel (black).

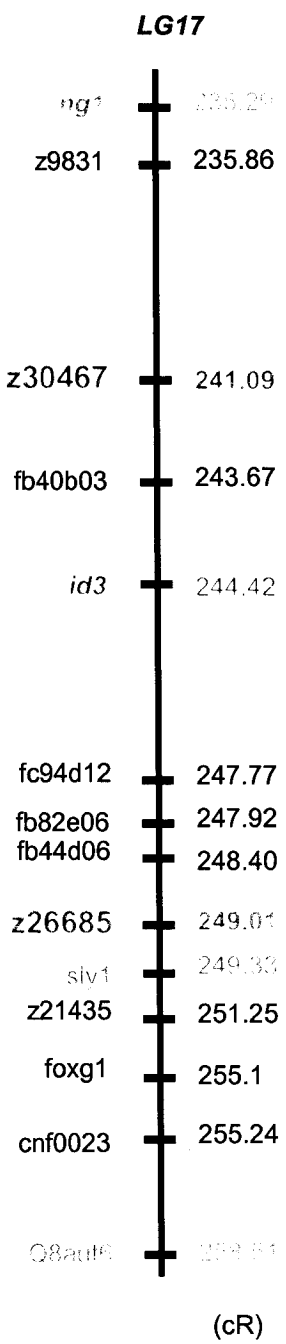
LG17
ng1
z9831
235.86
z30467
241.09
fb40b03
243.67
id3
244.42
fc94d12
247.77
fb82e06
247.92
fb44d06
248.40
z26685
siv1
z21435
251.25
foxg1
255.1
cnf0023
255.24
(cR)

3. Cloning of the *m196* mutation

In order to clone the *m196* mutation we used two separate approaches: analysis of candidate genes and positional cloning. The candidate gene approach involves using single strand conformation polymorphism (SSCP) analysis to map genes of interest to the mutation (see Materials and Methods). Meiotically-linked candidate coding sequences from wild type and *m196* mutants can then be cloned and sequenced in order to identify mutant-specific base pair changes. Positional cloning is used to isolate genomic clones spanning the critical interval. Both techniques are useful in isolating the random ENU-induced genomic mutations such as *m196*.

3.1 The candidate gene approach

Mapping experiments proceeded concurrently with our search for candidate genes. Frequently updated zebrafish resources were used for candidate identification including the meiotic and radiation hybrid mapping panels published on the ZFIN website (Sprague *et al.*, 2001) as well as the genome sequence releases from the Sanger Institute. Prior to the identification of the zCtg37A SSLP marker, we identified, analyzed, and ruled out four candidate genes within the mapping interval: *growth/differentiation factor 7* (*gdf7*), a novel gene (*novel gene 1, ng1*), *inhibitor of DNA binding/differentiation 3* (*id3*), and *e2f transcription factor 2* (*e2f2*). Upon the discovery of zCtg37A, we proceeded to primarily utilize the Sanger genomic sequence surrounding this marker for candidate selection. A substantial amount of sequence prediction data is provided with each Sanger

assembly release, including GENSCAN open reading frame prediction and EST, cDNA, and homology alignments with the genomic sequence. Currently we are in the process of cloning and sequencing an additional four candidates: putative homologs of *claudin*, *connector enhancer of kinase suppressor of ras 1* (*cnk1*), and *grainyhead-like 3* (*grhl3*) as well as the PHD zinc finger domain *phf17*. These candidates were isolated from sequence data associated with the genomic releases in close proximity to zCtg37A (Figure 41).

3.1.1 Growth and differentiation factor 7 (gdf7)

The earliest candidate analyzed was found on the MGH mapping panel found on ZFIN (Sprague *et al.*, 2001) between LG17 markers z22016 and z15715. *Gdf7*, a member of the TGF-ß superfamily of transcription factors, has been partially cloned by Davidson *et al.* (1999). During development, g*df7* can be amplified by RT-PCR in embryos approximately 5 through 120 hpf. At 48hpf transcripts are found in the precartilage condensations of the head, neurocranium, dorsal aorta in the trunk and the pronephros (Davidson *et al.*, 1999). Additionally other members of this family have been implicated in fin development (Bruneau *et al.*, 1997; Delot *et al.*, 1999; McPherron *et al.*, 1999). Based on these previously published data, *gdf7* appeared to be an appropriate candidate for *m196*. Using SSCP analysis we found a polymorphic fragment in the putative 3'UTR of the 2,404 bp *gdf7* partial coding sequence. We found *gdf7* remained recombinant with at least four of the mutant genomes recombinant with flanking marker z26685, therefore the mutation is not fully linked to *gdf7*. At the time this earliest candidate was tested only four z26685 recombinants had been recovered and

were subsequently tested with this candidate. Thus although possibly located within the critical interval, *gdf7* was not tested further. Its current placement within the meiotic map is unknown and is consequently not included within our up-to-date meiotic map.

3.1.2 Novel gene 1 *(ng1)*

The next potential candidate was identified from a predicted novel translation from a Fall 2003 release of the Sanger zebrafish genome assembly. Based on meiotic mapping results, we predicted the mutation to be located between z30467 and z26685 sequences found in the genomic release. Within approximately 84 kb (0.14 cM) of z30467 were a number of predicted novel translations supported by homology alignments with the teleost pufferfish *Takifugu rubripes*, mouse and human. ENSDARG00000006645, which we termed *novel gene 1*, encodes a 1,557 bp coding sequence containing a fibronectin type III domain as predicted by Sanger sequence analysis. We confirmed the location of *ng1* on LG17 by using the LN54 radiation hybrid panel to map this candidate to the 235.29 cR position (Figure 40). The fibronectin protein is an important factor in cell adhesion and is expressed in zebrafish in the somitic boundaries as well as dorsal trunk at 24hpf (Crawford *et al.*, 2003). It has been implicated in directing neural crest migration in mouse, chick, *Xenopus* and axolotl (Epperlein *et al.*, 1988). Specifically in *Xenopus*, fibronectin was found in the extracellular matrix lining the neural crest migration pathway before and during their migration. Therefore, based on these data, we considered the

fibronectin domain-containing novel gene *ng1* to be an interesting candidate for the *m196* mutation.

Ng1 was concurrently cloned, sequenced, and mapped using SSCP. The coding sequence of *novel gene 1* was amplified by RT-PCR from wild type strains AB and TL, as well as 2 *m196* homozygous embryos at 25 and 36 hpf. These fragments were then cloned and sequenced. Alignment of the resulting sequences together with the sequence from the genome release revealed no subsequent defect in *m196* compared to wild type strains. A polymorphic marker for SSCP analysis was found within the predicted 3'UTR of *ng1*. Mapping revealed that *ng1* retains 6 recombinants of z9831, including the three mutant genomes recombinant with z30467 (Figure 42). Therefore this predicted novel gene is located 0.28 cM away from *m196* outside of the critical interval between z30467 and z9831, and contains no *m196*-specific mutation within the coding sequence.

3.1.3 Inhibitor of DNA binding/differentiation 3 (id3*)*

Mapped between cR 44.5 and 47.1 of LG17 on the Tübingen radiation hybrid panel (T51) (Geisler *et al.*, 1999) is *inhibitor of DNA binding/differentiation 3* (*id3*) (Dickmeis *et al.*, 2002). The ID family of helix-loop-helix proteins are well characterized in *Drosophila* as the *extramacrochaetae (emc*) locus (Ellis *et al.*, 1990; Garrell and Modolel, 1990) and as dominant negative regulators of bHLH transcription factors in mouse (Riechmann *et al.*, 1994). The ID family is implicated in many aspects of development including differentiation and cell cycle regulation (Norton, 2000). In flies, the *emc* locus in part has been found to

regulate wing morphology (Baonza *et al.*, 2000; Baonza and Garcia-Bellido, 1999). Specifically in zebrafish the role of *id3* is not yet elucidated but is known to be expressed in late- and post-somitogenesis in the cephalic neural crest and pectoral fin buds as well as many structures of the developing brain, eye and kidney (Dickmeis *et al.*, 2002). Moreover homologs of *id3* are found in regions syntenic to zebrafish LG17 on *Fugu* Scaffold_137 from the *Fugu* sequencing project, mouse Chromosome 4 (MCh4), and human Chromosome 1 (HCh1) (Figure 43). Therefore because of its genomic location, expression pattern, and role in differentiation in other organisms *id3* is a very good candidate for the *m196* mutation.

This candidate was concurrently cloned, sequenced and mapped by SSCP in search of the *m196* mutation. In order to confirm the location of *id3* on LG17 we mapped the gene to the 244.42 cR position on the LN54 RH map. The wild type AB and TL and 2 separate *m196* transcripts of the candidate at 25 and 36 hpf were amplified by RT-PCR. Alignment of sequences from these cloned transcripts showed no difference between wild type and mutant *id3*. Polymorphic markers were isolated within the 3' UTR of the *id3* coding sequence and SSCP analysis of this marker revealed that *id3* shares 3 recombinants with z26685. Therefore *id3* transcripts contain no *m196*-specific mutation based on sequence alignments. Furthermore although the candidate is not completely linked to the *m196* allele, it maps within the critical region, closing the interval to 0.28 cM between it and flanking marker z30467.

3.1.4 Putative e2f2 *homolog*

The zebrafish putative homolog of human *E2F2* was also found within the Sanger genomic sequence on LG17 (Figure 41) as well as in syntenic regions in mouse, human and *Fugu* (Figure 43). This transcription factor binds the E2 recognition site found in the promoter region of genes commonly involved in cell cycle control or DNA replication *in vitro* (Ivey-Hoyle *et al.*, 1993). Polymorphic markers for SSCP analysis were found in the 3'UTR of the Sanger predicted coding sequence. Results of this analysis revealed the predicted *e2f2* gene retains 6 recombination events from those of flanking marker z26685 and is 0.28 cM away from *m196*. Therefore *e2f2* is located outside the critical region flanked by z30467 and *id3* is not fully linked to the *m196* mutation.

3.1.5 Putative claudin *homolog*

Upon discovery of the marker zCtg37A and the release of a more consistent and complete Sanger genomic release in Winter 2004, further SSCP mapping of candidates was deemed unnecessary. Located between z30467 and zCtg37A is the GENSCAN-predicted open reading frame (ORF) GENSCAN0000004736 (Figure 41). This GENSCAN data is substantiated by TBLASTX analysis of the translated coding sequence which finds homology with *Fugu claudin 23b* translated gene (AY554345, 57% identity), mouse *Claudin 23* translated cDNA clone (BC085262, 28% identity) located on MCh8, and human *CLAUDIN 23* translated cDNA (BC016047, 25% identity) located on HCh8.

Claudins are single or multiple exon genes of the tetraspanin superfamily encoding major transmembrane proteins of tight junctions. They are known to

play an important role among vertebrates in cell adhesion and migration of epithelial tissues (Kollmar *et al.*, 2001). Currently, there are over a dozen homologous Claudin proteins found for human, mouse, zebrafish, and pufferfish (Kollmar *et al.*, 2001; Loh *et al.*, 2004). *Claudin 23b* in *Fugu* has been identified in preliminary studies to be expressed only in adult intestine and muscle tissues by RT-PCR (Loh *et al.*, 2004), however detailed expression patterns during teleost development have not been analyzed to date. During development a number of *Claudins* in mouse, such as *Cldn4* and *Cldn6*, are expressed in the branchial arches and forelimbs (Kollmar *et al.*, 2001). In *Xenopus* development *cldna* is expressed in regions dramatically similar to those proposed to be affected in the *m196* mutation namely the branchial arch endoderm and dorsal neural epithelium of the tail tip, along with the otic vesicle and pronephros (Brizuela *et al.*, 2001). Over 15 *claudins* have been found in zebrafish, only two of which, *cldna* and *cldnb*, have been at all characterized to date (Kollmar *et al.*, 2001). Since zebrafish *claudin* function remains unknown, it is possible this predicted protein represents a yet unidentified member of the tight junction protein family.

Our putative *claudin* sequence aligns with none of the currently published zebrafish *claudin* sequences. We were able to amplify the 675 bp predicted single exon coding sequence in wild type AB and TL as well as mutant embryos at 25 and 36 hpf by RT-PCR. We can therefore conclude that this ORF is in fact expressed in zebrafish during development at these stages. Although an excellent candidate located close to the marker zCtg37A, cloning and

subsequent sequencing of this predicted novel zebrafish *claudin* coding sequence showed no mutant-specific differences within the *m196* mutant sequence compared with wild type AB and TL. This however does not rule out the possibility of a base pair change within promoter or regulatory sequences upstream. *In situ* hybridization analysis is currently underway in order to determine if this putative *claudin* is expressed in the zebrafish embryos whether ubiquitously or differentially. Therefore this putative *claudin* remains a hopeful candidate for the gene affected in the *m196* mutants despite its wild type in coding sequence.

3.1.6 Putative connector enhancer of KSR 1 *(*cnk1*) homolog:* est3

zCtg37A is in fact located directly within a predicted intron of the zebrafish EST sequence ENSDESTT00000026153 (Figure 41). BLAST analysis partially aligns this EST with a large 3,816 bp, uncharacterized mRNA sequence in zebrafish zgc:77200 (BC065587). Further BLAST analysis of this mRNA shows homology of the translated partial coding sequence to human Connector Enhancer of Kinase Suppressor of RAS 1 (CNKSR1), also known as CNK1 (AF100153, 33% identity), and mouse predicted Cnksr1 (XM_110525, 33% identity). These genes are also located in regions on HCh1 and MCh4 syntenic to LG17, and a putative *cnk1* is found in the syntenic region of *Fugu* Scaffold_137 (Figure 43). CNK1 was first isolated in *Drosophila* as a component of the RAS/MAPK (mitogen-activated protein kinase) pathway and was found to play a role in the activity and/or cellular localization of RAS-activated RAF (Therrien *et al.*, 1998). Mutant phenotypes in *Drosophila* show CNK1 to be essential for wing and eye formation

(Therrien *et al.*, 1998). Although this gene has yet to be identified in zebrafish, the regulation of the RAS/MAPK pathway plays an essential role in teleost development, particularly as an important component of the fgf signaling pathway (Tsang *et al.*, 2004). Disruption of the inhibitory pathway of FGF/RAS/MAPK signaling leads to defects in dorsoventral patterning in early zebrafish development (Tsang *et al.*, 2004) and defects in posterior neural specification in *Xenopus* (Ribisi *et al.*, 2000). Therefore especially considering the defects in *fgf8* signaling found within the posterior region of *m196* mutant embryos, this putative partial *cnk1* EST sequence, termed "*est3*", is an interesting candidate to be involved in the mutant phenotype.

The 250 bp *est3* fragment was amplified in wild type and *m196* embryos at 25 and 36 hpf by RT-PCR. We obtained cloned transcripts for wild type strains AB and TL as well as 2 copies of *m196* for initial sequence comparisons. GENSCAN and novel translation results, compared with a known zebrafish cDNA zgc:77200 (Strausberg *et al.*, 2002) with which *est3* partially aligns, give conflicting data as to the correct and full transcript. Although the full transcript of this candidate is currently unknown, our ability to amplify *est3* by RT-PCR suggests it is in fact expressed in zebrafish at this stage in development. Alignment of these preliminary wild type and mutant sequences reveals no *m196*–specific base pair change in this short sequence. When aligned with the Sanger genome sequence, the zgc:77200 mRNA sequence spans over 200 kb of genomic region. As well, *est3* only partially aligns with a small portion of this mRNA, yet we are able to amplify the entire sequence by RT-PCR. Therefore

further experiments are necessary in order to clarify these inconsistencies regarding the expressed sequence. 5' and 3' RACE experiments are currently underway to obtain the full coding sequence of this gene.

3.1.7 Phf17

Another candidate located on the Sanger genome sequence between z30467 and zCtg37A is the zebrafish *phf17* (BC046874; Figure 41). Known as *Jade1* in mouse, it encodes a PHD zinc finger protein involved in anteroposterior axis development. *Jade1* is expressed in mice during organogenesis and later fetal development, specifically in the neural tube, somites, primitive streak, facial muscle, limb bud muscle and around the digits, chordal neural hinge of the tail bud, heart, liver, and optic vesicle (Tzouanacou *et al.*, 2003). Murine homozygous *Jade1* null mutants are however viable and fertile. Additionally human, mouse and pufferfish homologs of *phf17* are not found within regions syntenic to LG17 (Figure 43). Nevertheless the expression pattern of *Jade1* during organogenesis, particularly in the face, limb bud, and tail, does not allow us to rule out its zebrafish homolog *phf17* as a candidate.

Analysis of the zebrafish phf17 protein sequence shows significant conservation between human (NM199320, 49% identity), mouse (NM172303, 49% identity) and putative *Fugu* (SINFRUG00000138885, 56% identity) translations. The 3,172 bp transcript contains two PHD zinc finger domains and one bipartite nuclear localization signal (Figure 44A). We cloned the *phf17* coding sequence in four overlapping fragments due to its large size. Sequencing of wild type AB and TL as well as two *m196* transcripts reveals a mutant specific

modification at base pairs 1777 and 1778 from adenine and cytosine to two thymines, changing residue 554 from a threonine (T) to a leucine (L) (Figure 44). However this segment of the protein is not found within regions conserved between mouse, human or *Fugu*. In fact the aligned residue in the pufferfish corresponding to the zebrafish residue 554 is found to be a leucine. Nonetheless motif prediction of the zebrafish protein suggests the presence of a putative proline-directed kinase phosphorylation site between residues 552 and 558 and/or a putative motif recognized by class 1 SH3 domains between residues 553 and 559. Since the pattern of *phf17* expression in zebrafish is to date unpublished, we are in the process of assessing embryonic expression of *phf17* by ISH in order to determine whether transcripts can be found in the affected structures. Despite the preliminary identification of the *m196*-specific base pair change resulting in an amino acid transformation, confirmation of *phf17* as the mutated gene causing the *m196* phenotype is dependent on expression and possible rescue experiments.

3.1.8 Putative grainyhead-like 3 *(grhl3) homolog*

The final candidate we are currently analyzing is based on a cluster of EST sequences located between z30467 and zCtg37A (Figure 41) including ENSDARESTG00000005566, wz8070, and I.M.A.G.E. clone 7001816. A 1741 bp consensus sequence of these ESTs, containing 15 predicted exons, was obtained through sequence alignment analyses of these ESTs. BLAST analysis of the translated sequence produces significant identity to both mouse (53% identity) and human (53% identity) Grainyhead-like 3 (Grhl3) proteins, also

known as Sister-of-Mammalian Grainyhead (SOM) or transcription factor CP2-like 4 (Tfcp2l4). The mouse and human *Grhl3* homologs are also located in syntenic regions of MCh4 and HCh1 respectively (Figure 43). The *Grainyhead*-like family of developmental transcription factors found in mouse and human consists of a number of phylogenetically related *Grh*-like homologs in mammals including *Grhl1* (also known as *Mammalian Grainyhead* (*MGR*)), *Grhl2* (also known as *Brother-of-MGR* (*BOM*)), and the recently cloned *Grhl3* (Ting *et al.*, 2003b). The three *Grhl3* isoforms in human show unique restricted expression patterns including adult brain, pancreas, testis, placenta, prostate, colon and kidney (Ting *et al.*, 2003b). During development *Grhl3* is expressed in mouse within the neural folds during neural tube folding and later in the entire surface ectoderm. Transcripts are also found in other tissues lined with squamous epithelium such as the oral cavity, urogenital sinus and the anal canal (Ting *et al.*, 2003a). *Grhl3* null mutant mice exhibit defects reminiscent of the tissues affected in *m196* mutants. Not only are the *Grhl3*$^{-/-}$ null embryos smaller in size, all display spina bifida and a curled tail (Ting *et al.*, 2003a). Ting and colleagues (2003a) have implicated *Grhl3* as a primary candidate affected in the *curly tail* mouse mutation, used as a model for neural tube defects for decades (Gruneberg, 1954). In fact, dominant negative expression of the epidermally-expressed *Xenopus grhl1* results in a poorly differentiated and bulky peridermis and partially collapsed pharynx (Tao *et al.*, 2005). Although the amphibian fin fold is only slightly affected in these mutants, these results are comparable to the

observed *m196* phenotype and implicate the *grhl* gene family in similar developmental processes.

The *Grainyhead, Grainyhead-like*, and *CP2* gene families contain a highly conserved DNA binding domain (DBD) and dimerization domain (DD) with a much less conserved N-terminal sequence (Kudryavtseva *et al.*, 2003). Through amino acid sequence alignments between human and mouse *grhl3* proteins we have predicted DBD/DD region to be located within the last 372 amino acids of the putative protein (Figure 45). We have cloned and sequenced transcripts of a wild type TL and *m196* mutant by RT-PCR. Sequence analysis reveals an *m196*-specific cytosine (C) to guanine (G) mutation within base pair 718, which changes residue 239 from a tyrosine (Y) to a stop (*; Figure 45). This nonsense mutation is located within the predicted DBD, creating a truncated protein lacking a significant amount of the DBD and DD region. Despite the *m196*-specific mutation within *phf-17*, the nonsense mutation within a highly conserved amino acid of the putative *grhl3* transcript, coupled with the *Grhl* expression pattern and phenotype within *Grhl* mouse and frog mutants, provides significant evidence that this candidate is involved in the *m196* mutation. We have currently begun expression analysis and rescue experiments in order to determine if this base pair change does in fact play a role in the *m196* phenotype.

3.2 Positional cloning using large genomic PAC clones

In order to positionally clone the *m196* mutation, we set out to obtain a series of large genomic clones spanning the critical interval created by meiotic mapping illustrated in Figure 39. Positional cloning experiments were initially based on

flanking markers and mapped candidates associated at the time with the critical interval. For example, prior to the complete mapping of *ng1* we used this gene to probe the genomic library for PAC clones within the region and obtained PAC ng1.2 and ng1.4 (Figure 46). Before mapping zCtg37A, we used the two mapped flanking elements, z30467 and *id3*, to screen the PAC library. We have obtained 3 clones associated with z30467 which we called PAC21, -23, and -24. Probing the library with *id3* we were able to isolate 2 clones: PACid3.5 and PACid3.6. The clone ends sequenced from the T7 and SP6 promoters of all 6 clones were found on LG17 within the Sanger zebrafish genome sequence by SSAHA analysis. The sequence fragments of PAC23 and PAC24 determined from SP6-end sequences were mapped using SSCP analysis. The PAC23 SP6 clone retains only 2 of the z30467 recombinants and therefore maps 0.095 cM away from the *m196* mutation within the critical interval. The PAC24 SP6 end retained all 3 recombinants for z30467 and was not tested any further. Thus this PAC end maps at least at, if not beyond, the interval border created by this flanking marker. These results however confirm the proximity of the PAC ends within the critical interval and reduce the meiotic distance between flanking markers to a mere 0.235 cM.

Upon discovery of the zCtg37A marker, we screened the PAC-based library with this marker for clones spanning the genomic region and isolated a single clone we termed PACB. This genomic clone does not overlap with any of the sequenced ends of clones isolated from flanking markers z30467 and *id3*, suggesting that there are still genomic regions not covered by the current PACs

at hand. However we are able to amplify all current candidates including *est3* and putative zebrafish homologs of *claudin* and *phf17* from PACB, therefore not only does this confirm the isolation of the correct genomic region, this clone contains a sufficient amount of the critical region surrounding zCtg37A for our purposes. At this point a further search for genomic clones is unnecessary.

Figure 41: The current genomic region of LG17 spanning the linked marker zCtg37A. Cartoon of the genomic sequence of LG17 from megabases (Mb) 15.00 to 15.60 based on the contemporary Sanger sequencing project assembly. Alternating light and dark blue stripe represents assembled Sanger contigs. Red lines mark mapping boundaries created by PAC23 SP6, zCtg37A, and *id3*. Coloured blocks represent annotated ESTs, GENSCANs, and Ensembl novel translations. Elements in quotations denote putative identities based on Sanger comparison data. Asmt, acetylserotonin O-methyltransferase; e2f2, e2f transcription factor 2; grhl3, grainyhead-like 3; id3, inhibitor of differentiation/DNA binding 3; recs, recombinants; rps6ka1, ribosomal protein S6 kinase polypeptide 1. Black blocks labelled 'unknown' represent ESTs, GENSCANS, and Ensemble novel translation with no predicted homology with genes of known function.

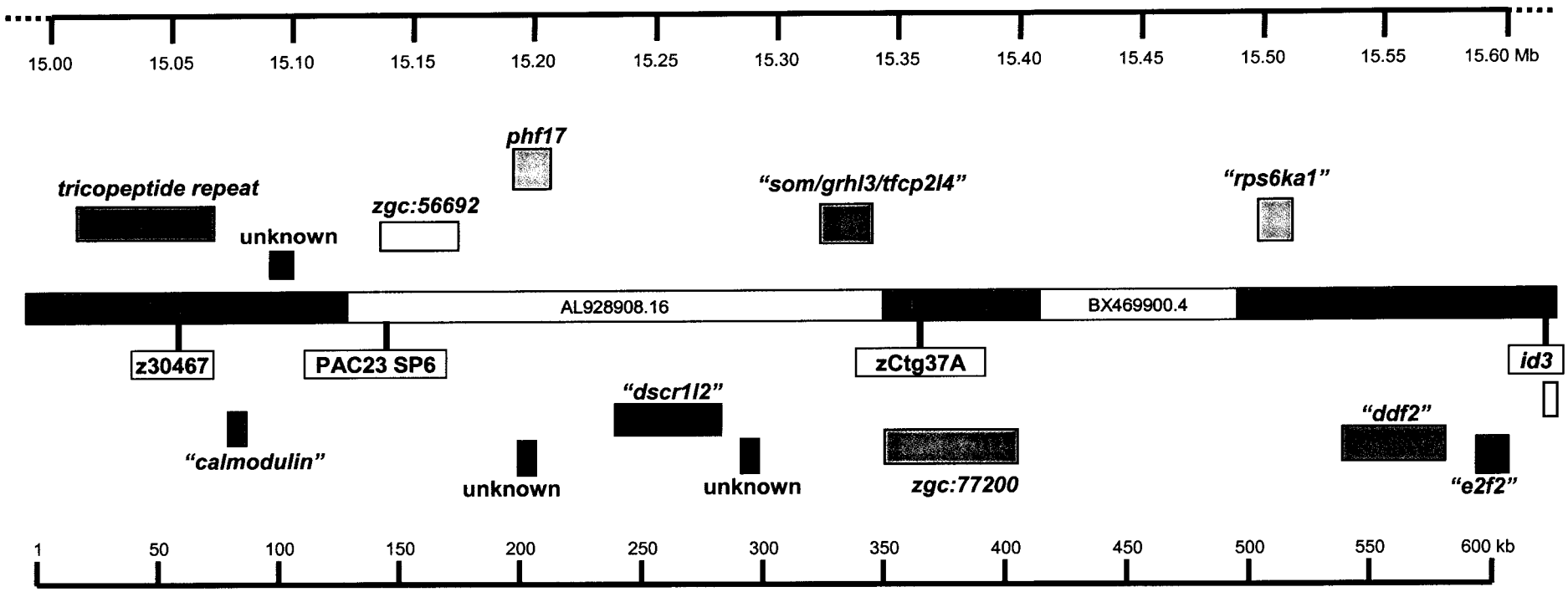
15.00
15.05
15.10
15.15
15.20
15.25
15.30
15.35
15.40
15.45
15.50
15.55
15.60 Mb
phf17
tricopeptide repeat
zgc:56692
"som/grhl3/tfcp2l4"
"rps6ka1"
unknown
AL928908.16
BX469900.4
z30467
PAC23 SP6
zCtg37A
id3
"dscr1l2"
"ddf2"
"calmodulin"
unknown
unknown
zgc:77200
"e2f2"
1
50
100
150
200
250
300
350
400
450
500
550
600 kb

Figure 42: Example of SSCP analysis: *novel gene 1* maps beyond the critical interval on the side of z30467. Separation by polyacrylamide gel electrophoresis of polymorphic alleles of *novel gene 1* amplified from the putative 3' UTR. Lanes 1-3 show fragments amplified from homozygous wild type TL/TL, heterozygous *m196*/TL and homozygous *m196*/*m196* respectively. Lanes 4-6 show fragments amplified from the three z30467 recombinants. Lanes 7-15 show fragments amplified from the recombinants associated with z26685.

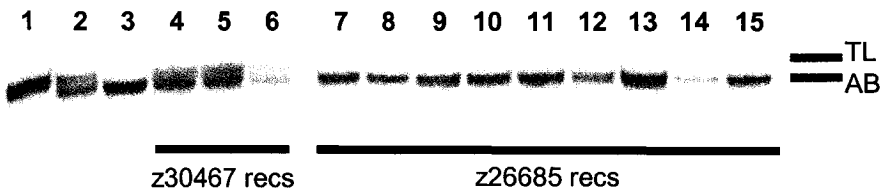
1 2 3 4 5 6 7 8 9 10 11 12 13 14 15
TL
AB
z30467 recs
z26685 recs

Figure 43: Comparative map of the regions of mouse, human, and pufferfish syntenic with zebrafish LG17. *Danio rerio* Linkage Group 17 (LG17). *Mus musculus* Chromosome 4 (MCh4). *Homo sapien* Chromosome 1 (HCh1). *Takifugu rubripes* Scaffold_137. ddf2, development and differentiation enhancing factor 2; dscr1l2, down syndrome candidate region gene 1-like 2 (calcipressin 3); e2f2, e2f transcription factor 2; id3, inhibitor of differentiation/DNA binding 3; grhl3, grainyhead-like 3; prox1, prospero-related homeobox 1; rps6ka1, ribosomal protein S6 kinase polypeptide 1.

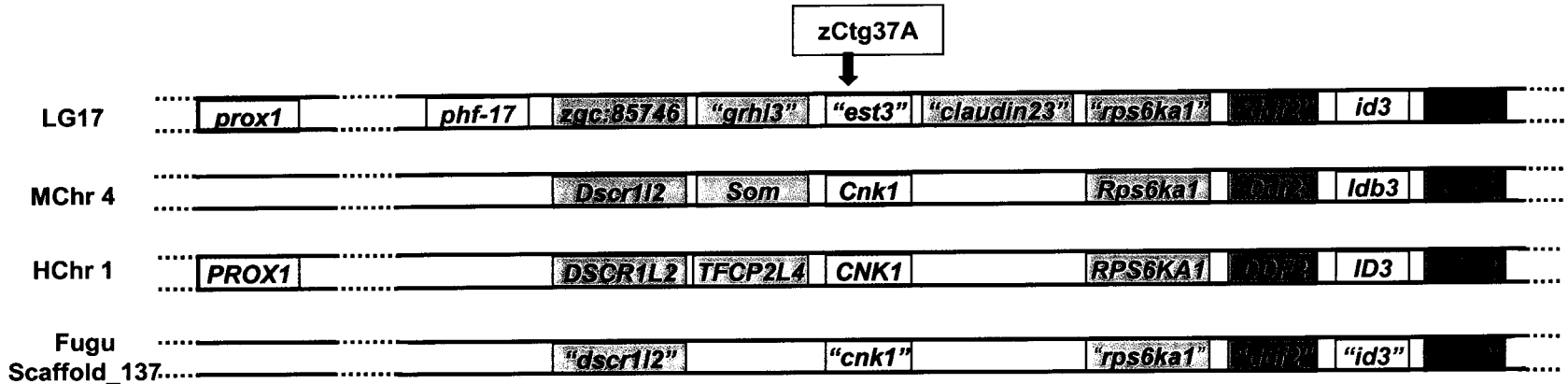
zCtg37A
LG17
prox1
phf-17
zgc:85746
"grhl3"
"est3"
"claudin23"
"rps6ka1"
id3
MChr 4
Dscr1l2
Som
Cnk1
Rps6ka1
Idb3
HChr 1
PROX1
DSCR1L2
TFCP2L4
CNK1
RPS6KA1
ID3
Fugu
Scaffold_137
"dscr1l2"
"cnk1"
"rps6ka1"
"id3"

Figure 44: Phf17 contains an *m196* mutant-specific alteration changing residue 554 from a threonine to a leucine. (A) Cartoon of the 831 amino acid phf17 protein including 2 zinc finger-like PHD domains and a bipartite nuclear localization signal. (B) Chromatograph of wild type TL, AB and *m196* mutant cDNA sequences between base pairs 1771-1796 and amino acids 552-560. Black rectangle outlines base pairs 1777 and 1778 in each sequence.

A

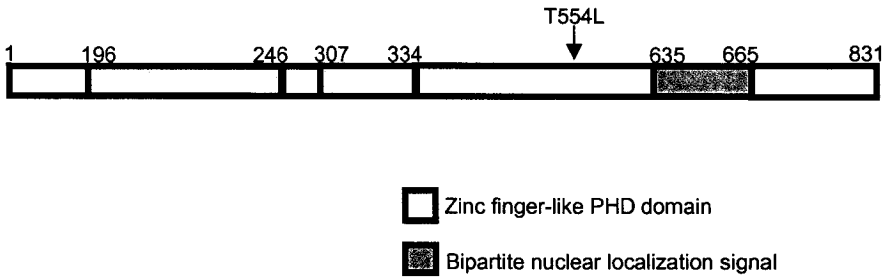
T554L
1
196
246
307
334
635
665
831
Zinc finger-like PHD domain
Bipartite nuclear localization signal

B

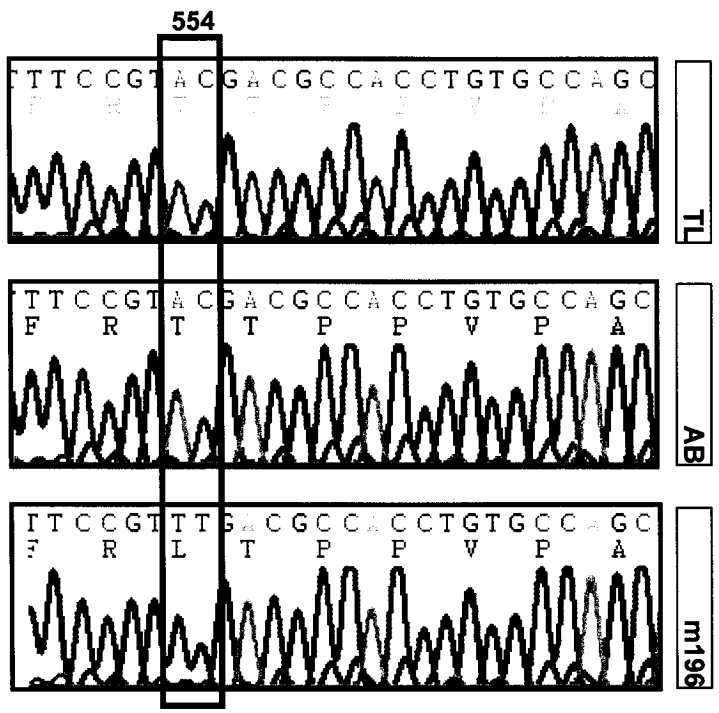
554
TTCCGTACGACGCCACCTGTGCCAGC
TL
TTCCGTACGACGCCACCTGTGCCAGC
F R T T P P V P A
AB
TTCCGTTTGCGCCACCTGTGCCAGC
F R L T P P V P A
m196

Figure 45: Grhl3 contains an *m196* mutant-specific alteration changing residue 239 from a tyrosine to a stop. (A) Cartoon of the grhl3 protein including a DNA binding domain and dimerization domain comprising the 372-amino acid C-terminus. (B) Chromatograph of wild type TL and *m196* mutant cDNA sequences between base pairs 710-724 and amino acids 237-241. Black rectangle outlines residue 239 in each sequence.

A

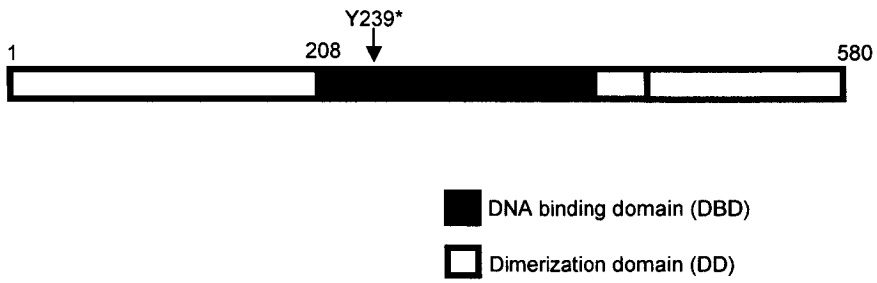
Y239*
1
208
580
DNA binding domain (DBD)
Dimerization domain (DD)

B

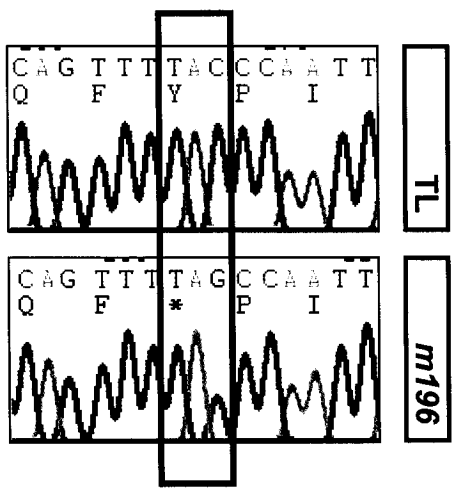
C A G T T T T A C C C A A T T
Q F Y P I
TL
C A G T T T T A G C C A A T T
Q F * P I
m196

Figure 46: Positional cloning of the m196 mutation. Meiotic map of the region spanning the m196 mutation including genomic PAC clones. Colored horizontal lines represent PAC clones isolated from library screening experiments. PAC ng1.2 and ng1.4 were isolated by probing with candidate *ng1*. PAC 21, 23 and 24 were isolated by probing with z30467. PAC id3.5 and id3.6 were isolated with *id3*. *E2f2* is also found on PAC id3.6. PAC B was isolated by probing with zCtg37A. The position of SP6 and T7 sequenced ends were estimated by searching the Sanger genomic sequence. Recs, recombinants.

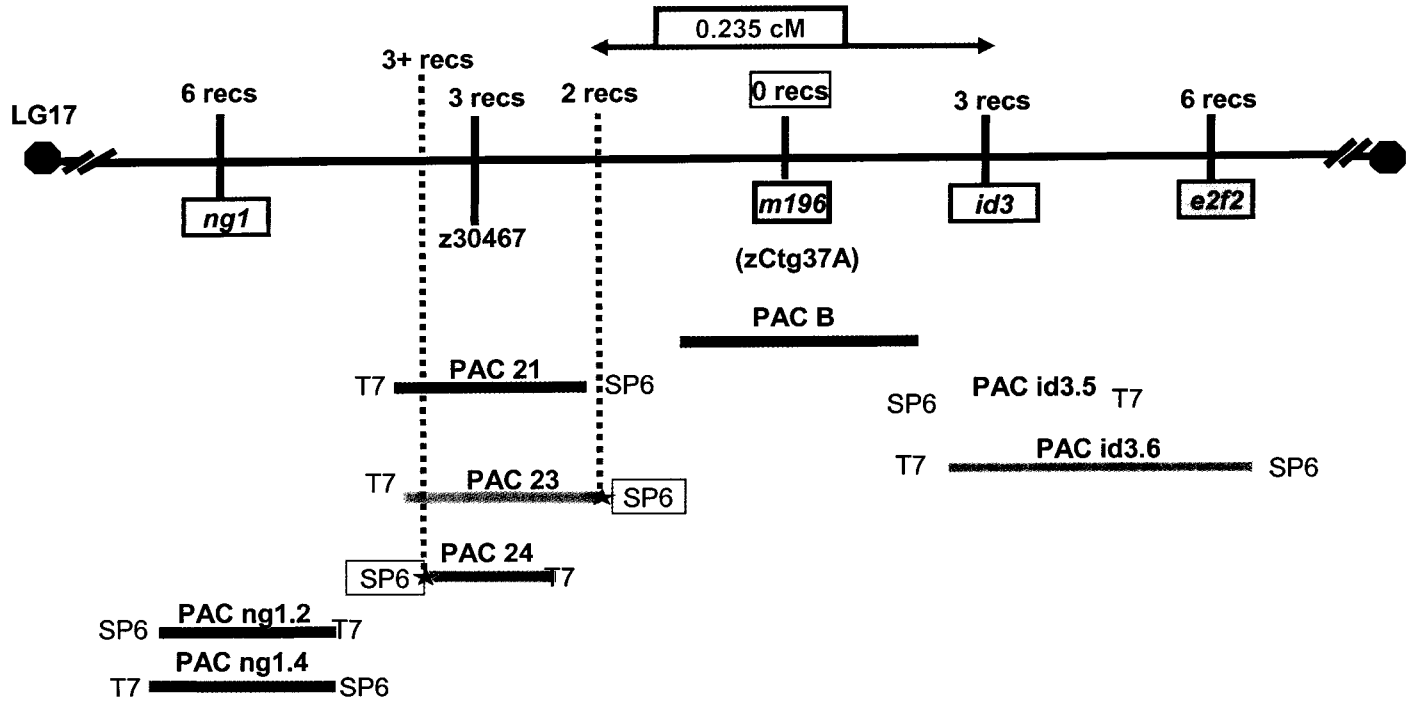
0.235 cM
3+ recs
6 recs
3 recs
2 recs
0 recs
3 recs
6 recs
LG17
ng1
z30467
m196
(zCtg37A)
id3
e2f2
PAC B
T7
PAC 21
SP6
SP6
PAC id3.5
T7
T7
PAC id3.6
SP6
T7
PAC 23
SP6
SP6
PAC 24
T7
SP6
PAC ng1.2
T7
PAC ng1.4
T7
SP6

IV. Discussion

In recent years zebrafish has become an invaluable tool for the study of human disease. Mutant analysis has led to much of our current understanding of genetic regulation during embryogenesis. Powerful tools, such as a large number of mutant zebrafish lines, genetic maps and mapping techniques, as well as gene knockdown technologies, have been and will continue to shed light on the genetic etiology of developmental diseases (Dooley and Zon, 2000; Penberthy *et al.*, 2002).

The *m196* mutant phenotype includes a variable disruption in craniofacial cartilage differentiation, an initial displacement of pharyngeal endoderm, and loss of proper median and pectoral fin fold extension. The variability in phenotype leads us to believe that the *m196* mutation is not in fact a null allele. Rather it is likely a hypomorphic allele causing a reduction but not a complete loss in gene activity. The eventual recovery in most cases of opercular and pharyngeal pouch lumen formation, proper cartilage differentiation and the development of a substantial amount of pectoral and median fin fold by 8-12 dpf suggests that the disrupted gene activity is significant only within the first few days of embryonic life, but is essential for zebrafish survival. It is possible that within this window of developmental time the affected tissues are competent and open to respond to the affected gene. It may also be the case however that this gene is only active during this specific time period. Maternal contribution of expressed factors until approximately the mid-blastula transition, may also contribute to the variability seen within the phenotype. In fact a stronger and possibly new phenotype can

occur in characterized ENU mutants in which maternal wild type expression of the zygotically mutant gene is lost by complete replacement of the germ line with those derived from homozygous mutants (Ciruna *et al.*, 2002). Thus maternal contribution, retained activity, and/or varying tissue competency or genetic regulation of the affected genetic element may play a role in the variation seen within the *m196* phenotype.

Current results regarding the craniofacial disruption in *m196* mutants remain somewhat elusive. The significant influence pharyngeal endoderm has over cranial cartilage and branchial arch development (see Introduction) may reflect the phenotype we observe in these mutants. In fact the presence of pharyngeal endoderm is necessary to maintain *dlx2* expression in the arches (David *et al.*, 2002). Initial oblong morphology of the branchial arches, determined by *dlx2* expression, mirrors the hyperlateral positioning of the pharyngeal pouches prior to cartilage differentiation. This initial displacement of both structures may play a role in the delay in chondrogenesis found in *m196* mutants. The subsequent normal cartilage formation by 6-8 dpf followed by a small number of 12 dpf embryos with a few non-alcian-stained gill arches suggests that, in a few mutants, some arches are unable to remain differentiated. Crowding of the five gill arches found in the *m196* mutants is more than likely associated with the closeness of the pouches prior to cartilage differentiation. This may be caused by a reduction in the number of cells migrating into the pouch and/or arch regions (Schilling and Kimmel, 1994).

The majority of *m196* mutants die on or around 12 dpf from unknown causes. It is unlikely that death is caused solely as a result of the disruption in fin fold development. There are a number of zebrafish mutants in which the disruption of median and pectoral fin fold growth does not hinder development into adulthood such as the *somitabun* dorsalizing mutation (Mullins *et al.*, 1995). In the region of the urogenital opening, just posterior to the yolk on the ventral side, the expression domains of *dlx3* (data not shown) and *msxC* (Figure 30) are expanded in *m196* mutants. These results, along with the early displacement of pharyngeal structures and an absence of an open mouth and pharynx at larval stages (Figure 12), indicate a more involved disturbance in *m196* endodermal formation. In fact a high mortality is normally seen in wild type larvae at approximately 2 weeks of age possibly due to the inability to feed properly (Akimenko, M.A., Knapik, E.W., personal communication). Therefore mortality at 12 dpf in the *m196* mutant may be attributable to an endodermal disruption leading to the inability to ingest or digest sufficient life-sustaining nutrients.

Future characterization of the pharyngeal region will focus on the genetic specification of the anterior endoderm as well as a closer look at the epithelial tissue integrity. A number of genetic markers have been shown to play a role in mouth and pharynx development such as *foxa2/axial* (Strahle *et al.*, 1996), *nkx2.3*, *nkx2.7* (Lee *et al.*, 1996), and *gata5/faust* (Yelon *et al.*, 1999). In fact, disrupted morphogenesis of the pharyngeal pouches similar to that of *m196* is also seen in the *gata5/faust* zebrafish mutants (Yelon *et al.*, 1999). Therefore

analysis of endodermal differentiation will provide insight into the nature of the *m196* phenotype.

The genetic mechanism of median fin fold extension is largely uncharacterized in zebrafish. Although the *m196* mutants display severe disruption in this process within the first few days of development, median fin fold extension is variably, though never completely, recovered by 8-12 dpf. This may reflect a loss of dependence on the factor perturbed in the *m196* mutants and may signal a change in genetic regulation of fin fold development. In fact zebrafish larvae boast the ability to regenerate the median fin fold (Kawakami *et al.*, 2004). Therefore the later partial rescue of the median fin fold disruption in the *m196* mutants may indicate the activation of such a regenerative process.

The results showing that the ventral fin is largely unaffected leads us to believe the *m196* fin fold defect may in fact involve neural crest migration in some way. Neural crest cells have previously been shown to contribute to the zebrafish fin mesenchyme (Smith *et al.*, 1994). In *Xenopus* it has more recently been found that differential cellular contributions populate the dorsal versus ventral fin fold (Tucker and Slack, 2004). Neural crest contribution to the dorsal fin is significant, whereas fewer neural crest cells migrate ventrally and invade the median fin forming area which is contributed to mostly by local mesenchyme (Tucker and Slack, 2004). Although this specific role of neural crest in the dorsal fin has not yet been confirmed in zebrafish, it is highly possible given the homology of the median fin structures in both *Xenopus* and zebrafish. The accumulation of *crestin*-expressing cells and black pigment cells in the posterior

regions of the *m196* tail during fin fold extension as well as ectopic position of these neural crest-derived melanocytes into the posterior-most fin fold suggests that migration of these cells is misguided in this region. The lack of dorsal fin fold and shortened tail length is also similar to that seen in 48 hpf zebrafish embryos in which the neural crest cells from the 14-26 somite level were ablated at approximately 20 hpf (Vaglia and Hall, 2000). Therefore the misexpression or absence of cell migration factors along the neural crest cell pathway may contribute to the median fin defect and account for the comparatively more wild type ventral fin fold development in the *m196* mutants.

The similar defect in anterior endodermal lumen formation and pouch migration and posterior epidermal fin fold extension suggests there may be a similar mechanism facilitating these epithelial cell movements. Both tissue movements rely on specific surrounding matrix elements for proper migration. This process often involves attractive or repulsive signals from surrounding tissues to guide movement. The ectopic pouch location may also be the result of the collapse of the main pharyngeal cavity or foregut. This however does not explain the eventual more medial position of the pouches at 2 dpf. Pharyngeal pouches may require such chemotactic cues for migration (Crump *et al.*, 2004a). The hyperlateral pouch migration in *m196* mutants prior to 2 dpf could be attributable to a loss of some factor from the surrounding branchial arches. Chick pouch movements have been found to involve the adhesion and migration protein N-cadherin (Quinlan *et al.*, 2004). Although they are reported to have no pharyngeal pouch or branchial arch defects, the zebrafish *parachute* mutants,

encoding a truncated N-cadherin, include a loss of the dorsal-most median fin fold (Lele *et al.*, 2002), a phenotype similar to that of the *m196* mutant. Additional adhesion molecules are found in dorsal trunk neural crest pathways in amphibians (Epperlein *et al.*, 1988) while some are actually differentially expressed in cranial and posterior fin regions during *Xenopus* and zebrafish development (Kollmar *et al.*, 2001; Loh *et al.*, 2004). Cross fibers within the ECM between early epithelial folding in zebrafish may be important for tissue stability (Dane and Tucker, 1985). Considering the presence of a large number of cells expressing fin fold-specific genes in the *m196* mutant, defects in epithelial tissues are more likely an effect of compromised tissue integrity than a disruption of the genetic signaling pathways necessary for fin differentiation. Thus the defects in epithelial and neural crest tissues of the *m196* mutant may reflect a disruption in migration or adhesion factors that mediate the coupled development of craniofacial and fin structure.

Disruption of fgf-signaling, specifically overexpression of *fgf8*, in *m196* mutants may indicate an important secondary defect pertaining to the disregulation of this important pathway. The fgf-signaling pathway is known to play an essential role in all areas affected in the mutants, namely craniofacial (Crump *et al.*, 2004a; David *et al.*, 2002; Trumpp *et al.*, 1999), pectoral fin (Fischer *et al.*, 2003) and posterior body development (Draper *et al.*, 2003; Fuerthauer *et al.*, 2004). Although *fgf8* expression is unaffected in the craniofacial regions of *m196* embryos, other members of this family involved in anterior development may be disregulated and contribute to the mutant

phenotype. Therefore the *m196* affected gene may play a role in differentially regulating the fgf-signaling mechanism along the anterior-posterior axis.

Future characterization work will focus on the later genetic specification in the median fin fold in order to understand how this structure is able to form in older mutant larvae. The possible initiation of the fin regeneration phenomena may explain this rescue in fin development especially considering the recent research revealing the regenerative capacity of larval fins (Kawakami *et al.*, 2004). Continued characterization of the large variation in pectoral fin fold development in these mutants will also be necessary. A further look at factors defining pectoral fin tissues and fin fold extension, such as the fin fold-specific markers recently cloned by our lab (Padhi *et al.*, 2004), is necessary to shed additional light on this aspect of the *m196* phenotype.

Meiotic mapping has greatly facilitated the identification of candidate genes by limiting the interval of interest on LG17. In spite of the zCtg37A meiotic marker linked to the *m196* allele out of over 2000 meioses, the markers flanking this region help to define the distance along the genome sequence in which the search for candidates can reach. Based on a map resolution of 0.1 cM (Knapik *et al.*, 1998), it is unlikely that cloning of the *m196* allele would be further facilitated by shortening the already 0.235 cM region surrounding the allele.

Although we have identified a number of PAC clones within the mapping interval including one spanning a substantial amount of sequence around zCtg37A, positional cloning has become almost obsolete with the increasing fidelity of the zebrafish genome sequencing project. Physical isolation of the

allele-containing genomic region is more and more unnecessary when genes can be easily identified and amplified based on published sequence. Therefore we have stopped short of officially completing a contig assembly spanning the critical interval.

A number of candidates are already ruled out within the critical region, but a few with great potential remain. It is unnecessary to determine linkage of these remaining candidates to the *m196* mutation due to their close proximity to zCtg37A within the genome. Previously published studies on the homologs of remaining candidate genes- the putative *claudin*, putative *cnk1*, *phf17*, and putative *grhl3*- provide substantial evidence illustrating their suitability as candidates for the *m196* mutation. The role of Claudins in cell adhesion could explain the defects in cell migration within the branchial and fin fold tissues in *m196* mutants, particularly when coupled with the dramatic expression of *Xenopus claudin* (Brizuela *et al.*, 2001) in tail bud stage embryos within these regions. Similarly, CNK1 and FGF are both involved in the RAS/MAPK pathway in human and zebrafish (Therrien *et al.*, 1998; Tsang *et al.*, 2004). Defects in the putative *cnk1* homolog could therefore explain components of the *m196* phenotype particularly the overexpression of *fgf8* expression in the tail. Finally, despite the presence of a possible *m196*-specific mutation in an unconserved, putative phosphorylation site within *phf17*, the nonsense mutation found within a highly conserved residue of the putative zebrafish *grhl3* homolog may be an exciting candidate for the *m196* mutant phenotype. Mouse *Grhl3* is expressed in the neural folds and epithelial tissues and has been proposed to play a role in the

neural tube defect mouse model (Ting *et al.*, 2003a). Although no neural tube defect has been observed in *m196* mutants, possibly due to the fact that zebrafish neural tube development involves neural keel cavitation (Kimmel *et al.*, 1995) rather than neuroectodermal folding, it may indicate a unique role for *grhl3* in zebrafish and be a useful model for understanding the mechanisms of *grhl3* activity. Additionally, coupled with its expression in frog, the significant phenotypic similarity between the dominant negative expression of *grainyhead-like* family member *Xgrhl1* (Tao *et al.*, 2005) and the *m196* mutant also supports the involvement of this candidate. Thus the current candidates, particularly the latter mentioned *grhl3*, each provide substantial evidence pointing to a possible participation in the *m196* phenotype.

Although coding sequence dissimilarities are not found between the wild type and mutant sequences of some current candidates, point mutations within the untranslated regions (Pesole *et al.*, 2001), introns (Muller *et al.*, 1999), or intergenic regions (Ghanem *et al.*, 2003) have the potential to affect the regulation of transcription, translation or degradation of resulting gene products. The search for such mutations is however rather difficult and tedious due to the fact that these sequences are less conserved between zebrafish strains and between species. Therefore determining mere polymorphisms from *m196*-specific mutations within such genomic sequence will only be initiated after coding sequences of all the current surrounding candidates have been screened. This also outlines the importance of expression analysis and rescue experiments,

the results from which may provide evidence for the role of the gene of interest in the *m196* mutation.

In situ hybridization experiments are in the process of being carried out for all contemporary candidates. Temporally appropriate expression of these genes within the affected regions provides a good indication of their role in zebrafish development. The tissue- and time-specific phenotype of the *m196* mutation suggests that the genetic element affected is also expressed in such a manner. Although transcripts could potentially be found ubiquitously throughout the embryo and/or throughout development, redundant expression of other members of the same gene family may compensate for the lack of phenotype in all transcript-containing tissues. As well differential post-transcriptional regulation may play a role in limiting the action of the peptides in an appropriate manner as to create the *m196* phenotype. For example the transcripts of *Jade1*, the candidate *phf17* homolog in mouse, may be alternatively spliced and polyadenylated (Tzouanacou *et al.*, 2003), creating multiple mRNA and protein isoforms. At the same time, conserved sequences, such as PEST domains found within Jade1, may play a role in the rate of protein or transcript degradation (Rechsteiner and Rogers, 1996). Therefore although expression analysis of candidates will be helpful in determining the location of transcripts during development, post-transcriptional regulation could function to alter their ultimate signaling properties.

In order to confirm the isolation of the *m196* mutation within the affected gene, it is necessary to demonstrate that the cloned candidate can functionally

rescue the mutant phenotype. This is accomplished by injection of a wild type mRNA or DNA copy of the coding sequence in question into one-cell stage fertilized zygotes from a single cross of two adult fish heterozygous for the mutation (Fishman *et al.*, 1997). This should result in at least a partial phenotypic rescue of the defects within the 25% of resultant progeny with the mutant phenotype. A large genomic PAC or BAC clone can also be injected in the instance that a candidate has not yet been isolated (Yan *et al.*, 1998). This would confirm the isolation of genomic area containing the mutation and would justify further analysis of the cloned region.

A powerful approach to confirming the mutant genotype versus phenotype would be the ability to reiterate the original mutation by generating an independent loss-of-function mutant. Synthetically-designed antisense oligo-nucleotides called morpholinos, injected into one- or two-cell stage zebrafish embryos, can bind to mRNA and block subsequent translation causing the functional knockdown of the targeted gene (Nasevicius and Ekker, 2000; Summerton, 1999). If the candidate is in fact affected in the mutant line, inhibited translation of the candidate protein in wild type embryos will likely phenocopy the mutation. However it should be noted that, given the hypothesis that the *m196* mutation is a hypomorph, these morphants may demonstrate a more severe phenotype. Thus comparison of phenotypes created by morpholino-induced functional knockdown of candidates with the *m196* mutant phenotype will play an important role in verifying isolation of the affected gene.

Based on the conserved mechanisms of branchial arch and paired limb development between species, this study will likely impact our understanding of vertebrate development of these structures. Ultimately the *m196* mutation will lead to the discovery of a gene or genetic element essential for fin and craniofacial development. It will provide new insight into the mechanisms of epithelial tissue movements as well as neural crest cell migration in the posterior embryo and represent an interesting case study for the coupled regulation of fin fold and cranial development.

V. References

Agathon, A., Thisse, C. and Thisse, B. (2003). The molecular nature of the zebrafish tail organizer. *Nature,* **424,** 448-452.

Akimenko, M. A. and Ekker, M. (1995a). Anterior Duplication of the *Sonic hedgehog* Expression Pattern in the Pectoral Fin Buds of Zebrafish Treated with Retinoic Acid. *Developmental Biology,* **170,** 243-247.

Akimenko, M. A., Ekker, M., Wegner, J., Lin, W. and Westerfield, M. (1994). Combinatorial Expression of Three Zebrafish Genes Related to *Distal-less*: Part of a Homeobox Gene Code for the Head. *Journal of Neuroscience,* **14,** 3475-3486.

Akimenko, M. A., Johnson, S. L., Westerfield, M. and Ekker, M. (1995b). Differential induction of four *msx* homeobox genes during fin development and regeneration in zebrafish. *Development,* **121,** 347-357.

Akiyama, H., Lyons, J. P., Mori-Akiyama, Y., Yang, X., Zhang, R., Zhang, Z., Deng, J. M., Taketo, M. M., Nakamura, T., Behringer, R. R., McCrea, P. D. and de Crombrugghe, B. (2004). Interactions between Sox9 and ß-catenin control chondrocyte differentiation. *Genes Dev.,* **18,** 1072-1087.

Amemiya, C. T., Ota, T. and Litman, G. (1996). *Construction of P1 artificial chromosome (PAC) libraries from lower vertebrates.* Academic Press, San Diego, pp. 223-256.

Amemiya, C. T., Zhong, T. P., Silverman, G. A., Fishman, M. C. and Zon, L. I. (1999a). Zebrafish YAC, BAC and PAC genomic libraries. *Methods Cell Biol,* **60,** 235-258.

Amemiya, C. T. and Zon, L. I. (1999b). Generation of a Zebrafish P1 Artificial Chromosome Library. *Genomics,* **58,** 211-213.

Amsterdam, A., Burgess, S., Golling, G., Chen, W., Sun, Z., Townsend, K., Farrington, S., Haldi, M. and Hopkins, N. (1999). A large-scale insertional mutagenesis screen in zebrafish. *Genes Dev,* **13,** 2713-2724.

Baonza, A., de Celis, J. F. and Garcia-Bellido, A. (2000). Relationships between *extramacrochaetae* and Notch signaling in *Drosophila* wing development. *Development,* **127,** 2383-2393.

Baonza, A. and Garcia-Bellido, A. (1999). Dual role of extramacrochaetae in cell proliferation and differentiation during wing morphogenesis in Drosophila. *Mechanisms of Development,* **80,** 133-146.

Bauer, H., Lele, Z., Rauch, G.-J., Geisler, R. and Hammerschmidt, M. (2001). The type I serine/threonine kinase receptor Alk8/Lost a fin is required for Bmp2b/7 signal transduction during dorsoventral patterning of the zebrafish embryo. *Development,* **128,** 849-858.

Beck, C. W., Whitman, M. and Slack, J. M. W. (2001). The role of BMP signaling in outgrowth and patterning of the *Xenopus* tail bud. *Developmental Biology,* **238,** 303-314.

Bee, J. and Thorogood, P. (1980). The role of tissue interactions in the skeletogenic differentiation of avian neural crest cells. *Developmental Biology,* **78,** 47-62.

Beerman, A., Aranda, M. and Schroder, R. (2004). The Sp8 zinc-finger transcription factor is involved in allometric growth of the limb in the beetle *Tribolium castaneum. Development,* **131,** 733-742.

Bell, S. M., Schreiner, C. M., Waclaw, R. R., Campbell, K., Potter, S. S. and Scott, W. J. (2003). Sp8 is crucial for limb outgrowth and neuropore closure. *Proc. Natl. Acad. Sci. USA,* **100,** 12195-12200.

Bodenstein, D. (1952). Studies on the development of the dorsal fin in amphibians. *J Exper Zool,* **120,** 213-243.

Bokel, C. and Brown, N. H. (2002). Integrins in development: moving on, responding to, and sticking to the extracellular matrix. *Dev Cell,* **3,** 311-321.

Bouvet, J. (1974). Différenciation et ultrastructure du squelette distal de la nageoire pectorale chez la truite indigène (*Salmo trutta fario* L.). I. Différenciation et ultrastructure des actinotriches. *Archives d'Anatomie microscopique,* **63,** 79-96.

Brizuela, B. J., Wessely, O. and De Robertis, E. M. (2001). Overexpression of the Xenopus Tight-Junction Protein Claudin Causes Randomization of the Left-Right Body Axis. *Developmental Biology,* **230,** 217-229.

Brownlie, A., Donovan, A., Pratt, S. J., Paw, B. H., Oates, A. C. and Brugnara, H. E. (1998). Positional cloning of the zebrafish *sauternes* gene: a model for congenital sideroblastic anaemia. *Nature Genetics,* **20,** 244-250.

Bruneau, S., P., M. and Rosa, F. M. (1997). Expression of *contact*, a new zebrafish DVR member, marks mesenchymal cell lineages in the developing pectoral fins and head and is regulated by retinoic acid. *Mechanisms of Development,* **65,** 163-173.

Brunet, L., McMahon, J., McMahon, A. and Harland, R. (1998). Noggin, cartilage morphogenesis, and joint formation in the mammalian skeleton. *Science,* **280,** 1455-1457.

Bryant, S. V. and Gardiner, D. M. (1992). Retinoic acid, local cell-cell interactions, and pattern formation in vertebrate limbs. *Developmental Biology,* **152,** 1-25.

Capdevila, J. and Belmonte, J. C. I. (2001). Patterning Mechanisms Controlling Vertebrate Limb Development. *Annu. Rev. Cell Dev. Biol.,* **17,** 87-132.

Charite, J., de Graaff, W., Shen, S. and Duchamps, J. (1994). Ectopic expression of *Hoxb-8* causes duplications of the ZPA in the forelimb and homeotic transformation of axial structures. *Cell,* **78,** 559-601.

Chiang, E. F.-L., Chin-I, P., Wyatt, M., Yan, Y. L., Postlethwait, J. H. and Chung, B.-C. (2001). Two *Sox9* Genes on Duplicated Zebrafish Chromosomes: Expression of Similar Transcription Activators in Distinct Sites. *Developmental Biology,* **231,** 149-163.

Childs, S., Weinstein, B. M., Mohideen, M. A., Donohue, S., Bonkovsky, H. and Fishman, M. C. (2000). Zebrafish *dracula* encodes ferrochelatase and it mutation provides a model for erythropoietic protoporphyria. *Current Biology,* **10,** 1001-1004.

Ciruna, B., Weidinger, G., Knaut, H., Thisse, B., Thisse, C., Raz, E. and Schier, A. F. (2002). Production of maternal-zygotic mutant zebrafish by germ-line replacement. *Proc. Natl. Acad. Sci. USA,* **99,** 14919-14924.

Coates, M. I. (1995). Limb evolution. Fish fins or tetrapod limbs--a simple twist of fate? *Current Biology,* **5,** 844-848.

Cole, L. K. and Ross, L. S. (2001). Apoptosis in the Developing Zebrafish Embryo. *Developmental Biology,* **240,** 123-142.

Collazo, A., Bronner-Fraser, M. and Fraser, S. E. (1993). Vital dye labeling of Xenopus trunk neural crest reveals multipotency and novel pathways of migration. *Development,* **118,** 363-376.

Connors, S. A., Trout, J., Ekker, M. and Mullins, M. C. (1999). The role of *tolloid/mini fin* in dorsoventral pattern formation of the zebrafish. *Development,* **126,** 3119-3130.

Cordier, A. C. and Haumont, S. M. (1980). Development of thymus, parathyroids, and ultimo-branchial bodies in NMRI and nude mice. *Am J Anat,* **157,** 227-263.

Couly, G. and LeDouarin, N. M. (1990). Head morphogenesis in embryonic avian chimeras: evidence for a segmental pattern in ectoderm corresponding to neuromeres. *Development,* **108,** 543-558.

Cox, D. R., Burmeister, M., Price, E. R., Kim, S. and Myers, R. M. (1990). Radiation hybrid mapping: a somatic cell genetic method for constructing high-resolution maps of mammalian chromosomes. *Science,* **250,** 245-250.

Crawford, B. D., Henry, C. A., Clason, T. A., Becker, A. L. and Hille, M. B. (2003). Activity and distribution of paxillin, focal adhesion kinase, and cadherin indicate cooperative roles during zebrafish morphogenesis. *Mol. Cell. Biol.,* **14,** 3065-3081.

Crump, J. G., Maves, L., Lawson, N. D., Weinstein, B. M. and Kimmel, C. B. (2004a). An essential role for Fgfs in endodermal pouch formation influences later craniofacial skeletal patterning. *Development,* **131,** 5703-5716.

Crump, J. G., Swartz, M. E. and Kimmel, C. B. (2004b). An Integrin-Dependent Role of Pouch Endoderm in Hyoid Cartilage Development. *PLoS Biology,* **2,** e244.

Dane, P. J. and Tucker, J. B. (1985). Modulation of epidermal cell shaping and extracellular matrix during caudal fin morphogenesis in the zebra fish *Brachydanio rerio*. *J Embryol Exp Morphol,* **87,** 145-161.

David, N. B., Saint-Etienne, L., Tsang, M., Schilling, T. F. and Rosa, F. M. (2002). Requirement for endoderm and FGF3 in ventral head skeleton formation. *Development,* **129,** 4457-4468.

Davidson, A. J., Postlethwait, J. H., Yan, Y. L., Beier, D. R., van Doren, C., Foernzler, D., Celeste, A. J., Crosier, K. E. and Crosier, P. S. (1999). Isolation of zebrafish gdf7 and comparative genetic mapping of genes belonging to the growth/differentiation factor 5, 6, 7 subgroup of the TGF-beta superfamily. *Genome Research,* **9,** 121-129.

Delise, A. M. and Tuan, R. S. (2002). Analysis of N-cadherin function in limb mesenchymal chondrogenesis *in vitro*. *Developmental Dynamics,* **225,** 195-204.

Delot, E., Kataoka, H., Goutel, C., Yan, Y.-L., Postlethwait, J. H., Wittbrodt, J. and Rosa, F. M. (1999). The BMP-related protein Radar: a maintenance factor for dorsal neurectoderm? *Mechanisms of Development,* **85,** 15-25.

Dickmeis, T., Rastegar, S., Lam, C. S., Aanstad, P., Clark, M., Fischer, N., Rosa, F., Korzh, V. and Strahle, U. (2002). Expression of the helix-loop-helix gene id3 in the zebrafish embryo. *Mechanisms of Development,* **113,** 99-102.

Dooley, K. and Zon, L. I. (2000). Zebrafish: a model system for the study of human disease. *Curr Opin Genet Dev,* **10,** 252-256.

Draper, B. W., Stock, D. W. and Kimmel, C. B. (2003). Zebrafish *fgf24* functions with *fgf8* to promote posterior mesodermal development. *Development,* **130,** 4639-4654.

Driever, W., Solnica-Krezel, L., Schier, A. F., Neuhauss, S. C., Malicki, J., Stemple, D. L., Stainier, D. Y., Zwartkruis, F., Abdelilah, S., Rangini, Z.,

Belak, J. and Boggs, C. (1996). A genetic screen for mutations affecting embryogenesis in zebrafish. *Development,* **123,** 37-46.

DuShane, G. P. (1935). An experimental study of the origin of pigment cells in Amphibia. *J Exper Zool,* **72,** 1-31.

Ekker, M., Akimenko, M. A., Allende, M. L., Smith, R., Drouin, G., Langille, R. M., Weinberg, E. S. and Westerfield, M. (1997). Relationships Among *msx* Gene Structure and Function in Zebrafish and Other Vertebrates. *Mol. Biol. Evol.,* **14,** 1008-1022.

Ellies, D. L., Stock, D. W., Hatch, G., Giroux, G., Wiess, K. M. and Ekker, M. (1997). Relationship between the Genomic Organization and the Overlapping Embryonic Expression Patterns of the Zebrafish *dlx* Genes. *Genomics,* **45,** 580-590.

Ellis, H. M., Spann, D. R. and Posakony, J. W. (1990). Extramacrochaetae, a negative regulator of sensory organ development in Drosophila, defines a new class of helix-loop-helix proteins. *Cell,* **61,** 27-37.

Epperlein, H. H., Halfter, W. and Tucker, R. P. (1988). Distribution of fibronectin and tenascin along migratory pathways of the neural crest in the trunk of amphibian embryos. *Development,* **103,** 743-756.

Fischer, S., Draper, B. W. and Neumann, C. J. (2003). The zebrafish *fgf24* mutant identifies an additional level of Fgf signaling involved in vertebrate forelimb initiation. *Development,* **130,** 3515-3524.

Fishman, M. C., Stainier, D. Y., Breitbart, R. E. and Westerfield, M. (1997). Zebrafish: genetic and embryological methods in a transparent vertebrate embryo. *Methods Cell Biol,* **52,** 67-82.

Foernzler, D., Her, H., Knapik, E. W., Clark, M., Lehrach, H., Postlethwait, J. H., Zon, L. I. and Beier, D. R. (1998). Gene Mapping in Zebrafish Using Single-Strand Conformation Polymorphism Analysis. *Genomics,* **51,** 216-222.

Fuerthauer, M., Thisse, C. and Thisse, B. (1997). A role for FGF-8 in the dorsoventral patterning of the zebrafish gastrula. *Development,* **124,** 4253-4264.

Fuerthauer, M., Van Celst, J., Thisse, C. and Thisse, B. (2004). Fgf signaling controls the dorsoventral patterning of the zebrafish embryo. *Development,* **131,** 2853-2864.

Gaiano, N., Amsterdam, A., Kawakami, K., Allende, M., Becker, T. and Hopkins, N. (1996). Insertional mutagenesis and rapid cloning of essential genes in zebrafish. *Nature,* **383,** 829-832.

Garrell, J. and Modolel, J. (1990). The Drosophila extramacrochaetae locus, an antagonist of pro-neural genes that like these genes encodes a helix-loop-helix protein. *Cell,* **61,** 39-34.

Garrity, D. M., Childs, S. and Fishman, M. C. (2002). The *heartstrings* mutation in zebrafish causes heart/fin Tbx5 deficiency syndrome. *Development,* **129,** 4635-4645.

Geisler, R., Rauch, G.-J., Baier, H., van Bebber, F. V., Brobeta, L., Dekens, M. P. S., Finger, K., Fricke, C., Gates, M. A., Geiger, H., Geiger-Rudolph, S., Gilmour, D., Glaser, S., Gnuegge, L., Habeck, H., Hingst, K., Holley, S., Keenan, J., Kirn, A., Knaut, H., Lashkari, D., Maderspacher, F., Martyn, U., Neuhauss, S., Neumann, C., Nicolson, T., Pelegri, F., Ray, R., Rick, J. M., Roehl, H., Roeser, T., Schauerte, H. E., Schier, A. F., Schoenberger, U., Schoenthaler, H.-B., Schulte-Merker, S., Seydler, C., Talbot, W. S., Weiler, C., Nuesslein-Volhard, C. and Haffter, P. (1999). A radiation hybrid map of the zebrafish genome. *Nature Genetics,* **23,** 86-89.

Geraudie, J. (1977). Initiation of the actinotrichial development in the early fin bud of the fish, *Salmo*. *Journal of Morphology,* **151,** 353-362.

Ghanem, N., Jarinova, O., Amores, A., Long, Q., Hatch, G., Park, B. K., Rubenstein, J. L. R. and Ekker, M. (2003). Regulatory Roles of Conserved Intergenic Domains in Vertebrate *Dlx* Bigene Clusters. *Genome Research,* **13,** 533-543.

Gibson-Brown, J. J., Agulnik, S. I., Chapman, D. L., Alexiou, M., Garvey, N., Silver, L. M. and Papaioannou, V. E. (1996). Evidence of a role for T-box genes in the evolution of limb morphogenesis and the specification of forelimb/hindlimb identity. *Mechanisms of Development,* **56,** 93-101.

Gilbert, S. F. (2000). *Developmental Biology*. Sinauer Associates, Inc., Sunderland, pp. 749.

Grandel, H. and Schulte-Merker, S. (1998). The development of the paired fins in the zebrafish (Danio rerio). *Mechanisms of Development,* **79,** 99-120.

Gravenson, A. C. and Armstrong, J. B. (1987). Differentiation of cartilage from cranial nerual crest in the axolotl (*Ambystoma mexicanum*). *Differentiation,* **35,** 16-20.

Gruneberg, H. (1954). Genetic studies on the skeleton of the mouse. VIII. Curly tail. *J. Genet.,* **52,** 52-67.

Haffter, P., Granato, M., Brand, M., Mullins, M. C., Hammerschmidt, M., Kane, D. A., Odenthal, J., van Eeden, F. J. M., Jiang, Y.-J., Heisenberg, C.-P., Kelsh, R. N., Furutani-Seiki, M., Vogelsang, E., Beuchle, D., Schach, U., Fabian, C. and Nuesslein-Volhard, C. (1996). The identification of genes with unique and essential functions in the development of the zebrafish, *Danio rerio*. *Development,* **123,** 1-36.

Hall, B. K. and Miyake, T. (1992). The membranous skeleton: the role of cell condensations in vertebrate skeletogenesis. *Anat Embryol,* **186,** 107-124.

Halpern, M. E., Ho, R. K., Walker, C. and Kimmel, C. B. (1993). Induction of muscle pioneers and floor plate is distinguished by the zebrafish *no tail* mutation. *Cell,* **75,** 99-111.

Heisenberg, C.-P., Brennan, C. and Wilson, S. W. (1999). Zebrafish *aussicht* mutant embryos exhibit widespread overexpression of *ace* (*fgf8*) and coincident defects in CNS development. *Development,* **126,** 2129-2140.

Hirsh, D. and Vanderslice, R. (1976). Temperature sensitive developmental mutants of *Caenorhabditis elegans*. *Developmental Biology,* **49,** 220-235.

Hukriede, N. A., Fisher, D., Epstein, J. A., Joly, L., Tellis, P., Zhou, Y., Barbazuk, B., Cox, K., Fenton-Noriega, L., Hersey, C., Miles, J., Sheng, X., Song, A., Waterman, R., Johnson, S. L., Dawid, I. B., Chevrette, M., Zon, L. I., McPherson, J. D. and Ekker, M. (2001). The LN54 Radiation Hybrid Map of Zebrafish Expressed Sequences. *Genome Research,* **11,** 2127-2132.

Hukriede, N. A., Joly, L., Tsang, M., Miles, J., Tellis, P., Epstein, J. A., Barbazuk, W. B., Li, F. N., Paw, B., Postlethwait, J. H., Hudson, T. J., Zon, L. I., McPherson, J. D., Chevrette, M., Dawid, I. B., Johnson, S. L. and Ekker,

M. (1999). Radiation hybrid mapping of the zebrafish genome. *Proc. Natl. Acad. Sci.,* **96,** 9745-9750.

Ivey-Hoyle, M., Conroy, R., Huber, H. E., Goodhart, P. J., Oliff, A. and Heimbrook, D. C. (1993). Cloning and characterization of E2F-2, a novel protein with the biochemical properties of transcription factor E2F. *Mol. Cell. Biol.,* **13,** 7802-7812.

Ivics, Z., Hackett, P. B., Plasterk, R. H. and Izsvak, Z. (1997). Molecular reconstruction of Sleeping Beauty, a Tc1-like transposon from fish, and its transposition in human cells. *Cell,* **91,** 501-510.

Johnson, S. L. and Zon, L. I. (1999). Genetic backgrounds and some standard stocks and strains used in zebrafish developmental biology and genetics. *Methods Cell Biol,* **60,** 357-359.

Jones, R. and Reid, L. (1973). The effect of pH on Alcian Blue staining of epithelial acid glycoproteins. I. Sialomucins and sulphomucins (singly or in simple combinations). *Histochem J,* **5,** 9-18.

Junquiera, L. C., Carneiro, J. and Kelley, R. O. (1998). *Basic Histology*. Appleton and Lange, Stamford, pp. 494.

Kanki, J. P., Chang, S. and Kuwada, J. Y. (1994). The molecular cloning and characterization of potential chick DM-GRASP homologs in zebrafish and mouse. *J. Neurobiol.,* **25,** 831-845.

Kanki, J. P. and Ho, R. K. (1997). The development of the posterior body in zebrafish. *Development,* **124,** 881-893.

Kawakami, A., Fukazawa, T. and Takeda, H. (2004). Early fin primordia of zebrafish larvae regenerate by a similar growth control mechanism with adult regeneration. *Developmental Dynamics,* **231,** 693-699.

Kawakami, K., Shima, A. and Kawakami, N. (2000). Identification of a functional transposase of the Tol2 element, an Ac-like element from the Japanese medaka fish, and its transposition in the zebrafish germ lineage. *Proc. Natl. Acad. Sci.,* **97,** 11403-11408.

Kawakami, Y., Capdevila, J., Buescher, D., Itoh, T., Esteban, C. R. and Belmonte, J. C. (2001). WNT signals control FGF-dependent limb initiation and AER induction in the chick embryo. *Cell,* **104,** 891-900.

Kawakami, Y., Esteban, C. R., Matsui, T., Rodriguez-Leon, J., Kato, S. and Belmonte, J. C. I. (2004). *Sp8* and *Sp9*, two closely related *buttonhead*-like transcription factors, regulate *Fgf8* expression and limb outgrowth in vertebrate embryos. *Development,* **131,** 4763-4774.

Kimmel, C. B., Ballard, W. W., Kimmel, S. R., Ullmann, B. and Schilling, T. F. (1995). Stages of Embryonic Development of the Zebrafish. *Developmental Dynamics,* **203,** 253-310.

Kimmel, C. B., Miller, C. T., Kruze, G., Ullmann, B., BreMiller, R. A., Larison, K. D. and Snyder, H. C. (1998). The Shaping of Pharyngeal Cartilages during Early Development of the Zebrafish. *Developmental Biology,* **203,** 245-263.

Knapik, E. W., Goodman, A., Ekker, M., Chevrette, M., Delgado, J., Neuhauss, S., Shimoda, N., Driever, W., Fishman, M. C. and Jacob, H. J. (1998). A microsatellite genetic linkage map for zebrafish (Danio rerio). *Nature Genetics,* **18,** 338-343.

Kollmar, R., Nakamura, S. K., Kappler, J. A. and Hudspeth, A. J. (2001). Expression and phylogeny of claudins in vertebrate primordia. *Proc. Natl. Acad. Sci.,* **98,** 10196-10201.

Krauss, S., Concordet, J. P. and Ingham, P. W. (1993). A functionally conserved homolog of the Drosophila segment polarity gene hh is expressed in tissues with polarizing activity in zebrafish embryos. *Cell,* **75,** 1431-1444.

Kudryavtseva, E. I., Sugihara, T. M., Wang, N., Lasso, R. J., Gudnason, J. F., Lipkin, S. M. and Andersen, B. (2003). Identification and Characterization of Grainyhead-like Epithelial Transactivator (GET-1), a Novel Mammalian Grainyhead-like Factor. *Developmental Dynamics,* **226,** 604-617.

LeDouarin, N. M., Dupin, E. and Ziller, C. (1994). Genetic and Epigenetic control in neural crest development. *Curr Opin Genet Dev,* **4,** 685-695.

Lee, K.-H., Xu, Q. and Breitbart, R. E. (1996). A New *tinman*-Related Gene, *nkx2.7*, Anticipates the Expression of *nkx2.5* and *nkx2.3* in Zebrafish Heart and Pharyngeal Endoderm. *Developmental Biology,* **180,** 722-731.

Lefebvre, V., Huang, W., Harley, V. R., Goodfellow, P. N. and De Crombrugghe, B. (1997). SOX9 is a potent activator of the chondrocyte-specific enhancer of the pro α1(II) collagen gene. *Mol. Cell. Biol.,* **17,** 2336-2346.

Lekven, A. C., Thorpe, C. J., Waxman, J. S. and Moon, R. T. (2001). Zebrafish wnt8 encodes two wnt8 proteins on a bicistronic transcript and is required for mesoderm and neuroectoderm patterning. *Developmental Cell,* **1,** 103-114.

Lele, Z., Folchert, A., Concha, M., Rauch, G. J., Geisler, R., Rosa, F., Wilson, S. W., Hammerschmidt, M. and Bally-Cuif, L. (2002). parachute/ n-cadherins required for morphogenesis and maintained integrity of the zebrafish neural tube. *Development,* **129,** 3281-3294.

Loh, Y. H., Christoffels, A., Brenner, S., Hunziker, W. and Venkatesh, B. (2004). Extensive Expansion of the Claudin Gene Family in the Teleost Fish, *Fugu rubripes*. *Genome Research,* **14,** 1248-1257.

Luo, R., An, M., Arduini, B. L. and Henion, P. D. (2001). Specific Pan-Neural Crest Expression of Zebrafish *Crestin* Throughout Embryonic Development. *Developmental Dynamics,* **220,** 169-174.

Macias, D., Ganan, Y., Sampath, T., Piedra, M., Ros, M. and Hurle, J. (1997). Role of BMP-2 and OP-1 (BMP-7) in programmed cell death and skeletogenesis during chick limb development. *Development,* **124,** 1109-1117.

Mansour, S., Hall, C. M., Pembrey, M. E. and Young, I. D. (1995). A clinical and genetic study of campomelic dysplasia. *J Med Genet,* **32,** 415-520.

McPherron, A. C., Lawler, A. M. and Lee, S. J. (1999). Regulation of anterior/posterior patterning of the axial skeleton by growth/differentiation factor 11. *Nature Genetics,* **22,** 260-264.

Michelmore, R. W., Paran, I. and Kesseli, R. V. (1991). Identification of markers linked to disease-resistance genes by bulked segregant analysis: A rapid

method to detect markers in specific genomic regions by using segregating populations. *Proc. Natl. Acad. Sci.,* **88,** 9828-9832.

Muller, F., Chang, B., Albert, S., Fischer, N., Tora, L. and Strahle, U. (1999). Intronic enhancers control expression of zebrafish sonic hedgehog in floor plate and notochord. *Development,* **126,** 2103-2116.

Mullins, M. C., Hammerschmidt, M., Kane, D. A., Odenthal, J., Brand, M., van Eeden, F. J. M., Furutani-Seiki, M., Granato, M., Haffter, P., Heisenberg, C.-P., Jiang, Y.-J., Kelsh, R. N. and Nuesslein-Volhard, C. (1995). Genes establishing dorsoventral pattern formation in the zebrafish embryo: the ventral specifying genes. *Development,* **123,** 81-93.

Nakamura, T., Aikawa, T., Iwamoto-Enomoto, M., Iwamoto, M., Higuchi, Y., Maurizio, P., Kinto, N., Yamaguchi, A., Noji, S., Kurisu, K. and Matsuya, T. (1997). Induction of osteogenic differentiation by hedgehog proteins. *Biochem Biophys Res Commun,* **237,** 465-469.

Nakao, T. and Ishizawa, A. (1984). Light- and electron-microscopic observations of the tail bud of the larval lamprey (*Lampetra japonica*). *Am J Anat,* **170,** 55-71.

Nasevicius, A. and Ekker, S. C. (2000). Effective targeted gene 'knockdown' in zebrafish. *Nature Genetics,* **26,** 216-220.

Nelson, C. E., Morgan, B. A., Burke, A. C., Laufer, E., DiMambro, E., Murtaugh, L. C., Gonzales, E., Tessarollo, L., Parada, L. F. and Tabin, C. (1996). Analysis of Hox gene expression in the chick limb bud. *Development,* **122,** 1449-1466.

Neumann, C. J., Grandel, H., Gaffield, W., Schulte-Merker, F. and Nuesslein-Volhard, C. (1999). Transient establishment of anterior-posterior polarity in the zebrafish pectoral fin bud in the absence of *sonic hedgehog* activity. *Development,* **126,** 4817-4826.

Newth, D. R. (1956). On the neural crest of the lamprey embryo. *J Embryol Exp Morphol,* **4,** 358-375.

Ng, J. K., Kawakami, Y., Büscher, D., Raya, A., Itoh, T., Koth, C. M., Esteban, C. R., Rodríguez-León, J., Garrity, D. M., Fishman, M. C. and Belmonte, J. C.

I. (2002). The limb identity gene *Tbx5* promotes limb initiation by interacting with *Wnt2b* and *Fgf10*. *Development,* **129,** 5161-5170.

Noden, D. M. (1988). Interactions and fates of avian craniofacial mesenchyme. *Development,* **103 Supplement,** 121-140.

Norton, J. D. (2000). ID helix-loop-helix proteins in cell growth, differentiation and tumorigenesis. *Journal of Cell Science,* **113,** 3897-3905.

Nuesslein-Volhard, C. and Dahm, R. (2002). *Zebrafish*. Oxford University Press, Oxford, pp. 303.

Nuesslein-Volhard, C. and Wieschaus, E. (1980). Mutations affecting segment number and polarity in Drosophila. *Nature,* **287,** 795-801.

Odenthal, J. and Nuesslein-Volhard, C. (1998). *fork head* domain genes in zebrafish. *Dev Genes Evol,* **208,** 245-258.

Padhi, B. K., Joly, L., Tellis, P., Smith, A., Nanjappa, P., Chevrette, M., Ekker, M. and Akimenko, M. A. (2004). Screen for Genes Differentially Expressed During Regeneration of the Zebrafish Caudal Fin. *Developmental Dynamics,* **231,** 527–541.

Penberthy, W. T., Shafizadeh, E. and Lin, S. (2002). The zebrafish as a model for human disease. *Front Biosci,* **7,** d1439-1453.

Pesole, G., Mignone, F., Gissi, C., Grillo, G., Licciulli, F. and Liuni, S. (2001). Structural and functional features of eukaryotic mRNA untranslated regions. *Gene,* **276,** 73-81.

Piotrowski, T., Ahn, D.-G., Schilling, T. F., Nair, S., Ruvinsky, I., Geisler, R., Rauch, G.-J., Haffter, P., Zon, L. I., Zhou, Y., Foott, H., Dawid, I. B. and Ho, R. K. (2003). The zebrafish *van gogh* mutation disrupts *tbx1*, which is involved in the DiGeorge deletion syndrome in humans. *Development,* **130,** 5043-5052.

Piotrowski, T. and Nuesslein-Volhard, C. (2000). The Endoderm Plays an Important Role in Patterning the Segmented Pharyngeal Region in Zebrafish (*Danio rerio*). *Developmental Biology,* **225,** 339-356.

Postlethwait, J. H., Johnson, S. L., Midson, C. N., Talbot, W. S., Gates, M., Ballinger, E. W., Africa, D., Andrews, R., Carl, T., Eisen, J. S., Horne, S., Kimmel, C. B., Hutchinson, M., Johnson, M. and Rodriguez, A. (1994). A Genetic Linkage Map for the Zebrafish. *Science,* **264,** 699-703.

Quinlan, R., Martin, P. and Graham, A. (2004). The role of actin cables in directing the morphogenesis of the pharyngeal pouches. *Development,* **131,** 593-599.

Rancourt, D. E., Tsuzuki, T. and Capecchi, M. R. (1995). Genetic interaction between hoxb-5 and hoxb-6 is revealed by nonallelic noncomplementation. *Genes Dev.,* **9,** 108-122.

Rawls, J. F., Frieda, M. R., McAdow, A. R., Gross, J. P., Clayton, C. M., Heyen, C. K. and Johnson, S. L. (2003). Coupled Mutagenesis Screens and Genetic Mapping in Zebrafish. *Genetics,* **163,** 997-1009.

Rechsteiner, M. and Rogers, S. W. (1996). PEST sequences and regulation by proteolysis. *Trends Biochem. Sci.,* **21,** 267-271.

Ribisi, S. J., Mariani, F. V., Aamar, E., Lamb, T. M., Frank, D. and Harland, R. M. (2000). Ras-Mediated FGF Signaling Is Required for the Formation of Posterior but Not Anterior Neural Tissue in *Xenopus laevis*. *Developmental Biology,* **227,** 183-196.

Riddle, R. D., Johnson, R. L., Laufer, E. and Tabin, C. (1993). *Sonic hedgehog* mediates the polarizing activity of the ZPA. *Cell,* **75,** 1401-1416.

Riechmann, V., van Cruchten, I. and Sablitzky, F. (1994). The expression pattern of Id4, a novel dominant negative helix-loop-helix protein is distinct from Id1, Id2 and Id3. *Nucleic Acids Res,* **22,** 749-755.

Rodriguez-Esteban, C., Tsukui, T., Yonei, S., Magallon, J., Tamura, K. and Izpisua-Belmonte, J. C. (1999). The T-box genes *Tbx4* and *Tbx5* regulate limb outgrowth and identity. *Nature,* **398,** 814-818.

Rubenstein, A. L., Lee, D., Luo, R., Henion, P. D. and Halpern, M. E. (2000). Genes dependent on zebrafish cyclops function identified by AFLP differential gene expression screen. *Genesis,* **26,** 86-97.

Russell, W., Kelly, E., Hunsicker, P., Bangham, J., Maddux, S. and Phipps, E. (1979). Specific-locus test shows ethylnitrosourea to be the most potent mutagen in the mouse. *Proc. Natl. Acad. Sci. USA,* **76,** 5818-5819.

Saunders, J. W. J. (1948). The proximo-distal sequence of origin of the parts of the chick wing and the role of the ectoderm. *J. Exp. Zool.,* **108,** 363-403.

Schilling, T. F., Concordet, J. P. and Ingham, P. W. (1999). Regulation of Left-Right Asymmetries in the Zebrafish by *Shh* and *BMP4*. *Developmental Biology,* **210,** 277-287.

Schilling, T. F. and Kimmel, C. B. (1994). Segment and cell type lineage restrictions during pharyngeal arch development in the zebrafish embryo. *Development,* **120,** 483-494.

Schmid, B., Furthauer, M., Connors, S. A., Trout, J., Thisse, B., Thisse, C. and Mullins, M. C. (2000). Equivalent roles for *bmp7/snailhouse* and *bmp2b/swirl* in dorsoventral pattern formation. *Development,* **127,** 957-967.

Seufert, D. W. and Hall, B. K. (1990). Tissue interactions involving cranial neural crest in cartilage formation in *Xenopus laevis* (Daudin). *Cell Differ Dev,* **32,** 153-165.

Shih, J. and Fraser, S. E. (1996). Characterizing the zebrafish organizer: microsurgical analysis at the earlyshield stage. *Development,* **122,** 1313-1322.

Shukunami, C., Ohta, Y., Sakuda, M. and Hiraki, Y. (1998). Sequential progression of the differentiation program by bone morphogenetic protein-2 in chondrogenic cell line ATDC5. *Exp Cell Res,* **241,** 1-11.

Singer, B. and Grunberger, D. (1983). *Molecular Biology of Mutagens and Carcinogens*. Plenum Press, New York.

Smith, L. and Thorogood, P. (1983). Transfilter studies on the mechanism of epitheliomesenchymal interaction leading to chondrogenic differentiation of neural crest cells. *J. Embryol. Exp. Morphol.,* **75,** 165-188.

Smith, M., Hickman, A., Amanze, D., Lumsden, A. and Thorogood, P. (1994). Trunk neural crest origin of caudal fin mesenchyme in the zebrafish *Brachydanio rerio*. *Proc. R. Soc. Lond.*, **256,** 137-145.

Smith, M. M. and Hall, B. K. (1990). Development and evolutionary origins of vertebrate skeletogenic and odontogenic tissues. *Biol Rev,* **65,** 277-373.

Smithberg, M. (1954). The origin and development of the tail in the frog, *Rana pipiens*. *J Exper Zool,* **127,** 397-425.

Sordino, P., van der Hoeven, F. and Deboule, D. (1995). Hox gene expression in the teleost fin and the origin of vertebrate digits. *Nature,* **375,** 678-681.

Spemann, H. and Mangold, H. (1924). Induction of embryonic primordia by implantation of organizers from a different species. In: *Foundations of Experimental Embryology*, B. H. Willier and J. M. Oppenheimer, Eds, Hafner, New York, pp. 144-184.

Sprague, J., Doerry, E., Douglas, S. and Westerfield, M. (2001). The Zebrafish Information Network (ZFIN): a resource for genetic, genomic and developmental research. *Nucleic Acids Res,* **29,** 87-90.

Strahle, U., Blader, P. and Ingham, P. W. (1996). Expression of axial and sonic hedgehog in wildtype and midline defective zebrafish embryos. *Int. J. Dev. Biol.,* **40,** 929-940.

Stratford, T., Horton, C. and Maden, M. (1996). Retinoic acid is required for the initiation of outgrowth in the chick limb bud. *Current Biology,* **6,** 1124-1133.

Strausberg, R. L., Feingold, E. A., Grouse, L. H., Derge, J. G., Klausner, R. D., Collins,F.S., Wagner,L., Shenmen,C.M., Schuler,G.D., Altschul, S. F., Zeeberg,B., Buetow,K.H., Schaefer,C.F., Bhat,N.K., Hopkins, R. F., Jordan,H., Moore,T., Max,S.I., Wang,J., Hsieh,F., Diatchenko, L., Marusina,K., Farmer,A.A., Rubin,G.M., Hong,L., Stapleton, M., Soares,M.B., Bonaldo,M.F., Casavant,T.L., Scheetz, T. E., Brownstein,M.J., Usdin,T.B., Toshiyuki,S., Carninci, P., Prange,C., Raha,S.S., Loquellano,N.A., Peters,G.J., Abramson, R. D., Mullahy,S.J., Bosak,S.A., McEwan,P.J., McKernan, K. J., Malek,J.A., Gunaratne,P.H., Richards,S., Worley, K. C., Hale,S., Garcia,A.M., Gay,L.J., Hulyk,S.W., Villalon, D. K., Muzny,D.M., Sodergren,E.J., Lu,X., Gibbs,R.A., Fahey, J., Helton,E., Ketteman,M., Madan,A., Rodrigues,S., Sanchez, A.,

Whiting,M., Madan,A., Young,A.C., Shevchenko,Y., Bouffard, G. G., Blakesley,R.W., Touchman,J.W., Green,E.D., Dickson, M. C., Rodriguez,A.C., Grimwood,J., Schmutz,J., Myers,R.M., Butterfield, Y. S., Krzywinski,M.I., Skalska,U., Smailus,D.E., and Schnerch, A., Schein,J.E., Jones,S.J. and Marra,M.A. (2002). Generation and initial analysis of more than 15,000 full-length human and mouse cDNA sequences. *Proc. Natl. Acad. Sci.,* **99,** 16899-16903.

Summerton, J. (1999). Morpholino antisense oligomers: the case for an RNase H-independent structural type. *Biochem Biophys Acta,* **1489,** 141-158.

Takeuchi, J. K., Koshiba-Takeuchi, K., Matsumoto, K., Vogel-Hopker, A., Naitoh-Matsuo, M., Ogura, K., Takahashi, N., Yasuda, K. and Ogura, T. (1999). *Tbx5* and *Tbx4* genes determine the wing/leg identity of limb buds. *Nature,* **398,** 810-814.

Talbot, W. S., Trevarrow, B., Halpern, M. E., Melby, A. E., Farr, G., Postlethwait, J. H., Jowett, T., Kimmel, C. B. and Kimelman, D. (1995). A homeobox gene essential for zebrafish notochord development. *Nature,* **378,** 150-157.

Tao, J., Kuliyev, E., Wang, X., Li, X., Wilanowski, T., Jane, S. M., Mead, P. E. and Cunningham, J. M. (2005). BMP4-dependent expression of *Xenopus* Grainyhead-like 1 is essential for epidermal differentiation. *Development,* **132,** 1021-1034.

Therrien, M., Wong, A. M. and Rubin, G. M. (1998). CNK, a RAF-Binding Multidomain Protein Required for RAS Signaling. *Cell,* **95,** 343-353.

Thisse, B., Wright, C. V. and Thisse, C. (2000). Activin- and Nodal-related factors control antero-posterior patterning of the zebrafish embryo. *Nature,* **403,** 425-428.

Thorogood, P. and Wood, A. (1987). Analysis of *in vivo* cell movement using transparent tissue systems. *J Cell Sci Suppl,* **8,** 395-413.

Ting, S. B., Wilanowski, T., Auden, A., Hall, M., Voss, A. K., Thomas, T., Parekh, V., Cunningham, J. M. and Jane, S. M. (2003a). Inositol- and folate-resistant neural tube defects in mice lacking the epithelial-specific factor Grhl-3. *Nature Medicine,* **9,** 1513-1519.

Ting, S. B., Wilanowski, T., Cerruti, L., Zhao, L.-L., Cunningham, J. M. and Jane, S. M. (2003b). The identification and characterization of human Sister-of-Mammalian Grainyhead (SOM) expands the *grainyhead*-like family of developmental transcription factors. *Biochem. J.,* **370,** 953-962.

Todt, W. L. and Fallon, J. F. (1984). Development of the apical ectodermal ridge in the chick wing. *J. Embryol. Exp. Morphol.,* **80,** 21-41.

Trainor, P. A., Tan, S. S. and Tam, P. P. L. (1994). Cranial paraxial mesoderm: regionalisation of cell fate and impact on craniofacial development in mouse embryos. *Development,* **120,** 2397-2408.

Treichel, D., Schock, F., Jackle, H., Gruss, P. and Mansouri, A. (2003). mBtd is required to maintain signaling during murine limb development. *Genes Dev.,* **17,** 2630-2635.

Trumpp, A., Depew, M. J., Rubenstein, J. L., Bishop, J. M. and Martin, G. R. (1999). Cre-mediated gene inactivation demonstrates that FGF8 is required for cell survival and patterning of the first branchial arch. *Development,* **13,** 3136-3148.

Tsang, M., Maegawa, S., Kiang, A., Habas, R., Weinberg, E. and Dawid, I. B. (2004). A role for MKP3 in axial patterning of the zebrafish embryo. *Development,* **131,** 2769-2779.

Tucker, A. S. and Slack, J. M. W. (1995). The *Xenopus laevis* tail-forming region. *Development,* **121,** 249-262.

Tucker, A. S. and Slack, J. M. W. (2004). Independent Induction and Formation of the Dorsal and Ventral Fins in *Xenopus laevis*. *Developmental Dynamics,* **230,** 461-467.

Twitty, V. C. and Bodenstein, D. (1941). Experiments on the determination problem. I. The roles of ectoderm and neural crest in the development of the dorsal fin in Amphibia. II. Changes in ciliary polarity associated with the induction of fin epidermis. *J Exper Zool,* **86,** 343-380.

Tzouanacou, E., Tweedie, S. and Wilson, V. (2003). Identification of *Jade-1*, a Gene Encoding a PHD Zinc Finger Protein in a Gene Trap Mutagenesis

Screen for Genes Involved in Anteroposterior Axis Development. *Mol. Cell. Biol.,* **23,** 8553-8562.

Vaglia, J. L. and Hall, B. K. (1999). Regulation of neural crest cell populations: occurrence, distribution and underlying mechanisms. *Int. J. Dev. Biol.,* **43,** 95-110.

Vaglia, J. L. and Hall, B. K. (2000). Patterns of migration and regulation of trunk neural crest cells in Zebrafish (*Danio rerio*). *Int. J. Dev. Biol.,* **44,** 867-881.

van Eeden, F. J. M., Granato, M., Schach, U., Brand, M., Furutani-Seiki, M., Haffter, P., Hammerschmidt, M., Heisenberg, C.-P., Jiang, Y.-J., Kane, D. A., Kelsh, R. N., Mullins, M. C., Odenthal, J., Warga, R. M. and Nuesslein-Volhard, C. (1996). Genetic analysis of fin formation in the zebrafish, *Danio rerio*. *Development,* **12,** 255-262.

Wagner, G. P. and Chui, C.-H. (2001). The Tetrapod Limb: A Hypothesis on Its Origin. *Journal of Experimantal Zoology (Mol Dev Evol),* **291,** 226-240.

Wang, H., Long, Q., Marty, S. D., Sassa, S. and Lin, S. (1998). A zebrafish model for hepatoerythropoietic porphyria. *Nature Genetics,* **20,** 239-243.

Warga, R. M. and Stainier, D. Y. (2002). The guts of endoderm formation. *Results Probl Cell Differ,* **40,** 28-47.

Westerfield, M. (1995). *The Zebrafish Book.* University of Oregon Press, Eugene.

Wood, A. and Thorogood, P. (1984). An analysis of *in vivo* cell migration during teleost fin morphogenesis. *J Cell Sci,* **66,** 205-222.

Wood, A. and Thorogood, P. (1987). An ultrastructural and morphometric analysis of an *in vivo* contact guidance system. *Development,* **101,** 363-381.

Yan, Y. L., Hatta, K., Riggleman, B. and Postlethwait, J. H. (1995). Expression of a type II collagen gene in the zebrafish embryonic axis. *Developmental Dynamics,* **203,** 363-376.

Yan, Y. L., Talbot, W. S., Egan, E. S. and Postlethwait, J. H. (1998). Mutant Rescue by BAC Clone Injection in Zebrafish. *Genomics,* **50,** 287-289.

Yelon, D., Patient, R., Holder, N. and Stainier, D. Y. R. (1999). Gata5 is required for the development of the heart and endoderm in zebrafish. *Genes Dev,* **13,** 2983-2995.

Zon, L. I. (1999). Zebrafish: A New Model for Human Disease. *Genome Research,* **9,** 99-100.

Zou, H., Wieser, R., Massague, J. and Niswander, L. (1997). Distinct roles of type I bone morphogenetic protein receptors in the formation and differentiation of cartilage. *Genes Dev.,* **11,** 2191-2203.

Sequence data were produced by the Danio rerio Sequencing Group at the Sanger Institute and can be obtained from http://www.ensembl.org/Danio_rerio.

SSLP marker data for this thesis were retrieved from the Zebrafish Information Network (ZFIN), the Zebrafish International Resource Center, University of Oregon, Eugene, OR 97403-5274; World Wide Web URL: http://zfin.org/; February 8, 2005.

Appendix 1: Probes used for *in situ* hybridization experiments

Probe	Reference	Size (kb)	Linearized with	RNA polymerase
2-H06	(Padhi *et al.*, 2004)	2.5	*EcoR*I	T7
collagen 2a1	(Yan *et al.*, 1995)	1.7	*Hind*III	T3
crestin	(Rubenstein *et al.*, 2000)	4	*EcoR*I	T7
dlx2	(Akimenko *et al.*, 1994)	1.7	*BamH*I	T7
fgf8	(Fuerthauer *et al.*, 1997)	2.1	*EcoR*I	T7
foxD3	(Odenthal and Nuesslein-Volhard, 1998)	1.8	*BamH*I	T7
msxC	(Akimenko *et al.*, 1995b)	2-2.1	*BamH*I	T7
sox9b	(Chiang *et al.*, 2001)	2.0	*Xho*I	T7

Appendix 2: Sequence reference numbers

NAME	GenBank/Ensembl/RZPD ID	Primers for cloning (5'→3'; Forward, Reverse)	Primers for mapping (5'→3'; Forward, Reverse)
id3	AY065841	acgcgtccgggagttcaaca, ccaaactgcagccatgctga	gcgggacagaacttttctcc, ccaaatagtcaggaatgtagcc
gdf7	AF113022	N/A	ttgagtgctcattcctgcac, ttagcccctgttggaagatg
e2f2	ENSDART00000002343	N/A	atgaaagccatcaacatcca, gcaggcagaaataccttgct
claudin	GENSCAN0000004736	ccattgacgagatgcact, gagtctcttgagtcctctgaa	N/A
zgc:77200	BC065587	N/A	N/A
est3	ENSDESTT00000026153	tctgtaccacagatcagcaaca, tttcctctcttagtcctgccata	N/A
ng1	ENSDARG00000006645	atacggatctgtgtttcagg, agcaagactgtccactcaac	ctcgtctcttacacaaagagg, agcacaacaatcacatcaca
phf17.1	BC046874	atttccgcatcacttgaagg, acgcagatgttgcacttgtc	N/A
phf17.2	BC046874	tgcgatgtctgtcagtctcc, cgccttaaaagcacttcctg	N/A
phf17.3	BC046874	ggacgagttctatcgcttcg, cgatccgctgtacatgtttg	N/A
phf17.4	BC046874	caagctatgggaccaggtgt, tgccacagcagaagtaatgg	N/A
grhl3	ENSDARESTG00000005566	atcagcactgcctgtacaaggag, ctataactccataagtgtgacctgg	N/A
z30467	N/A	N/A	ctctctcccacagtcatgca, ggggtttgatgaatggtgac
z26685	G47976	N/A	tgttcaccagcgaagaacag, agcctcacaggtgagcatct
z9831	G41660	N/A	gaatccctgtgccagttgtt, tcaggtgtcttaggaaaattgtt
zCtg37A	N/A	N/A	caggcataaaccgccataat, tgaggacatacgagctttgc
PAC21	BUSMP706M112	N/A	N/A
PAC23	BUSMP706P1397	N/A	tggtgcaacctcaagttcaa, cctccatcgaatgcagtttt
PAC24	BUSMP706J05236	N/A	cggactgtctggcaacatct, acagactgctccctcttcca
PACid3.5	BUSMP706M02159	N/A	N/A
PACid3.6	BUSMP706B13171	N/A	N/A
PACB	BUSMP706O155	N/A	N/A

Appendix 3: Statistical Analyses of Mapping Results

# recombinants/meioses	95% Confidence Interval	
	cM (% recombination)	kb
2/2114	0.0115<0.0950<0.341	6.90<57.0<205
0/2114	0<0<0.174	0<0<104
3/2148	0.0281<0.140<0.407	16.9<84.0<244

Marker	LN54 LOD score
ng1	14.8
z30467	15.7
id3	17.7
z26685	15.7
sly1	13.9
Q8aut6	13.2